Nanoparticle Catalysts for Carbon-Carbon Coupling Reactions

A thesis submitted to

The College of Graduate Studies and Research

In Partial Fulfillment of the Requirements

For the Degree of Master of Science

In the Department of Chemistry

University of Saskatchewan

Saskatoon

By

Qian Bai

PERMISSION TO USE

In presenting this thesis in partial fulfillment of the requirements for a Postgraduate degree from the University of Saskatchewan, I agree that the Libraries of this University may make it freely available for inspection. I further agree that permission for copying of this thesis in any manner, in whole or in part, for scholarly purposes may be granted by the professor or professors who supervised my thesis work or, in their absence, by the Head of the Department or the Dean of the College in which my thesis work was done. It is understood that any copying or publication or use of this thesis or parts thereof for financial gain shall not be allowed without my written permission. It is also understood that due recognition shall be given to me and to the University of Saskatchewan in any scholarly use which may be made of any material in my thesis.

Requests for permission to copy or to make other uses of materials in this thesis in whole or part should be addressed to:

Head of the Department of Chemistry

University of Saskatchewan

Saskatoon, Saskatchewan (S7N5C9)

Canada

ABSTRACT

My research is focused on two main objectives, the study of catalytic efficiency and mechanism of palladium nanoparticles stabilized by poly(vinylpyrrolidone) (PVP) for carbon-carbon coupling reactions, and to rationally synthesize metal nanoparticles stabilized by metal-carbon bonds and apply them to catalyze carbon-carbon coupling reactions.

In the first project, Pd nanoparticles stabilized by PVP were used to catalyze carbon-coupling reactions, specifically the Stille and Suzuki reactions. The mechanism of carbon-carbon coupling reactions was studied. The uncertainty of whether nanoparticles or Pd salts are the catalyst was also examined using the same experimental procedure with Pd salts to examine their catalytic activity in carbon-carbon coupling reactions. Results show that the presence of O_2 is crucial to the Stille reaction with the Pd nanoparticles, which are nearly completely inert under N_2, while the K_2PdCl_4 precursor is itself quite active for the Stille reaction. However, the Pd nanoparticles were found to be active for the Suzuki reaction with high yields in the absence of O_2. The yields for 4-chlorobenzoic acid are higher than 4-bromobenzoic acid and occur for un-catalyzed reactions, for reasons that are still unknown. Finally Au nanoparticles have been tested by the same experimental procedure and have no catalytic activity for these two reactions.

In the second project, the synthesis of Au and Pd monolayer protected clusters

(MPCs) with metal carbon covalent linkages was examined, and the stability of the resulting MPCs was tested. UV-Vis spectra and TEM images show the formation of Au and Pd nanoparticles and ^{1}H NMR was used to characterize the ligands attached to the surface of the nanoparticles. The decylphenyl-stabilized Pd MPCs were synthesized successfully and quite stable in air, while decylphenyl-stabilized Au MPCs prepared with the same protocol have less stability and are easily decomposed. XPS spectra indicate the composition of decylphenyl-stabilized Pd MPCs is a combination of Pd^{0} and Pd^{2+} species with the Pd^{2+} species in excess. In addition, alkylphenyl-stabilized Pd nanoparticles were shown to be effective catalysts for carbon-carbon coupling reactions such as Suzuki and Stille reactions as well as hydrogenation reactions. Finally, it was noted that Pd-C bonds could be easily reduced by H_2 when performing hydrogenation reactions resulting in nanoparticle aggregation and precipitation under hydrogenation conditions.

ACKNOWLEDGEMENTS

Foremost, I would like to express my sincere gratitude to my supervisor, Dr. Robert W. J. Scott for the continuous support of my Master study and research, for his patience, motivation, enthusiasm, and immense knowledge. His guidance helped me in all the time of research and writing of this thesis. I could not have imagined having a better advisor and mentor for my Master study. I will always cherish that. I would also like to thank Dr. S. R. Foley, my advisory committee member, for his assistance throughout my research work.

My sincere thanks to all the past and present Scott Group members, especially Priyabrat Dash, Tesfalidet Lamma and Mita Dasog, for helping me during my research work. Thanks to all of members in Dr. Burgess' group for all of their help.

In addition, thanks to the Natural Sciences and Engineering Research Council (NSERC), the University of Saskatchewan and Department of Chemistry for financial support for my Masters research.

Finally, I would like to thank my family: my parents Zhimin Bai and Xiuqin Sun, for their unlimited love, support and encouragement throughout my life.

TABLE OF CONTENTS

LIST OF FIGURES

LIST OF SCHEMES

LIST OF TABLES

LIST OF ABBREVIATIONS

AFM	Atomic Force Microscopy
APy	1-Allylpyrene
BE	Binding Energy
C-C	Carbon-Carbon
CD	Cyclodextrin
C-N	Carbon-Nitrogen
DSC	Differential Scanning Calorimetry
EDS	Energy Dispersive X-ray Spectroscopy
EXAFS	Extended X-ray Absorption Fine Structure
FTIR	Fourier Transform Infrared Spectroscopy
FWHM	Full Width at Half Maximum
IR	Infrared Spectroscopy
LDI-MS	Laser Desorption-Ionization Mass Spectrometry
MA	Maleic Acid
MALDI-MS	Matrix Assisted Laser Desorption Ionization-Mass Spectrometry
MPACs	Monolayer-Protected Alloy Clusters
MPCs	Monolayer Protected Clusters
NHC	N-Heterocyclic Carbene

NMR	Nuclear Magnetic Resonance
PAMAM	Poly(amidoamine)
PATP	Poly(2-aminothiophenol)
PVP	Poly(vinylpyrrolidone)
SAM	Self-Assembled Monolayer
SAXS	Small-Angle X-ray Scattering
STM	Scanning Tunneling Microscopy
TBP	4-Tertbuthylphenol
TEM	Transmission Electron Microscopy
THF	Tetrahydrofuran
TGA	Thermal Gravimetric Analysis
TOAB	Tetraoctylammonium Bromide
TOF	Turnover Frequency
TON	Turnover Number
UV–Vis	Ultraviolet Visible
XPS	X-ray Photoelectron Spectroscopy
XRD	X-ray Diffraction
VPy	1-Vinylpyrene

CHAPTER 1: LITERATURE SURVEY- MONOLAYER - PROTECTED METAL CLUSTERS AND THEIR APPLICATIONS

1.1 Introduction to "Quasi-Homogeneous" Nanoparticle Catalysts

Catalysis is a central field of nanoscience and nanotechnology [1], and much work on nanoparticle-supported catalysts in the petrochemical community predates the nanotechnology revolution [2]. Product selectivity can be major problem in heterogeneous catalysis [3-6], while on the other side of the catalysis world, mononuclear transition-metal complexes have recently achieved amazing levels of performance in terms of selectivity [7-9] but can be extremely difficult to separate from products [7]. Recently, the ultimate goals of recoverable catalysts, their criteria of evaluation and their role in "green chemistry" have been emphasized [10]. Many homogeneous catalysts are used in industry in biphasic systems or by fixation on supports [11, 12]. A bridge between these two approaches is now being built through the use of nanoparticle catalysts suspended in liquid media; this domain is called "quasi-homogeneous" catalysis [13].

The interest in catalysis by metal nanoparticles is increasing dramatically, as reflected by the large number of publications in the last ten years. It can be seen that transition metal nanoparticles are very attractive to use as catalysts due to their high surface-to-volume ratio and their high surface energy, which makes their surface atoms very active [14-16]. The first use of nanoparticles in catalysis appeared in the 19^{th} century

with photography (Ag nanoparticles) and the decomposition of hydrogen peroxide [17]. A breakthrough of catalytic applications of nanoparticles came with Haruta's seminal studies on oxide-supported Au nanoparticle-catalyzed CO oxidation by O_2 at low temperatures [18, 19] and olefin hydrogenation reactions[20]. Since these studies, there have been numerous types of reactions that have been catalyzed using colloidal nanoparticles, for example, oxidations of alcohols and alkenes [21], carbon cross-coupling reactions [22], electron-transfer reactions [23, 24], hydrogenations of unsaturated substrates [3, 25], and many others.

Chemical reduction methods such as alcohol reduction, hydrogen reduction, and sodium borohydride reduction [26, 27], have been the most common ways of synthesizing colloidal metal nanoparticles. Other reduction methods such as electrochemical, photochemical and sonochemical reduction methods have also been used to a smaller extent [28, 29]. However, having very active surface atoms can also result in the nanoparticles being unstable in liquid media during the course of a catalytic reaction. Thus stabilizers need to be applied to prevent nanoparticles from aggregation, agglomeration and growth and thereby losing their catalytic activity. Many different stabilizers have been used as capping agents for the synthesis of colloidal metal nanoparticles such as polymers, dendrimers, block copolymer micelles, surfactants and other ligands [30-33].

One modern stabilization strategy, inspired by the 150-year old method of Faraday [34] and popularized by Schiffrins' group [35] in 1993, involves reduction of a

metal precursor such as $HAuCl_4$ or Na_2PdCl_4 by $NaBH_4$ in a biphasic organic-solvent-water system in the presence of a phase transfer reagent $[N(C_8H_{17})_4]Br$ and thiol stabilizer. These particles, called monolayer protected clusters (MPCs), have been studied widely from the aspects of stability and solubility [36-38]. In this thesis, I will focus on the synthesis of nanoparticles protected by different stabilizers and characterize them with diverse methods. The catalytic activity of nanoparticles in solution and possible mechanisms for carbon-carbon coupling reaction and hydrogenation reactions over nanoparticle surfaces will also be studied.

1.2 Monolayer-Protected Metal Clusters (MPCs)

Since metal nanoparticles possess unique physical and chemical features compared to equivalent larger-scale materials [18], it is often necessary to stabilize or functionalize such nanoparticles for applications. One of the most common ways to do so is to attach suitable organic groups to the surface atoms. One class of stabilized nanoparticles are commonly known as monolayer-protected clusters (MPCs), in which discrete ligands pack as monolayers on the surface of particles, while alternatively polymeric stabilizers (or other stabilizers) which have multiple points of attachment can be used [35]. There are several advantages for modifying nanoparticles. First of all, surface modification can stabilize nanoparticles against aggregation and agglomeration, which enables them to remain stable during a catalytic reaction [39]. A second aspect for modifying nanoparticles is to render them compatible with different liquid media. For

example, water-soluble nanoparticles can be functionalized with appropriate hydrophilic stabilizing groups, while hydrophobic groups can allow solubility in organic solutions. This modification can avoid homogeneity and compatibility problems between two phases [40]. A third aspect is to enable self-organization of the modified nanoparticles. Functional groups on the surface of particles may allow deliberate interactions of the nanoparticles with molecules, other nanoparticles, surfaces or solids [41].

In this introduction the stabilization of nanoparticles will be discussed and general approaches of stabilizing the surface of nanoparticles by different methods will be outlined.

1.2.1 Traditional Capping Groups on Metal Nanoparticles

The use of polymer stabilizers is a general way to prevent the aggregation of nanoparticles by providing steric stabilization for metal nanoparticles through the steric bulk of their framework and by binding weakly to the nanoparticle surface through heteroatoms [42]. Particularly, poly(vinylpyrrolidone) (PVP) is one of the most used polymers for nanoparticle stabilization and catalysis because the relatively low cost of PVP and the ease of access to the surface of the nanoparticle in aqueous reactions [43]. In fact, PVP is the best polymer stabilizer in aqueous solution and PVP-stabilized nanoparticles have been used as catalysts for a variety of reactions [44]. However, some drawbacks of PVP-stabilized metal nanoparticles, such as agglomeration and even precipitation during or after catalytic reactions and the problematic separation of the

catalytic nanoparticles from the polymer, limit the wide use of PVP stabilizers [45].

MPCs have been widely studied and reported in recent years due to the variety of effective ligands which can allow for the prevention from aggregation and for the resulting particles to be easily recycled and reused after catalytic reaction, as well as being compatible with organic solutions. Traditionally, noble metal nanoparticles can be stabilized by thiols [46, 47], disulfides [48], amines [40, 49], nitriles, carboxylic acids and phosphines [50, 51]. Selected examples of each will be provided in the following sections.

1.2.1.1 Thiols and Disulfides

The number of direct syntheses of thiol-stabilized nanoparticles has expanded in recent years since Brust and Schiffrin reported the preparation of dodecanethiol-stabilized MPCs in 1994 [40]. The Brust-Schiffrin synthesis provides ready access to functionalized nanomaterials with properties analogous to those of large molecules, as they are stable under ambient conditions and can exist in solvent-free forms. Because organosulfur groups are able to strongly coordinate to various metals, numerous metal nanoparticles, such as Ag, Cu, Pt, Fe, or Au [47, 52-54] and alloys [55] have been prepared in this way. Sulfur possesses a huge affinity for metal surfaces, and organosulfur compounds thus will adsorb spontaneously [56]. The metal-sulfur interaction is strong enough to immobilize the thiol groups on the surface of metal nanoparticles. For example, the chemisorption energy between gold and sulfur is estimated at 126 kJ /mol [57].

The exact nature of the metal-sulfur interaction was not completely resolved in most cases. It was found by elemental analysis and theoretical calculations that approximately two gold atoms are required on the surface per thiol [57]. In the special case of aromatic thiols it was shown that the thiol head group can occupy various adsorption sites on the metal surface, with very small energy differences. The difference consists in the additional electrostatic interaction between the aromatic ring and the surface, depending on the ring orientation relative to the gold surface [58]. Thiols can interact with metal nanoparticles in two different ways. The first possibility is the adsorption of the intact R-SH molecule on the surface [59]. The second possibility is chemisorption of thiols or disulfides on metal surfaces which generates thiolate (SR) groups [36]. Chemisorption of thiols on the metal surface typically occurs with breaking of the S–H bond. Spectroscopic and theoretical investigations of the interaction of chemisorbed methylthiolate with gold surfaces found there was no charge transfer between methylthiolate radicals and Au. Intact disulfides are not adsorbed as such, but are split in two thiolate moieties upon chemisorption [59]. Several groups have recently shown that the thiolate ligands adopt a bridging "staple" bonding mode rather than a terminal one by x-ray single-crystal crystallographic analysis [60]. For $[Au_{25}(SCH_2CH_2Ph)_{18}]^-TOA^+$ crystals, each of the exterior Au−Au pairs (six in total) is bridged by an −SR ligand and with two other −SR ligands bridging between the exterior Au atoms and the icosahedral Au_{13} core [60]. The bridging −SR ligands form an extended "staple" motif, where three sulfur and two gold atoms are arranged in a 'V-shaped'

−S−Au−S−Au−S− pattern (Figure 1.1), which binds to the icosahedral core through S−Au and Au−Au bonds. Similarly, a staple motif was seen in the crystal structure of $Au_{102}(SR)_{44}$ as well [61].

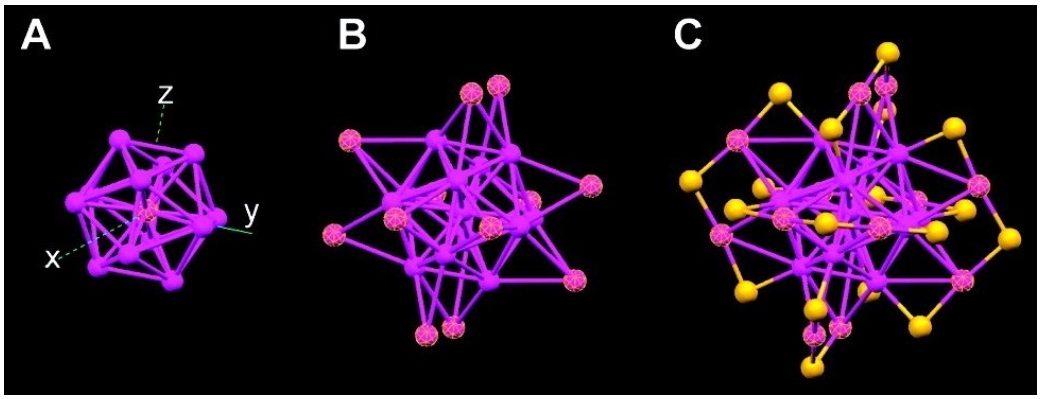

Figure 1.1 Anatomy of the Au-S framework of $[Au_{25}(SCH_2CH_2Ph)_{18}]^-TOA^+$. Only Au and S atoms are shown. Reprinted with permission from [60]. Copyright 2008 American Chemical Society

1.2.1.2 Amines and Ammonium Ions

Modification of metal nanoparticles by adsorbing alkylamines onto their surfaces is another way to stabilize particles. For example, coverage of Pd nanoparticles by hexadecylamine leads to a better dispersion and stability of the particles provided that the hexadecylamine coverage is sufficient [50]. The main difference between modification by means of thiols and amines is the stability of the nanoparticles. The interaction between amine groups and metal nanoparticle surfaces is much weaker than that of thiolate groups, and thus amine-modified nanoparticles are typically much larger than their organosulfur-modified equivalents and free amines cannot be completely removed from

the system [49]. However, both groups can be used simultaneously, for example, peptides can be linked to silver nanoparticles through both thiol and amine functionalities [40].

A wide-spread method to stabilize noble metal nanoparticles is by adsorption of tetraalkylammonium halides, which are often used because of their amphiphilic properties. The stabilization of the metal nanoparticles is due to the attachment of $R_4N^+X^-$ ion pairs to the metal surface. The anion adsorption gives an anchoring point for the charge-balancing quaternary ammonium ions and the hydrocarbon chains provide further stabilization by dispersion forces [62]. Hydrophobic metal nanoparticles stabilized with functionalized long chain ammonium ions can be solubilized in aqueous solutions via formation of bilayers, which is useful for biological applications [63]. Meanwhile, ammonium ions with shorter chain lengths, such as 4–8 carbons, have also been used to stabilize transition metal nanoparticles synthesized electrochemically, and the obtained nanoparticles were perfectly size-controlled and monodisperse, ranging from 1.2 to 5 nm [64-66].

1.2.1.3 Carboxylic Acids

Infrared spectroscopy as well as theoretical calculations has revealed that metal surfaces can interact with negatively charged carboxylate groups, obtained by deprotonation of carboxylic acids. Moskovits and Suh studied the geometry and conformation of a number of the ions of monocarboxylic and dicarboxylic acids adsorbed on Ag colloid surfaces. The carboxylate group of monocarboxylic acids is responsible for

the surface stability, probably via chelation to silver surface sites. Similarly, the dicarboxylate acids bind through both carboxylate groups [67]. If more than one functionality exists within a ligand, multifunctional adsorption may occur on a metal nanoparticle surface [68]. Calculations have revealed a bi-functional attachment of N-isobutyryl-L-cysteine on gold nanoparticles through the thiol and carboxylate functions, and a tri-functional coordination of penicillamine with simultaneous interaction of the thiol, amine and carboxylate groups with the particle surface (structures shown in Figure 1.2) [69, 70]. The stability of the nanoparticles can be dramatically increased due to the multiple attachments [70]. FTIR studies of the interactions between these ligands and the surface indicated that the coordination of the carboxylic acid group is largely through carboxylate chemisorption, while the amine coordination occurs by interaction of RNH_3^+ with the surface [69].

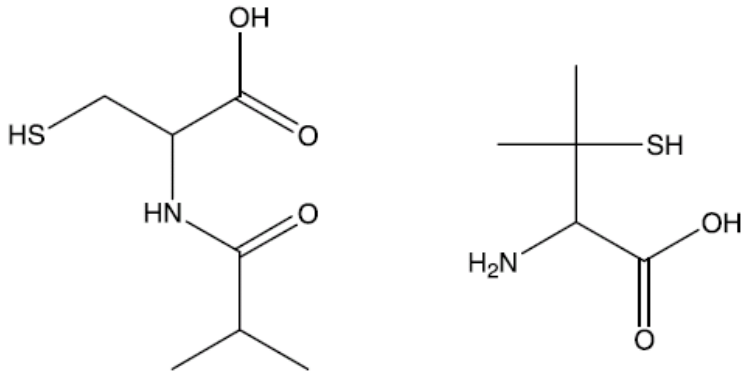

(a) (b)

Figure 1. 2 Structure of (a) N-isobutyryl-L-cysteine and (b) D-penicillamine [69, 70].

1.2.1.4 Phosphines

Hutchison and coworkers showed that gold nanoparticles can be protected by triphenylphosphine stabilizers[51]. The drawback of this method compared to the thiolate method is that phosphine interactions with the metal nanoparticle is weak and thus results in poor stability of the nanoparticles. However, the lack of stability can allow the exchange with other ligands, like thiolates, which are more strongly bonded to the metal surface [71]. The Brust method of nanoparticle synthesis is a valuable technique for preparing thiol-stabilized nanoparticles, where functional groups are limited only by the compatibility of thiols. However, the identification of a unique set of reaction conditions is often required for the preparation of each functionalized target, and it is often difficult to access smaller MPCs by this route. The approach of producing a nanoparticle precursor having a temporary stabilizing ligand shell, amenable to ligand exchange reactions with an incoming molecule that has the desired chemical functionality is quite attractive, and phosphine-stabilized nanoparticles have been a good option [51]. A very noticeable feature of such phosphine exchange reactions is that, contrary to the thiol–thiol exchanges, every phosphine ligand is exchanged. The exchange of phosphine ligands by thiol ligands is accompanied by a higher stability of the resulting nanoparticles. The lack of stability of phosphine ligands can be overcome by the use of polyphosphine ligands. For example, palladium nanoparticles were stabilized with di- or tri-phosphines, such as bis-(diphenylphosphino)decane or bis-(diphenylphosphinoethyl)phenylphosphine [50].

1.2.2 MPC Synthesis

The direct preparation of ligand-stabilized nanoparticles provides a simple route to functionalized materials, usually in a single step, one-pot procedure, imparting stability and chemical functionality to the nanoparticle products [46, 47]. Since alkanethiolate MPCs have been studied widely, we will mainly focus on the discussion of metal MPCs coated with alkanethiolate monolayers. Thiolate-stabilized nanoparticles can be prepared by the Brust-Schiffrin reaction. This reaction was first developed within a biphasic context, taking advantage of phase transfer compounds such as tetraoctylammonium bromide (TOAB) to shuttle ionic reagents to an organic phase where particle nucleation, growth, and passivation occur [35]. In the original Brust-Schiffrin reaction, the addition of dodecanethiol to $TOA^{+}AuCl_4^{-}$ in an organic phase (1:1 mole:mole) followed by reduction with $NaBH_4$ leads to dodecanethiolate-protected Au nanoparticles having a 1-3 nm range of core diameters. A single phase adaptation of the Brust-Schiffrin method of nanoparticle synthesis was developed by the desire to eliminate issues posed by the use of phase transfer reagents, including cytotoxicity and the potential for persistent contamination [72]. For example, in 1999, Murray *et al.* reported water soluble nanoparticles with an average diameter of 1.8 nm synthesized in the aqueous phase in which $HAuCl_4$ was reduced by $NaBH_4$ in the presence of tiopronin (N-2-mercaptopropionylglycine) [72].

The details of MPC synthesis reactions are not been completely understood;

however, they can be described in terms of two processes competing with each other. The first process is the growth of the particles leading to a reduction of the total surface area. At some point, coordination of the ligands to the surface atoms of the nanoparticles becomes more favorable and stops further growth. Usually, larger thiol:gold mole ratios give smaller average MPCs core sizes [57] and fast reductant addition and cooled solutions produce smaller, more monodisperse MPCs [73]. When the reaction is quenched immediately, it produces higher abundances of very small core sizes (≤2 nm) [36, 74, 75].

Subsequent variations of this procedure demonstrated the full scope of this reaction, substituting a wide range of alkanethiols (C_3-C_{24}), ω-functionalized alkanethiols, and dialkyl disulfides and varying the ratio of reagents in order to control the average diameter of the products. This basic protocol can give access to nanoparticles protected by a range of alkanethiolates, some of which are listed in Figure 1.3 [47, 68, 72, 76-79]. The Brust-Schiffrin reaction tolerates considerable modification in regard to the protecting ligand structures, and smaller metal core sizes can be synthesized based on the ligand chosen. The cone angle of the ligand is one of the major factors to influence the metal core size when alkanethiol coverage on the metal substrate is limited [80].

The metal core of MPCs can also be varied and reports of MPCs with different metals, as well as alloy cores have appeared. Hostetler *et al.* synthesized nanometer-sized monolayer-protected alloy clusters (MPACs) with Au/Ag, Au/Cu, Au/Ag/Cu, Au/Pt, Au/Pd, and Au/Ag/Cu/Pd as alloy cores. MPACs, like their MPC counterparts, are

generally air- and solvent-stable and obtained in high yield. The MPACs were found to be generally more thermally stable than their corresponding mono-metallic MPCs, and the presence and proportion of certain metals was found to enhance stability (Ag) or instability (Cu) [55].

1)

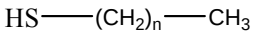

2)

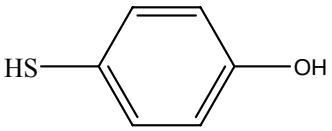

3)

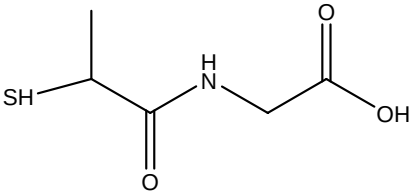

4)

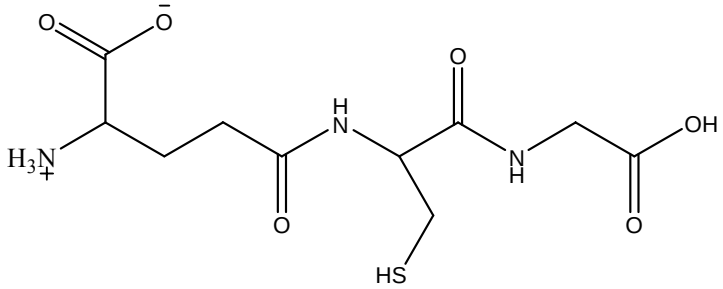

5)

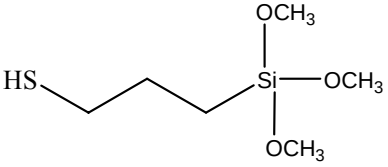

6)

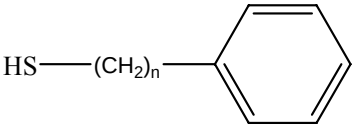

7)

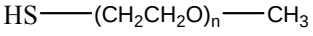

Figure 1.3 Examples of thiol ligands used to prepare Au MPCs. 1) Straight-chain alkanethiols [47] 2) p-mercaptophenol [68] 3) tiopronin [72] 4) glutathione [76] 5) (γ-mercaptopropyl)trimethoxysilane [79] 6) phenyl alkanethiols [78] 7) thiolated

poly(ethylene glycol) [77].

1.2.3 Characterization of MPCs

The excellent handling properties of metal MPCs, *i.e.* the ability to remove them from solution, remove impurities by washing and re-disperse the MPCs in solution, make structural and compositional analysis of MPCs quite simple. Analytical information about both the central core and the surrounding monolayer can be obtained, which enables a more complete understanding of the nanoparticle chemistry for applications.

Knowing how to control the dispersity of core size is quite important and the core dimensions of MPCs have been measured with many methods. Some of these techniques give substantial information about the core size, such as scanning tunneling microscopy (STM), x-ray diffraction (XRD), while other methods such as atomic force microscopy (AFM), laser desorption-ionization mass spectrometry (LDI-MS), light scattering and small-angle x-ray scattering (SAXS) can be used for measurement of the whole particle (core+ligand) size. The oxidation state and electronic interactions can be measured by x-ray photoelectron spectroscopy (XPS). For the determination of bimetallic structures and compositions, EXAFS and energy dispersive x-ray spectroscopy (EDS, an x-ray fluorescence technique) are the most commonly used methods.

Figure 1.4 illustrates the use of LDI-MS to track the solubility-fractionation of dodecanethioate MPC core sizes, conducted in concert with theoretical modeling to predict the core size and shape of isolated fractions [59]. The number of atoms per core

tends toward closed shell structures with an equilibrium truncated octahedral shape. However, MS is less useful when analyzing water-soluble MPCs with highly polar ligands because of difficulty of isolation of metal MPCs from water. Schaaff [76] and Templeton [72] have resolved this problem by gel and capillary electrophoresis and fractions collected using gel electrophoresis were examined via MALDI-MS.

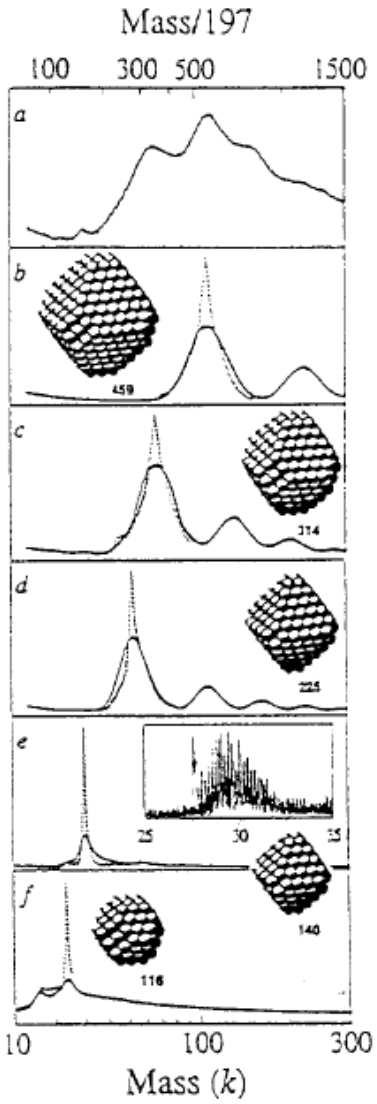

Figure 1.4 Mass spectra (abundance vs. mass, in k=103amu, and in mass equivalent number N of gold atoms, mAu= 197 amu) for (a) a crude dodecanethiolate MPC mixture,

(b-e) fractionated MPCs, and (f) a mixture of the two lightest fractions. Higher mass peaks in traces d and e are gas-phase, trimers, etc. Inset structures are predicted optimal core structures, and the inset in trace e is a high resolution mass spectrum plotted on a linear mass scale with an arrow marking the first peak at 27609 (2 amu). Reprinted with permission from [73]. Copyright 1996 Wiley-VCH Publishing.

Organic shells of MPC monolayers have also been examined with multiple techniques, including infrared spectroscopy (IR), nuclear magnetic resonance (NMR), and differential scanning calorimetry (DSC) and data can be obtained based on polydisperse MPCs. The fractional amounts of C, H, and S found in the elemental analysis has shown that the ligands on MPCs are consistent with intact RS- ligands [81]. Luedtke and Landman found that the packing arrangements and densities of the monolayers passivating the facets of the core Au nanocrystallites exhibit organization into molecular bundles of preferred orientations which upon heating undergo a reversible melting transition from the ordered bundled state to a uniform intermolecular orientation distribution [82]. The passivating monolayers are mainly formed on the (111) and (100) facets of the Au nanocrystallites (Figure 1.5). By applying thermogravimetric and core size analyses, the average number of ligands per core can be estimated [82]. 50% (ligand:surface Au atom) or greater coverages of MPC ligands are observed, which are larger than the 33% coverages characteristic of 2D-SAMs on Au (111) terraces; theoretical calculations indicate that such high coverage results from larger ligand:Au

binding ratios on core edges and vertexes [83].

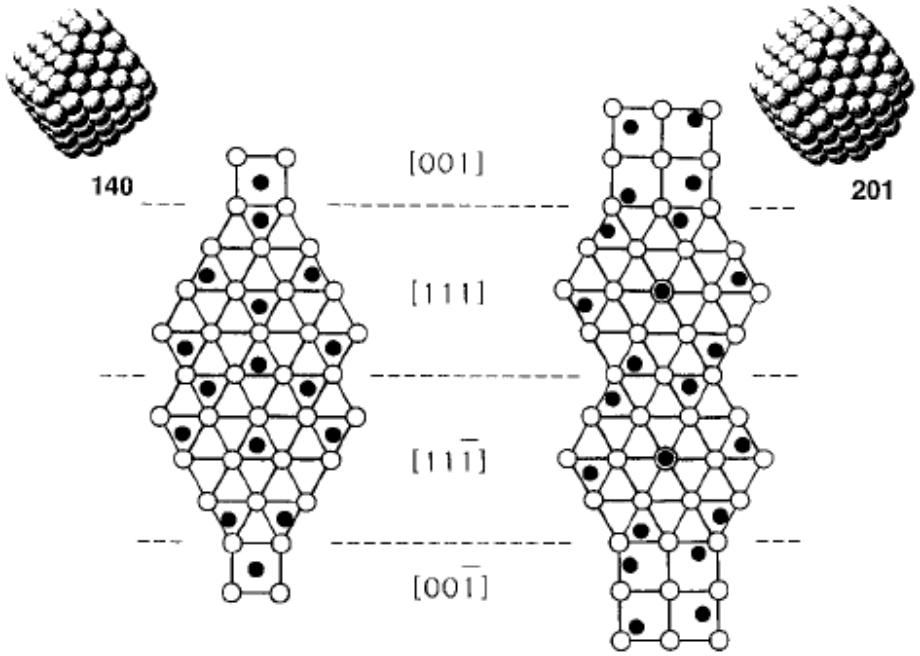

Figure 1.5 Arrangement of the thiols (filled circles) on the facets (gold atoms shown as open circles) of the equilibrium structures of isolated Au_{140} and Au_{201} crystallites, at left and right, respectively. Reprinted with permission from [82], Copyright 1996 American Chemical Society

NMR spectroscopy is a particularly useful technique to get information about the structure and content of MPC monolayers. ^{1}H and ^{13}C NMR resonances of MPC monolayers are characteristically broadened relative to those of free alkanethiols. The factors of broadened peaks include spin-spin relaxation (T2) broadening, a distribution in chemical shifts due to differences in Au-SR binding sites, and a gradient in monolayer

packing density from near-core to chain terminus with associated dipolar broadening [36, 47]. Figure 1.6 illustrates the broadening of ^{1}H NMR resonances of dodecanethiolate MPCs with increased core size, from top to bottom[36]. The methyl resonance (δ=0.9) is thought to exhibit primarily T2 broadening. Another broad resonance at 1.4 ppm corresponds to protons on methylene chain, which become broadened with an increased size of nanoparticles.

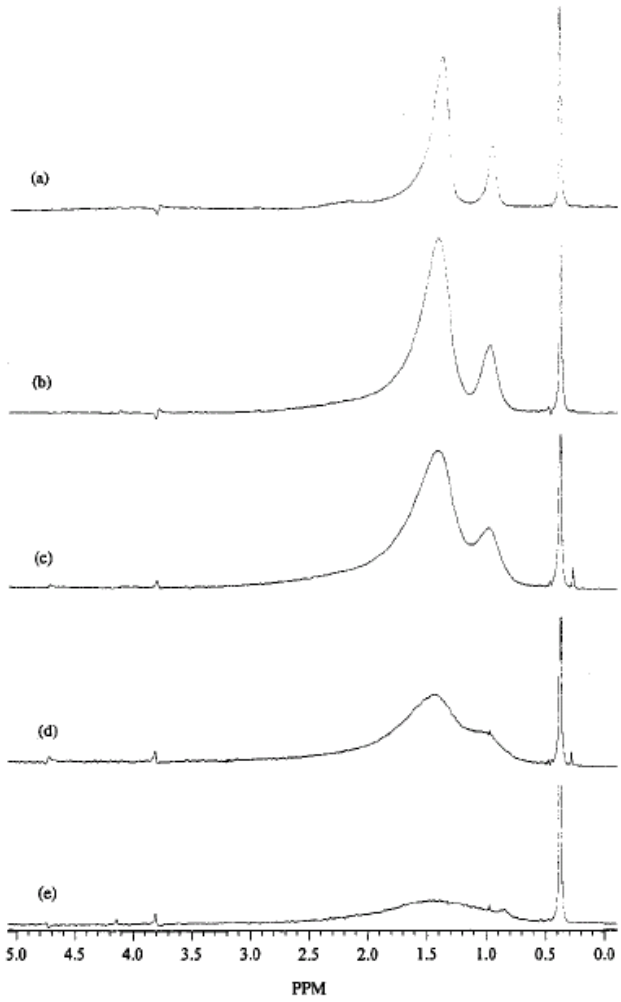

Figure 1.6 The ^{1}H NMR spectra (C_6D_6) of dodecanethiolate – protected Au clusters. (a) 0.76 nm (b) 0.96 nm (c) 1.5 nm (d) 2.2 nm (e) 2.6 nm. The peak at 0.4 ppm comes from a

solvent impurity. Reprinted with permission from [36], Copyright 1998 American Chemical Society.

1.2.4 Functionalization of MPCs

Synthesizing MPCs via the Brust-Schiffrin method can provide a direct route toward functionalized MPCs that provide the desired surface chemistry if the functional group does not react with $NaBH_4$ or show strong affinity for the surface of metal nanoparticles [84]. In situations where functional groups need to be added post MPC synthesis, many groups have found they can functionalize the surface of nanoparticles through surface modification. Surface modification methods can be categorized into two major classes as shown in Scheme 1.1 [84]: post-synthetic modification of the existing ligand shell, involving simple transformations of pendant functionalities or grafting, and ligand exchange, where an existing ligand shell is displaced by a different incoming ligand.

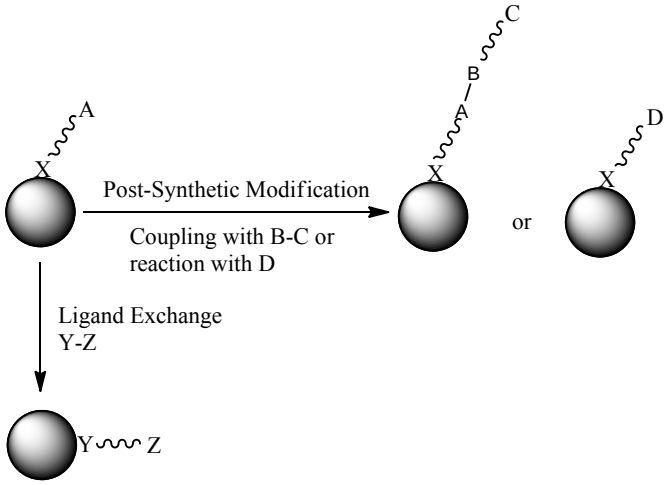

Scheme 1.1 Strategies for nanoparticle functionalization [84].

Post-synthetic modification methods allows for the introduction of a new chemical functionality to the surface of the MPCs which have been directly synthesized and stable enough to undergo secondary reactions. The success of such transformations relies on the stability and tolerance of nanoparticles themselves and also the steric environment of functional groups on the nanoparticle surface. Modification reactions include polymerizations [85-87], coupling reactions [88, 89], or transformation of an existing chemical moiety [90-92] and amino, carboxylate, bromo-, and iodo- terminal groups are commonly used as functional groups on the MPC surface. When considering the efficiency of post-synthetic modification, several factors, such as the length of the ligand composing the stabilizing shell, the spatial density of groups, and the bulk of the incoming nucleophile, can impact the results [93]. One major problem of post-synthetic modification methods is the characterization of the final MPCs, as it can be hard to assess the extent of modification.

Ligand exchange methods are a hybrid technique, as they require the direct synthesis of a versatile precursor MPC stabilized by a labile ligand shell. Then the original ligand shell is partially or fully displaced by another ligand in a ligand exchange step, thus introducing the desired chemical functionality to the surface of the MPC. Basically, the incoming ligand used in the exchange reaction has equal or greater affinity for the metal surface than the ligand composing the original stabilization shell for the MPC. Thus, one may start from a product that is stabilized by weakly coordinating ligands, such as organic acids (citrate, ascorbate, tannic acid) and surfactants, or more

robust ligand such as phosphines, amines, or thiols [71]. Usually, phosphines are the most versatile and well studied original protecting shell in favor of incoming ligands when applying ligand exchange reactions [94, 95]. Ligand exchange reactions can be carried out under a range of solution conditions that can be tailored to achieve the desired product, including aqueous, organic, and biphasic conditions. Several different ligand exchange examples with a variety of stabilizing ligand shells are illustrated below.

For the phosphine-to-phosphine exchange method, the functionalization of triphenylphosphine-stabilized gold clusters by the introduction of ω-functionalized aminophosphine ligands such as $Ph_2PC_6H_4SO_3$ to produce water soluble nanoparticles has been shown [96]. However, this method is limited by the instability of the phosphine-stabilized clusters and the inability to perform complete ligand exchanges. Thiol-to-thiol exchanges, because thiolate ligands have almost the same affinity to the surface of particles, often yield products with mixed ligand shells. Usually, exchange is initiated at the metal atoms that form the vertices and edges of a nanoparticle surface. The exchanged species then diffuse toward the terraced regions of the surface, eventually leading to an equilibrium state [41, 93, 97]. It is generally believed that the chain length and steric bulk of an incoming ligand are major factors which impact exchange rates, with smaller, simpler ligands exchanging most rapidly. Phosphine-to-thiol exchange can be the most versatile type of exchange reaction, since it is capable of producing homogenously mono-substituted nanoparticles bearing a wide variety of terminal functional groups. The exchange reaction can be carried out in a single organic phase to

introduce organic soluble thiols [94, 98, 99] or in a biphasic manner, using water soluble thiols to convert the hydrophobic precursor particles to water soluble materials without disrupting the original size of the gold core [94, 100]. Phosphine-to-amine exchange reactions can also undergo the displacement of phosphine ligands in a single phase [101]. One unique aspect of this reaction is that the size of the gold cores may become larger as the reaction progresses, transforming 1.4 nm triphenylphosphine-stabilized particles to larger monodisperse amine-stabilized particles, ranging in size from the original 1.4 nm up to 8 nm, depending on the exchange conditions [98, 101].

1.2.5 Catalysis with MPCs

The modification of metal and semiconductor nanoparticles with organic monolayers is attractive for the development of catalysts. MPCs were not thought to be catalytically active because the organic ligands can act as stabilizer of nanoparticles and the same time, inhibit the catalytic activity of metal nanoparticles, due to strong bonding between the capping ligands group and the metal nanoparticle surface [102]. The possible catalytic activity of MPCs can be extrapolated on the basis of comparisons with two-dimensional self-assembled monolayers (2D-SAMs) on metal surfaces and an assumed complete coverage of the MPCs by the ligands. The metal centers of MPCs do not consist of perfect two-dimensional surfaces with perfect faces, as significant edges and vertexes exist, resulting in a more exposed metal core [36, 103]. Hostetler and co-workers showed that for Au MPCs the thiol coverage for a three-dimensional

monolayer is only a percentage of that for a complete 2D-SAM. Also unlike 2D-SAMs, where the terminal ends of the thiol chains are tightly packed and block access to the metal surface, the high radius of curvature of MPCs causes the thiol chain density to decrease away from the metal core down the length of the thiol chains [103]. It is possible that this feature leaves open space between the MPC thiol chains that can allow the presence of unsaturated surface sites between the MPC ligands which can be accessed by small substrates. As such, metal MPCs may possess moderate catalytic activity.

Many groups have applied MPCs for different catalytic reactions for which they have interest. Shestakov revealed that gold nanoparticles stabilized by a 1-dodecanethiol monolayer can oxidize methane in a methylene chloride medium, presumably by an active oxygen species formed at the surface of the nanoparticles during their synthesis, to yield methanol (in stoichiometric amounts), ethane, and an unidentified product [104]. The only product of methane activation in toluene was ethylene. The same nanoparticles catalyzed the oxidation of cyclohexene by molecular oxygen to produce allyl hydroperoxide (11%), alkylhydroperoxide (84%), and allyl ketone (5%), with toluene inhibiting this reaction. These results obtained on the oxidation of hydrocarbons suggest that, in the presence of gold nanoparticles, oxygen can form active surface species on MPC surfaces.

In the case of hydrogenation reactions, many groups have examined the use of metal MPCs as catalysts. Cliffel and Eklund have reported that Pt MPCs with SC_6, SC_{12}, tiopronin, glutathione and mercaptoammonium as ligands, can be used as catalysts to

hydrogenate allyl alcohol to n-propanol [102]. Mercaptoammonium-stabilized Pt MPCs were also used as catalysts in the hydrogenation of maleic acid to succinic acid [102]. They found the rates of catalysis were higher for monosubstituted allyl alcohol compared to disubstituted maleic acid, and the rate of catalysis of allyl alcohol for mercaptoammonium-stabilized Pt MPCs is 4 times that of succinic acid using the same catalyst. It was postulated that this effect was caused by steric hindrance of the slightly larger maleic acid molecule by the thiol monolayer or from interactions between the negatively charged carboxylate groups on the substrates and the ammonium groups on the Pt-MA^+ MPC. Changes in solvents and the size of the Pt MPCs also led to differences in the catalytic hydrogenation rates among the various monolayer coatings for MPCs [102].

Alvarez and Kaifer tested the hydrogenation reaction of allylamine by Pt and Pd nanoparticles modified with thiolated β-cyclodextrin. The structure of HS-β-CD is shown in Figure 1.7 [105].

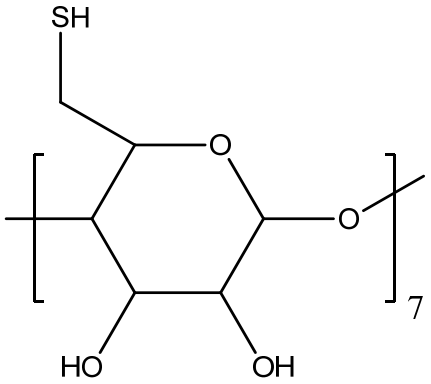

Figure 1.7 Structure of thiolated -β-cyclodextrin [105].

From TEM measurements, they found the average diameters were 14.1 ± 2.2 and 15.6 ± 1.3 nm for the Pt and Pd particles, respectively. Under the surveyed reaction conditions, both CD-modified Pt and Pd MPCs catalyzed the hydrogenation of allylamine to propylamine [105]. In a set of experiments, using 10 mg of each catalyst and 6 h reaction time, the surface modified Pt and Pd MPCs achieved full conversion. In a second series of experiments, using 5 mg of each catalyst and a shorter reaction time of 1 h, the CD-modified Pd nanoparticles were more efficient than the CD-modified Pt nanoparticles. It should note here that both types of CD-modified metal nanoparticles were soluble in the reaction medium and could be easily recovered at the end of the reaction by precipitation with ethanol. Similarly, Denicourt-Nowicki studied various catalytic reactions such as hydrogenations and cross-coupling reactions by using cyclodextrin-stabilized metal nanoparticles with good yields and selectivities according to the relevant choice of the cyclodextrin [106].

Jin's group recently studied the catalytic activity of $Au_{25}(SR)_{18}$, $Au_{38}(SR)_{24}$, and $Au_{144}(SR)_{60}$ MPCs, which are 1 nm, 1.3 nm, and 1.6 nm in diameter, for selective oxidation and hydrogenation processes [107]. They chose selective oxidation of styrene by O_2 to test the utility of the MPCs as an oxidation catalyst. They found the catalytic properties of the MPC are mainly determined by the metal core rather than by the ligand shell. Smaller MPCs give rise to a much higher catalytic activity, while the selectivity is not significantly changed. Larger sizes of Au MPCs (~3nm in diameter) showed a much-lower conversion activity and the ligands did not affect the catalytic activity and

product selectivity. They attribute the enhanced catalytic activities in smaller $Au_n(SR)_m$ nanoparticles to the electronic properties of small $Au_n(SR)_m$ nanoparticles rather than the higher surface area of smaller nanoparticles. Other important factors that may contribute to the high activity include the low coordination numbers of surface Au atoms and the high curvatures of small nanoparticles, which should facilitate adsorption and activation of reactant molecules as well. Meanwhile, Au MPCs were capable of hydrogenating benzalacetone with remarkable chemoselectivity toward the formation of the unsaturated alcohol, whereas only small amounts of unsaturated ketones and saturated alcohols were seen at 60^oC [107].

Murakami and coworkers have demonstrated the use of dodecanethiolate-stabilized Au MPCs as the co-catalyst towards the enhanced activity of a Mn porphyrin catalyst for styrene oxidation with iodosylbenzene [108]. The unique ability of the MPCs is to regenerate the active catalyst from catalytically ineffective Mn(IV) species to Mn(V). They found the surface dodecyl groups of dodecanethiol-stabilized Au MPCs could be oxidized into aldehydes (dodecanal) by the reaction with PhIO and are eliminated from the nanoparticle surface. However, no severe aggregation was observed, which means some dodecanethiolate ligands are remaining. They suggest the partial oxidation of dodecyl groups due to the thiolate reactivity varies with the attached gold sites on the nanoparticle surface (edge, vertex, etc.). One possible mechanism of catalyst reactivation on the gold surface is illustrated in Scheme 1.2.

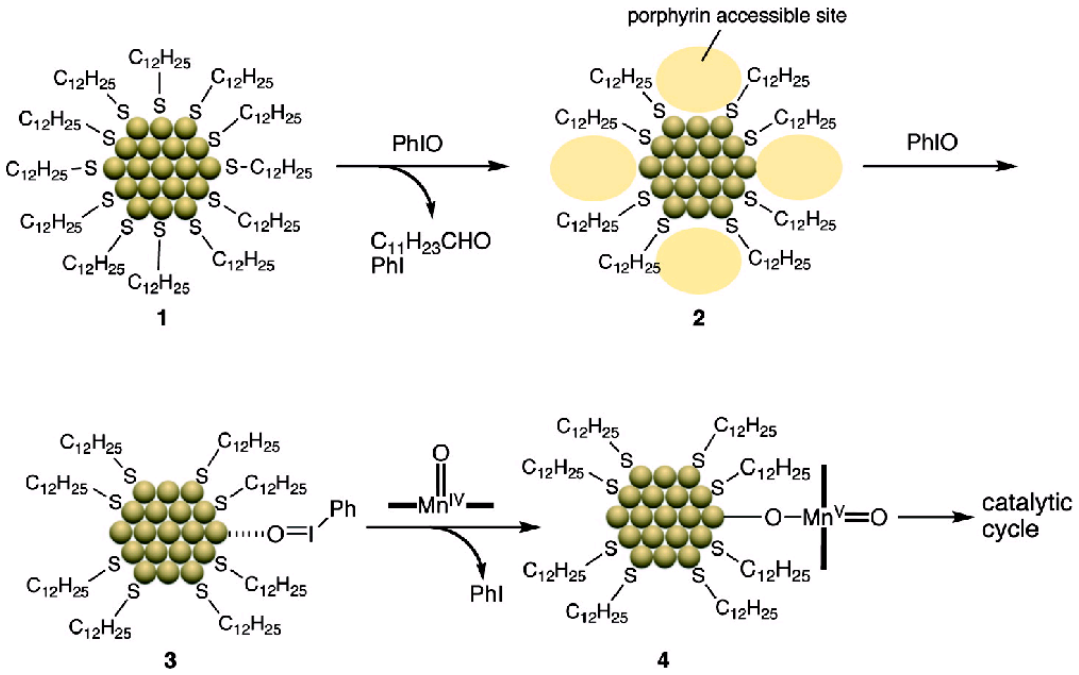

Scheme 1.2 Schematic illustration of a possible catalytic mechanism in the Au:SC_{12}/Mn(TPP)Cl System. (Reprinted with permission from [108]. Copyright (2007) American Chemical Society).

Li and Choi reported the synthesis of palladium nanoparticles using n-alkylamines (C_n-NH_2) as stabilizing ligands [109]. Electrochemical reactions between CH_4 and C_n-NH_2-Pd MPCs on Pd electrodes were studied by cyclic voltammetry and chronoamperometry [109]. The electrocatalytic activity to CH_4 oxidation was correlated to the particle size of the MPC which can be tuned by varying the mole ratio of $PdCl_2$/ligand and changing the n-alkyl chain length of C_n-NH_2. It was determined that Pd MPCs synthesized from 1:7 $PdCl_2$/C_{18}-NH_2 ratios displayed the most active and stable response to CH_4 as compared to bare Pd and other Pd MPC modified Pd electrodes. The

C_{18}-NH_2-Pd MPC (5.6 nm) modified electrode could be used repeatedly and had a stable and reproducible response to CH_4. They elucidated that CH_4 on the Pd MPCs is oxidized to CH_3OH first and then to HCHO by electrogenerated PdO/PdO_2 [109].

In our group, catalysis reactions with thiolated nanoparticles also have been examined. Dasog and Hou examined the catalytic activity of 1-dodecanethiolate-, dithiolate-, and 1:1 mixed 1-dodecanethiolate/dithiolate-protected Au MPCs for the reduction of 4-nitrophenol by $NaBH_4$ to 4-aminophenol. The reaction is shown in Scheme 1.3 below:

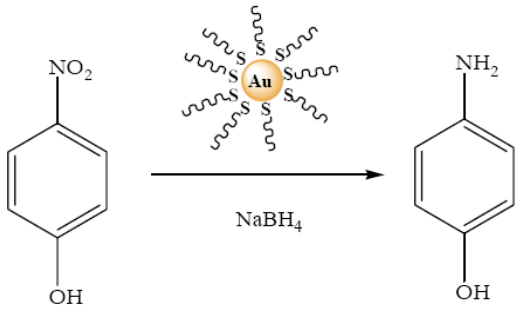

Scheme 1.3 Reduction of 4- nitrophenol to 4-aminophenol by Au MPCs.

They found the reduction rate was pseudo first order with regard to 4-nitrophenol when plotting UV-Vis absorption changes at 400 nm (due to 4-nitrophenol) vs. time. All three Au MPC samples had a high catalytic activity for the reduction of 4-nitrophenol, despite major differences in their surface accessibility. The rate decreases drastically with decrease in the concentration of Au and the particles seem to be stabilized by the aminophenol product during the reaction [110]. They further examined the effect of ligand length on different substrates and found the rate decreases with increasing ligand

length, and that more sterically crowded substrates, such as 2- and 3-nitrophenol and Eosin B, showed negligible reactivity.

Metal MPCs have also been used for carbon-carbon coupling reactions with high catalytic activity. Gopidas and Fox synthesized a palladium-nanoparticle-cored G-3 dendrimer having approximately 300 Pd atoms in the metallic core and an average diameter of 2.0 nm, to which were attached an average of fourteen G-3 dendrons [111]. The synthesis process is shown below in Scheme 1.4.

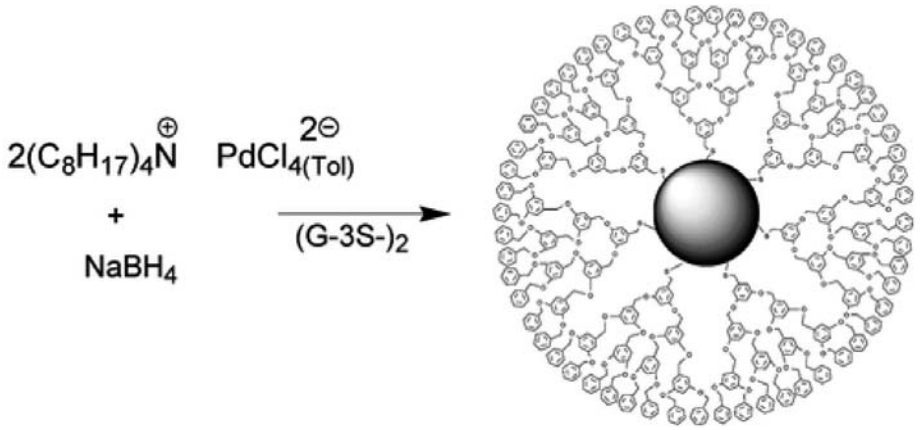

Scheme 1.4 Synthesis of Pd-G-3, in which seven of the fourteen G-3 wedges are shown. Reprinted with permission from [111]. Copyright (2003) American Chemical Society.

They found nearly 90% of the metal nanoparticle surface is unpassivated and available for catalysis. The dendrons could inhibit metal agglomeration without adversely affecting chemical reactivity. Thus, the Pd-G-3 MPCs efficiently catalyzed Heck and Suzuki reactions, with iodobenzene and bromobenzene as substrates and achieved decent

yields. Meanwhile, separation of the reactants and products from the catalyst was quite easy, and the Pd-G-3 recovered from the reactions was freely soluble in CH_2Cl_2, indicating that the Pd core had not agglomerated under the reaction conditions [111]. They also found the Pd-G-3 cannot be employed as a catalyst for hydrogenation reactions because the Pd metal gradually precipitated upon stirring for 3−4 h. It is likely the metal−sulfur bonds in Pd-G-3 undergo reduction under these conditions, leading to loss of the dendritic cap from the nanoparticles and metal precipitation.

Strimbu and Kaifer synthesized perthiolated cyclodextrin-capped Pd MPCs with average 3.5 nm diameter, which demonstrated effective catalytic activity for Suzuki cross-coupling reactions between aryl halides and phenylboronic acid [112]. They also found experimental conditions in which the sluggish reaction between iodoferrocene and phenylboronic acid was improved by the use of CD-capped Pd nanoparticles compared to the same reaction homogeneously catalyzed by homogeneous Pd molecular compounds. Their findings suggest that the binding of substrate to the CD cavities on the Pd nanoparticle surfaces plays a beneficial role in the overall catalytic efficiency.

1.3 Metal Nanoparticles Protected via Metal – Carbon Bonds

Metal nanoparticles with an organic functional shell have attracted much interest due to their applications as catalysts. Beyond providing solubility and preventing aggregation, the organic shell can also induce selectivity in catalytic reactions and compatibility in physiological systems as well [46]. As mentioned earlier, many different

organic ligands such as alkanethiols and phosphines have been used extensively as the ligands of choice to stabilize metal nanoparticles by taking advantage of the affinity of the organic groups for transition metal surfaces [42, 46, 106]. In order to synthesize metal and alloy nanoparticles with strong stabilizing ligands, which are less reliant on the chemisorptions of ligands containing soft atoms (S, N or P), a general and alternative synthetic approach needed to be developed. Recently, transition-metal nanoparticles protected by carbon-metal capping groups have also been reported. Metal–carbon covalent linkages should be strong enough to stabilize nanosized Pd particles because the bonding energy for a Pd–C single bond is 436 kJ mol^{-1}, which is even larger than that of the Pd–S linkage (380 kJ mol^{-1}) [113]. Thus, fundamentally, it will be of great interest to examine the effect of the metal–carbon ligand bonding interactions on nanoparticles stability.

Schiffrin's group first reported a simple and efficient method for the preparation of MPCs stabilized by metal-carbon bond formation [114]. They prepared Au and Pt nanoparticles by simultaneously reducing 4-diazoniumdecylbenzene tetrafluoroborate and hydrogen tetrachloroaurate or hydrogen hexachloroplatinate with $NaBH_4$. There is no phase transfer reagent required because the hydrophobic diazonium salt cation acts as the phase transfer reagent, as shown in Equation 1.1 below:

$$AuCl_4^- (aq) + RPhN{\equiv}N^+ (tol) \rightarrow AuCl_4^-N_2Ar^+ (tol) \qquad (1.1)$$

The individual reduction reactions taking place can be described by Equations 1.2-1.4 below:

$$n\ Au(III)\ (tol) \rightarrow Au_n\ (tol) \quad (1.2)$$

$$m\ RPhN{\equiv}N^{+}\ (tol) \rightarrow m\ RPh \bullet\ (tol) + N_2\ (g) \quad (1.3)$$

$$Au_n\ (tol) + m\ RPh \bullet\ \ (tol) \rightarrow Au_nAr_m\ (tol) \quad (1.4)$$

The TEM images of the decylphenyl-stabilized Au and Pt MPCs showed that an average particle size of 8.1 ± 0.8 nm for Au and 3 ± 1 nm for Pt was obtained. The length of the fully extended capping ligand was estimated at 1.6 nm for the Au nanoparticles, and based on the particle-particle distance in TEM some degree of interdigitation between the capping molecules must take place. FTIR spectra of the nanoparticles showed the complete removal of the diazonium group on reduction based on the lack of diazonium and aromatic C-N bands. The ^{13}C and ^{1}H NMR spectra of nanoparticles showed the aliphatic hydrogen similar to those of the free ligand and a broadening of the NMR peaks for atoms close to the nanoparticle core center and two very broad peaks in the aromatic region which provided strong evidence that the decylphenyl ligand is indeed chemically bonded to the metal core at the para position [114].

Recently, Ghosh and Chen successfully prepared stable palladium nanoparticles by functionalization with palladium–carbon covalent linkages through the reduction of diazonium derivatives and studied their electronic conductivity [113]. They found that Pd nanoparticles stabilized with decylphenyl and biphenyl ligands exhibit good stability and solubility in apolar solvents, however, ethylphenyl-protected Pd particles gradually lost

their solubility in solvents when exposed to air for an extended period of time. The core size was 3.6 ± 0.8 nm for decylphenyl-stabilized Pd MPCs and 3.1 ± 0.6 nm for biphenyl-stabilized Pd MPCs, which are comparable to that of the platinum nanoparticles synthesized under similar conditions, but substantially smaller than that of the gold counterparts (*ca.* 8 nm). They ascribed the larger Au core sizes to weaker Au–C bond as compared to Pt–C and Pd–C counterparts, as the metal–ligand bond strength largely dictates the passivation of the core during particle growth [115]. FTIR results showed that the samples are free of excess diazonium ligands and ^{1}H NMR spectra demonstrated the ligands are likely bound onto the Pd particle surface, as only the peaks for the methyl and methylene protons were seen and were substantially broadened for decylphenyl-stabilized Pd MPCs as compared to their counterparts in the free ligands. Chen's group also successfully synthesized biphenyl-stabilized Ti MPCs by reducing $TiCl_4$ and biphenyldiazonium salt under N_2 using a similar protocol [116]. The average core diameter was 2.3±0.6 nm, and characterization by ^{1}H NMR and FTIR, further supported the notion that the particles were passivated by metal–ligand covalent bonds [116].

Kumar and Gopidas applied a similar method to synthesize Au nanoparticles stabilized by dendritic ligands from $HAuCl_4$ and dendrons with a diazonium group at the focal point. The particles were formed by reducing both species simultaneously with $NaBH_4$ as shown in Figure 1.8 [117]. The dendron-stabilized MPCs consisted of a gold core of approximately 4.7 to 5.5 nm in diameter. The AuG_n dendrimers were quite stable in solution and did not oxidize after bubbling oxygen through the solution for 4 h. By

comparing the TEM and TGA data, they found the number of dendrons attached on the surface of Au nanoparticles is much larger than reported previously for thiolate-based nanoparticles, which was attributed to multiple layering of dendrons on the surface of the metal nanoparticles [117].

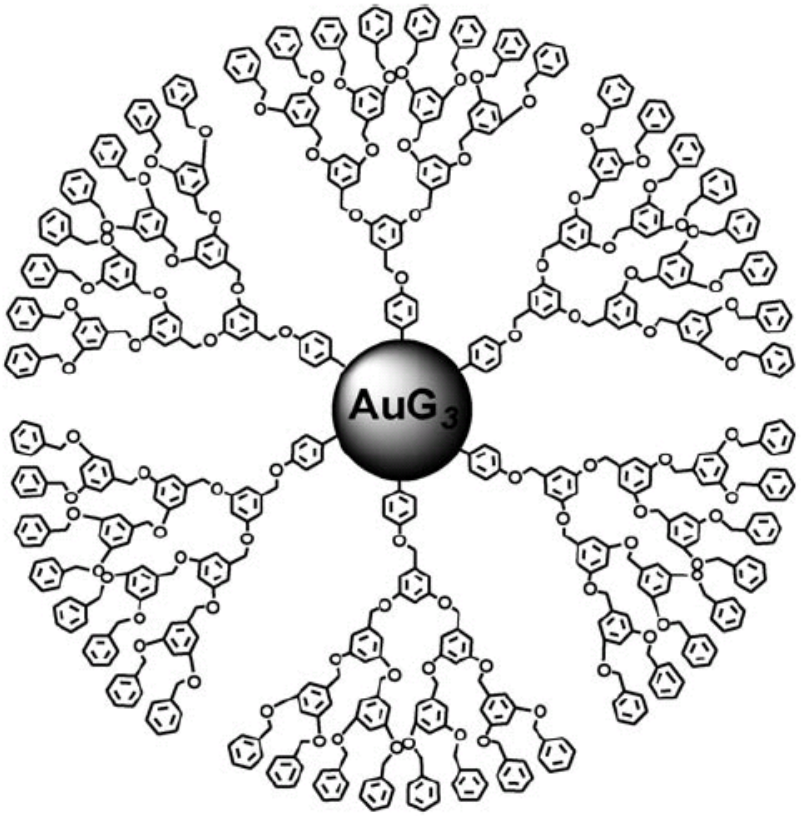

Figure 1.8 Idealized structure of AuG_3. Reprinted with permission from [117], Copyright 2010 Wiley-VCH Verlag GmbH & Co. KGaA, Weinheim.

Chen and coworkers synthesized stable ruthenium nanoparticles by protecting the particles with diazoacetate molecules that reacted readily with the ruthenium surface

forming Ru=C carbene bonds [118]. Instead of using diazonium salt, they chose to use octyl diazoacetate as ligands. Ru nanoparticles were synthesized by reduction of ruthenium chloride in 1,2-propanediol with sodium acetate trihydrate, followed by the addition of octyl diazoacetate dissolved in toluene. The overall average core diameter was 2.1 ± 0.7 nm. After they successfully prepared the Ru nanoparticles, 11-bromo-1-undecene was introduced to the Ru=C_8 MPC solution to exchange the carbene ligands with a 6:1 molar ratio of 11-bromo-1-undecene to particle-bound carbene ligands. The process is shown in Scheme 1.5 below:

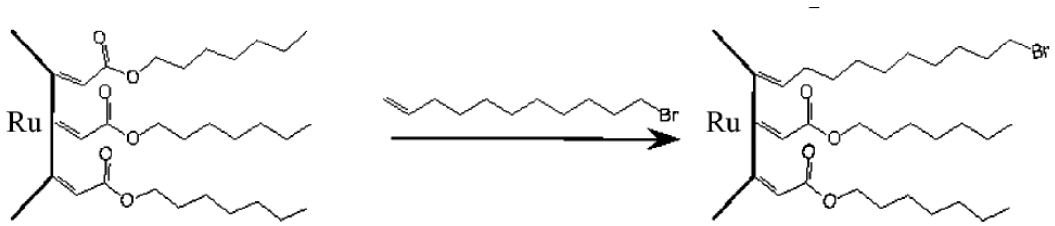

Scheme 1.5 Metathesis-based exchange reaction of carbene-functionalized ruthenium nanoparticles. Reprinted with permission from [118]. Copyright (2006) American Chemical Society.

From the ratio of the peak areas from protons of octyldiazoacetate and 11-bromo-1-undecene, the extent of the exchange reaction was estimated to be 90%, after 35 h. The exchange reaction corresponds to the second-order reaction and the rate constant is about twice as much as that observed with Au-thiolate MPCs upon ligand exchange reaction with another thiol ligand. They postulated that the Ru particles with terminal bromide groups can be potentially used for further chemical decoration by

coupling reactions through the labile Br moieties [118]. Recently, Chen's group synthesized pyrene-functionalized Ru (Ru=VPy and Ru=APy) nanoparticles, which were prepared by olefin exchange reactions of carbene-stabilized nanoparticles with 1-vinylpyrene and 1-allylpyrene in 3:1 molar ratio of pyrene to particle-bound carbene ligands [119]. The structure of 1-vinylpyrene and 1-allylpyrene are shown in Figure 1.9.

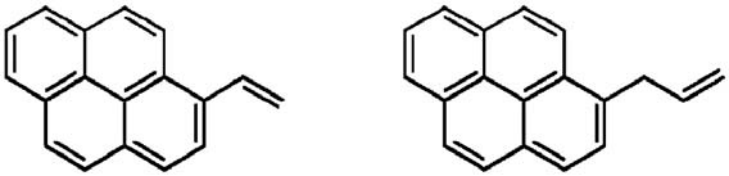

1-vinylpyrene 1-allylpyrene

Figure 1.9 Structure of 1-vinylpyrene and 1-allylpyrene [119].

The concentration of the pyrene functional groups on the nanoparticle surface was quantitatively evaluated by ^{1}H NMR measurements and there were approximately 20 pyrene functional groups per nanoparticle. Both of the pyrene monomers exhibited very well-defined absorption features and the successful incorporation of the pyrene moieties into the nanoparticle protecting layer was further confirmed by FTIR measurements. The resulting particles exhibited unique fluorescence properties which were found to vary significantly with the structure of the chemical linker. For Ru=VPy nanoparticles, the particle-bound pyrene moieties behaved equivalently to conjugated pyrene dimers. In contrast, the Ru=APy nanoparticles exhibited a fluorescence profile consistent with those of monomeric pyrene derivatives (vinylpyrene and allylpyrene). Furthermore,

fluorescence dynamics studies showed that the Ru=VPy nanoparticles exhibited a much longer lifetime, and were less prone to photo-bleaching than conjugated pyrene dimers. All these results suggest that the optical characteristics of fluorophore-functionalized nanoparticles might be readily and effectively controlled by metal-ligand bonding interactions as well as the structure of the chemical linkages [119].

Finally, Tilley's group applied a facile, one-phase method to synthesize Au nanoparticles based on reduction of single source N-heterocyclic carbene (NHC) – AuCl complexes [120]. They found the nature of different substituents on the NHC ligand allows for the control of nanoparticle size, and nanoparticles that were ~2 nm in diameter were obtained with bulky and rigid isopropyl substituents on the NHC ligand, while ~ 6 – 7 nm nanoparticles are formed with flexible, long linear alkyl chains on the NHC. The Au nanoparticles were terminated with Au=C bonds, which was supported by ^{1}H NMR spectroscopy and mass spectrometry. Importantly, monodisperse, high quality nanoparticles were obtained with use of the relatively weak reducing agent 9-borabicyclo[3.3.1]nonane, which ultimately led to their self-assembly into 3D superlattices without the requirement of a post-treatment procedure for narrowing the size distribution. They believed the NHCs possess desirable properties as capping agents for Au nanoparticle stabilization in a manner that is complementary to that of thiols [120].

1.4 Goals of My Research

The modification of metal nanoparticles with stabilizers and use as catalysts has

led to the very fruitful and active field of quasi-homogeneous catalysis in modern chemistry. An attractive aspect of recent developments in this area is that the final materials may exhibit combined properties from their inorganic nuclei and their organic surfaces. However, their compositions, stability, catalytic activity and selectivity and catalytic mechanisms over their surfaces still need to be explored for many systems. In this thesis, I will mainly focus on two main objectives, the first is the study of catalytic efficiency and mechanism of palladium nanoparticles stabilized by poly(vinylpyrrolidone) (PVP) for carbon-carbon coupling reactions, and the second is to rationally synthesize metal nanoparticles stabilized by metal-carbon bonds and exploit the resulting nanoparticles as carbon-carbon coupling and hydrogenation catalysts and comparing the activity and stability of the particles with Pd nanoparticles protected by PVP.

The first project involves using palladium nanoparticles stabilized by PVP for carbon-carbon coupling reactions, especially for the Stille and Suzuki reactions. Biaryls (Ar_1-Ar_2) are an important class of organic compounds and the two of the most commonly used catalytic methods in biaryl synthesis are the Stille and Suzuki reactions [121]. These reactions enable the preparation of both symmetrical and unsymmetrical biaryls in a cross-coupling reaction and are extremely versatile, proceed under mild conditions and can tolerate a wide range of substituents on both coupling partners [122]. Since the turn of the millennium, interest in nanoparticle catalysis has considerably increased and Pd now appears as the most frequently investigated metal for catalytic coupling in the synthesis of C-C bonds. As a stabilizer, polyvinylpyrrolidone (PVP) has been widely used

because of its solubility in water and the excellent ability to stabilize nanoparticles. However, although Pd nanoparticles have been extensively studied as catalysts, there are still many uncertain factors in the whole catalysis process, including what the actual catalytic mechanisms are. Thus in my first project, Pd nanoparticles protected by PVP stabilizers are used to catalyze Stille and Suzuki carbon-coupling reactions in mild aqueous conditions, as shown in Scheme 1.6, and an examination of the possible catalytic mechanism(s) is attempted via careful control experiments.

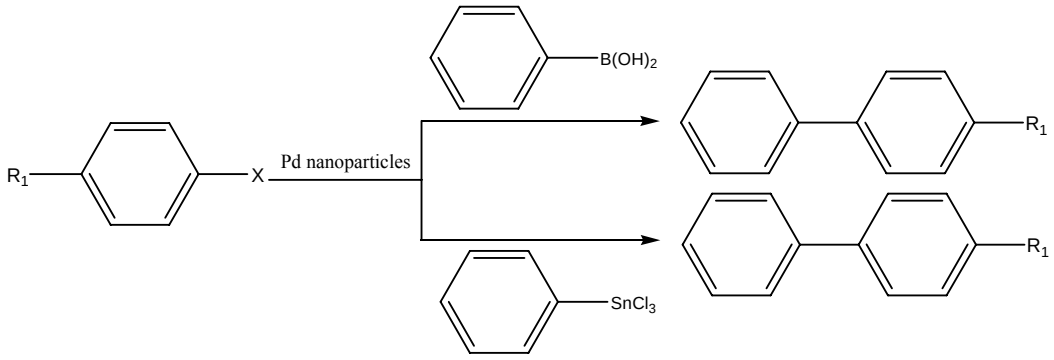

Scheme 1.6: Pd-catalyzed Suzuki and Stille cross-couplings reaction carried out under mild conditions.

The second project focuses on synthesizing nanoparticles stabilized by metal-carbon bonds by reducing diazonium ligands in the presence of the metal salts. Both the stability of these nanoparticles and their use as catalysts are to date unreported. Thus goal of the second project is to synthesize and study the catalytic activity of Pd nanoparticles protected by decylphenyl ligands for carbon–carbon coupling and hydrogenation reactions. Stabilized-Au and Pd nanoparticles will be synthesized and fully

characterized via techniques such as x-ray photoelectron spectroscopy (XPS), ^{1}H NMR and TEM, in order to determine the composition of metal core and organic ligands. Finally a detailed examination of the catalytic activity of Pd nanoparticles stabilized by metal-carbon bonds will be examined to provide insights on what the effect of such protecting ligands are on the catalytic efficiency of the Pd nanoparticles and enable a better understanding of the catalytic mechanisms at work.

1.5 References

[1] J. Grunes, J. Zhu, and G. A. Somorjai, *Chem. Commun.*, **2003**, 2257 - 2260

[2] C. Marcilly, *J Catal.*, **2003**, 216, 47-62

[3] J. M. Thomas, B. F. G. Johnson., *Acc. Chem. Res.*, **2003**, 36, 20–30

[4] A. S. Eppler, G. Rupprechter., *J. Phys. Chem. B*, **1997**, 101, 9973–9977

[5] J. M. Thomas and R. Raja, *Chem. Rec.* , **2001**, 1, 448–466

[6] S. GA and R. RM, *Catal. Today* **2005**, 100, 201-215

[7] W. A. Herrmann and B. Cornils, *Angew. Chem. Int. Ed. Engl.*, **2003**, 36, 1048-1067

[8] L. Resconi, L. Cavallo., *Chem. Rev.*, **2000**, 100, 1253–1346

[9] P. G. Jessop, Y. Hsiao., *J. Am. Chem. Soc.*, **1996**, 118, 344–355

[10] J. A. Gladysz, *Pure Appl. Chem.*, **2001**, 73, 1319-1324

[11] G. Schmid, *Chem. Rev.*, **1992**, 92, 1709-1727

[12] M. T. Reetz, R. Breinbauer, and K. Wanninger, *Tetrahedron Lett.*, **1996**, 37, 4499-4502

[13] X. Chaoxian, Y. Ning, and K. Yuan, *Chinese J.Catal*, **2009**, 30, 753 -764

[14] N. Toshima and T. Yonezawa, *New J. Chem.*, **1998**, 22, 1179-1201

[15] M. Moreno-Mañas and R. Pleixats, *Acc. Chem. Res.*, **2003**, 36, 638–643

[16] A. Roucoux, J. Schulz, and H. Patin, *Chem. Rev.*, **2002**, 102, 3757–3778

[17] J. S. Bradley, *Clusters and Colloids: From Theory to Applications*. Vol. 6. 1994, VCH: Weinheim. 459.

[18] G. Schmid and B. Corain, *Eur. J. Inorg. Chem.*, **2003**, 3081-3098

[19] M. Haruta, S. Tsubota., *J. Catal.* , **1993**, 144, 175-192

[20] H. Hirai, Y. Nakao, and N. Toshima, *J. Macromol. Sci. Chem.*, **1979**, 13, 727-750

[21] W. Hou, N. A. Dehm, and R. W. J. Scott, *J. Catal.*, **2008**, 253, 22-27

[22] A. F. Littke, C. Dai, and G. C. Fu, *J. Am. Chem. Soc.*, **2000**, 122, 4020–4028

[23] P. V. Kamat, *J. Phys. Chem. C*, **2007**, 111, 2834–2860

[24] X. Luo, A. Morrin., *Electroanal.*, **2006**, 18, 319-326

[25] O. M. Wilson, M. R. Knecht., *J. Am. Chem. Soc.*, **2006**, 128, 4510-4511

[26] T. Teranishi and M. Miyake, *Chem. Mater.*, **1998**, 10, 594–600

[27] A. Gniewek, A. M. Trzeciak., *J Catal.*, **2005**, 229, 332-343

[28] N. A. Dhas, C. P. Raj, and A. Gedanken, *Chem. Mater.*, **1998**, 10, 1446–1452

[29] S. Gorer, J. A. Ganske., *J. Am. Chem. Soc.*, **1998**, 120, 9584–9593

[30] R. M. Crooks, M. Zhao., *Acc. Chem. Res.*, **2001**, 34, 181-190

[31] A. M. Alkilany and C. J. Murphy, *Langmuir*, **2009**, 25, 13874–13879

[32] M. Antonietti, E. Wenz., *Adv. Mater.*, **1995**, 7, 1000 - 1005

[33] B. Nikoobakht and M. A. El-Sayed, *Langmuir*, **2001**, 17, 6368-6374

[34] M.-C. Daniel and D. Astruc, *Chem. Rev.*, **2004**, 104, 293-346

[35] M. Brust, M. Walker., *J. Chem. Soc., Chem. Commun.*, **1994**, 801-802

[36] M. J. Hostetler, J. E. Wingate., *Langmuir*, **1998**, 14, 17-30

[37] D. M. Shewchuk and M. T. McDermott, *Langmuir*, **2009**, 25, 4556–4563

[38] L. Civit, A. Fragoso, and C. K. O'Sullivan, *Electrochem. Commun.*, **2010**, 12, 1045–1048

[39] B. Pukánszky and E. Fekete, *Adv Polym Sci*, **1999**, 139, 109-153

[40] R. C. Doty, T. R. Tshikhudo., *Chem. Mater.*, **2005**, 17, 4630–4635

[41] R. S. Ingram, M. J. Hostetler, and R. W. Murray, *J. Am. Chem. Soc.*, **1997**, 119, 9175-9178

[42] D. Astruc, F. Lu, and J. R. Aranzaes, *Angew. Chem. Int. Ed.*, **2005**, 44, 7852 – 7872

[43] H. Tsunoyama, H. Sakurai., *J. Am. Chem. Soc.*, **2005**, 127, 9374-9375

[44] P. Dash, Towards the Rational Design of Nanoparticle Catalysts, 2010, University of Saskatchewan, 36

[45] R. Narayanan and M. A. El-Sayed, *J. Am. Chem. Soc.*, **2003**, 125, 8340-8347

[46] S. Chen, K. Huang, and J. A. Stearns, *Chem. Mater.*, **2000**, 12, 540-547

[47] S. Chen and R. W. Murray, *Langmuir*, **1999**, 15, 682–689

[48] W. Hou, M. Dasog, and R. W. J. Scott, *Langmuir*, **2009**, 25, 12954–12961

[49] M. Schulz-Dobrick, K. V. Sarathy, and M. Jansen, *J. Am. Chem. Soc.*, **2005**, 137, 12816–12817

[50] E. Ramirez, S. Jansat., *J Organomet Chem*, **2004**, 689, 4601–4610

[51] G. H. Woehrle and J. E. Hutchison, *Inorg. Chem.*, **2005**, 44, 6149–6158

[52] T.-Y. Dong, H.-H. Wu, and M.-C. Lin, *Langmuir*, **2006**, 22, 6754-6756

[53] B. A. Korgel, S. Fullam., *J. Phys. Chem. B*, **1998**, 102, 8379–8388

[54] S. Chen and K. Kimura, *J. Phys. Chem. B*, **2001**, 105, 5397–5403

[55] M. J. Hostetler, C.-J. Zhong., *J. Am. Chem. Soc.*, **1998**, 120, 9396-9397

[56] J. J. Gooding, F. Mearns., *Electroanal.*, **2003**, 15, 81-96

[57] D. V. Leff, P. C. Ohara., *J. Phys. Chem.*, **1995**, 99, 7036-7041

[58] P. Jiang, A. Nion., *J. Am. Chem. Soc.*, **2006**, 128, 12390–12391

[59] A. C. Templeton, W. P. Wuelfing, and R. W. Murray, *Acc. Chem. Res.*, **2000**, 33, 27–36

[60] M. Zhu, C. M. Aikens., *J. Am. Chem. Soc.*, **2008**, 130, 5883–5885

[61] P. D. Jadzinsky, G. Calero., *Science*, **2007**, 318, 430 - 433

[62] J. Fink, C. J. Kiely., *Chem. Mater.*, **1998**, 10, 922-926

[63] H. Fan, Z. Chen., *J. Am. Chem. Soc.*, **2005**, 127, 13746–13747

[64] M. T. Reetz and W. Helbig, *J. Am. Chem. Soc.*, **1994**, 116, 7401–7402

[65] M. T. Reetz and M. Maase, *Adv Mater* **1999**, 11, 773-777

[66] M. T. Reetz, M. Winter., *Chem Eur J*, **2001**, 7, 1084-1094

[67] M. Moskovits and J. S. Suh, *J. Am. Chem. Soc.*, **1985**, 107, 6826-6829

[68] M. Brust, J. Fink., *J. Chem. Soc., Chem. Commun.*, **1995**, 1655-1656

[69] M. Bieri and T. Bürgi, *Langmuir*, **2006**, 22, 8379–8386

[70] C. Gautier and T. Bürgi, *J. Am. Chem. Soc.*, **2006**, 128, 11079–11087

[71] M.-A. Neouze and U. Schubert, *Monatsh Chem*, **2008**, 139, 183–195

[72] A. C. Templeton, S. Chen., *Langmuir*, **1999**, 15, 66–76

[73] R. L. Whetten, J. T. Khoury., *Adv. Mater.*, **1996**, 8, 428-433

[74] T. G. Schaaff, M. N. Shafigullin., *J. Phys. Chem. B*, **1997**, 101, 7885–7891

[75] M. M. Alvarez, J. T. Khoury., *Chem.Phys. Lett.*, **1997**, 266, 91-98

[76] T. G. Schaaff, G. Knight., *J. Phys. Chem. B*, **1998**, 102, 10643–10646

[77] W. P. Wuelfing, S. M. Gross., *J. Am. Chem. Soc.*, **1998**, 120, 12696–12697

[78] S. R. Johnson, S. D. Evans., *Langmuir*, **1997**, 13, 51–57

[79] P. A. Buining, B. M. Humbel., *Langmuir*, **1997**, 13, 3921–3926

[80] S. Mitra, B. Nair., *J. Phys. Chem. B*, **2002**, 106, 3960–3967

[81] R. H. Terrill, T. A. Postlethwaite., *J. Am. Chem. Soc.*, **1995**, 117, 12537–12548

[82] W. D. Luedtke and U. Landman, *J. Phys. Chem.*, **1996**, 100, 13323–13329

[83] W. D. Luedtke and U. Landman, *J. Phys. Chem. B*, **1998**, 102, 6566–6572

[84] J. A. Dahl, B. L. S. Maddux, and J. E. Hutchison, *Chem. Rev.*, **2007**, 107, 2228-2269

[85] S. Nuû, H. Böttcher., *Angew. Chem. Int. Ed.*, **2001**, 40, 4016-4018

[86] K. Kamata, Y. Lu, and Y. Xia, *J. Am. Chem. Soc.*, **2003**, 125, 2384–2385

[87] D. Li, G. L. Jones., *Langmuir*, **2006**, 22, 3344–3351

[88] A. C. Templeton, D. E. Cliffel, and R. W. Murray, *J. Am. Chem. Soc.*, **1999**, 121, 7081–7089

[89] A. H. Latham and M. E. Williams, *Langmuir*, **2006**, 22, 4319–4326

[90] Q. Dai, J. G. Worden., *J. Am. Chem. Soc.*, **2005**, 127, 8008–8009

[91] A. J. Kell, R. L. Donkers, and M. S. Workentin, *Langmuir*, **2005**, 21, 735–742

[92] F. Hua, M. T. Swihart, and E. Ruckenstein, *Langmuir*, **2005**, 21, 6054–6062

[93] M. J. Hostetler, A. C. Templeton, and R. W. Murray, *Langmuir*, **1999**, 15, 3782–3789

[94] G. H. Woehrle, L. O. Brown, and J. E. Hutchison, *J. Am. Chem. Soc.*, **2005**, 127,

2172–2183

[95] R. Balasubramanian, R. Guo., *J. Am. Chem. Soc.*, **2005**, 127, 8126–8132

[96] G. Schmid, M. Baumle, and N. Beyer, *Angew. Chem., Int. Ed.*, **2000**, 39, 181-183

[97] R. Hong, J. M. Ferna´ndez., *Chem. Commun.*, **2006**, 2347–2349

[98] L. O. Brown and J. E. Hutchison, *J. Phys. Chem. B*, **2001**, 105, 8911–8916

[99] L. O. Brown and J. E. Hutchison, *J. Am. Chem. Soc.*, **1997**, 119, 12384–12385

[100] M. G. Warner, S. M. Reed, and J. E. Hutchison, *Chem. Mater.*, **2000**, 12, 3316–3320

[101] L. O. Brown and J. E. Hutchison, *J. Am. Chem. Soc.*, **1999**, 121, 882–883

[102] S. E. Eklund and D. E. Cliffel, *Langmuir*, **2004**, 20, 6012-6018

[103] G. A. Attard, A. Ahmadi., *J. Chem. Phys. Chem.*, **2003**, 4, 123-130

[104] V. S. Kulikova and A. F. Shestakov, *Russ. J. Phys. Chem. B*, **2007**, 1, 507–511

[105] J. Alvarez, J. Liu., *Chem. Commun.*, **2000**, 1151-1152

[106] D.-N. A and R. A, *Curr. Org. Chem.*, **2010**, 14, 1266-1283

[107] Y. Zhu, H. Qian., *Adv. Mater.*, **2010**, 22, 1915-1920

[108] Y. Murakami and K. Konishi, *J. Am. Chem. Soc.*, **2007**, 129, 14401–14407

[109] Z. Li, J. Gao., *J. Phys. Chem. C*, **2010**, 114, 723–733

[110] W. Hou, Quasi-Homogeneous Gold and Bimetallic Nanoparticle Catalysts, 2008, University of Saskatchewan, 106-109

[111] K. R. Gopidas, J. K. Whitesell, and M. A. Fox, *Nano Letters*, **2003**, 3, 1757–1760

[112] L. Strimbu, J. Liu, and A. E. Kaifer, *Langmuir*, **2003**, 19, 483–485

[113] D. Ghosh and S. Chen, *J. Mater. Chem.*, **2008**, 18, 755–762

[114] F. Mirkhalaf, J. Paprotny, and D. J. Schiffrin, *J. Am. Chem. Soc.*, **2006**, 128, 7400-7401

[115] S. Chen, A. C. Templeton, and R. W. Murray, *Langmuir*, **2000**, 16, 3543–3548

[116] D. Ghosh, S. Pradhan., *Chem. Mater.*, **2008**, 20, 1248-1250

[117] V. K. R. Kumar and K. R. Gopidas, *Chem. Asian J.*, **2010**, 5, 887-896

[118] W. Chen, J. R. Davies., *Chem. Mater.*, **2006**, 18, 5253-5259

[119] W. Chen, N. B. Zuckerman., *J. Phys. Chem. C*, **2009**, 113, 16988–16995

[120] J. Vignolle and T. D. Tilley, *Chem. Comm.*, **2009**, 7230-7232

[121] W. M. Seganish, M. E. Mowery., *Tetrahedron*, **2005**, 61, 2117-2121

[122] Y. Li, E. Boone, and M. A. El-Sayed, *Langmuir*, **2002**, 18, 4921-4925

CHAPTER 2: CARBON – CARBON COUPLING REACTIONS IN AQUEOUS SOLUTIONS USING PALLADIUM NANOPARTICLES

2.1 Introduction

Since the turn of the millennium, interest in quasi-homogeneous nanoparticle catalysis has considerably increased as such methods can allow for efficient reactions under mild, environmentally friendly-conditions in the context of green chemistry [1-6]. These particles have several advantages as they can be easily recovered from the reaction mixture and recycled, provided the nanoparticle catalyst does not deactivate too quickly under catalytic conditions. Specifically, Pd nanoparticles have emerged as an extremely powerful catalyst and Pd is the most frequently investigated metal for catalytic reactions involving the cross-coupling synthesis of C-C bonds [7-9]. Amongst coupling reactions forming biphenyl products, Suzuki and Stille cross-coupling reactions have been found to be some of the most effective routes [10, 11]. For Suzuki reactions, the relative thermal stability, insensitivity to air or moisture, and low toxicity of boronic acid derivatives constitute valuable practical advantages for both academic and industrial applications [12-14]. In the Stille reaction, the tin reagents used can be easily synthesized and purified, but do have some known toxicity issues, particularly for triorganotin compounds [15, 16].

Different stabilizers have been used to protect Pd nanoparticles for high stability, leading to remarkable achievements in this field with regards to systems with high catalytic activity and selectivity [17-19]. El-Sayed and coworkers [20] have found the

surface atoms of Pd nanoparticles do not all have the same reactivity in this reaction when applying the poly(vinylpyrrolidone) (PVP)-stabilized Pd nanoparticles with varying particle size to the Suzuki reaction. The catalytic activity of the Pd nanoparticles suggests that the low-coordination number vertex and edge atoms on the particle surface are active sites for the Suzuki reaction. They also indicated that the lower catalytic activity for the smallest Pd nanoparticles (~3.0 nm) might be due to stronger adsorption of the reaction intermediates on the particle surface, in which the strongly adsorbed species act as a poison to the reaction thereby decreasing the rate of the reaction. Later studies by the same group [21] using PVP stabilized Pd nanoparticles as catalysts for the Suzuki reaction indicated the addition of phenylboronic acid leads to the stability of the size distribution of the nanoparticles during the reaction as it binds to the particle surface through the O of the OH group and acts as a stabilizer. Iodobenzene has no effect and thus probably does not bind strongly to the surface during the catalytic process. Crooks and coworkers [17] have shown that Pd nanoparticles encapsulated within the interior of PAMAM dendrimers which have a diameter of ~1.7 nm are catalytically active for the Stille reaction for different substrates. Moreover, the reaction takes place under very mild conditions (in aqueous solution at 23^{o}C, and using only 0.100 atom % of Pd as catalyst) and with good yields. Montingelli and coworkers [22] studied catalysts composed of Pd nanoparticles stabilized by tetraalkylammonium salts bearing long alkyl chains, which behaved efficiently for Suzuki and Stille carbon-carbon coupling reactions. They also found the longer alkyl chains of the ammonium cation allowed nanoparticle stabilization

by protecting the metal core and sterically inhibiting access to the core. Meanwhile, due to the nucleophilicity of the bromide anion, it can play a role as the cocatalyst, by entering into the metal sphere and forming more active Pd^0 anionic species and also as an accelerating agent, by assisting in the transmetalation step. Recently, Guo and coworkers [23] found that poly (2-aminothiophenol)-stabilized Au nanoparticles were active catalysts for Suzuki-Miyaura crosscoupling reaction of aryl halides with arylboronic acids in water and air resulting in decent yields of product.

However, despite this remarkable progress, there are still a number of issues in this field. In view of their increased availability and decreased expense, aryl chlorides are much desirable coupling reagents compared to aryl bromides and iodides [24, 25]. Moreover, more detailed exploration of the possible catalytic mechanisms at work with Pd nanoparticle catalysts in solution are needed, such as whether catalytic reactions are indeed catalyzed by Pd^0 atoms on the particle surface or alternatively whether oxidized Pd^{2+} species are responsible for the catalytic activity of the particles [26, 27]. Herein we examine the activity of polymer stabilized Pd nanoparticles in aqueous solution for both Suzuki and Stille reactions towards understanding which mechanisms are dominant.

In this chapter, poly (vinylpyrrolidone) (PVP)-stabilized Pd nanoparticles were used to catalyze carbon-carbon coupling reactions, namely Stille and Suzuki reactions. In order to further understand the mechanism and the uncertainty of whether nanoparticles or Pd salts are the catalyst, control reactions using Pd salts were also examined using the same experimental procedure to examine their catalytic activity in carbon-carbon

coupling reactions. Results show that the presence of O_2 is crucial for the Stille reaction with the Pd nanoparticles, which are nearly completely inert under N_2, while the K_2PdCl_4 precursor is itself quite active for the Stille reaction. However, the Pd nanoparticles were found to be active for the Suzuki reaction with high yields in the absence of O_2. The yields for 4-chlorobenzoic acid are higher than 4-bromobenzoic acid and occur for un-catalyzed reactions, for reasons that are still unknown. Finally Au nanoparticles have been tested by the same experimental procedure and have no catalytic activity for these two reactions.

2.2 Experimental

2.2.1 Chemicals and Materials

Poly(n-vinyl-2-pyrrolidone) (PVP, M.W. 58,000), hydrogen tetrachloroaurate hydrate (99.9%), potassium tetrachloropalladate (99.99%), 4-iodobenzoic acid, 4-bromobenzoic acid, 4-chlorobenzoic acid, iodobenzene, potassium iodide, 4-tert-buthylphenyl (99%) and phenyltin trichloride were purchased from Alfa and used as received. Sodium borohydride and magnesium sulfate (anhydrous) was obtained from EMD Chemicals Inc. Deuterated solvents were purchased from Cambridge Isotope Laboratories. 18 MΩ.Cm Milli-Q deionized water (Millipore, Bedford, MA) was used throughout.

2.2.2 Preparation of PVP-Stabilized Pd Nanoparticles

The procedure used to prepare PVP stabilized Pd nanoparticles was the same as previous procedures published by our group [28]. First, 0.10 ml of a 10.0 mM potassium tetrachloropalladate solution was added to 10.0 ml of deionized water with stirring. Next, 0.28 ml of a 1.0 mM PVP solution was added. This mixture was then stirred for 15 minutes at room temperature in air. Finally, 0.10 ml of a fresh 0.10 M sodium borohydride solution was added to give a brown solution which is typical of Pd nanoparticles [29]. Au nanoparticles were prepared as stated above keeping the total molar amount of metal salt constant.

2.2.3 Catalytic Reactions

2.2.3.1 The Stille Reaction

Previously published procedures were used for most of the catalytic reactions [30], however small deviations were necessary in some cases. These are identified in the appropriate locations in the results and discussion sections. The reaction conditions used for the Stille coupling of 4-iodobenzoic acid with phenyltin trichloride are presented as an example of the default procedure. 124 mg (0.50 mmol) of 4-iodobenzoic acid and 604 mg (2.00 mmol) of phenyltin trichloride were completely dissolved in 6.00 mL of 3.0 M aqueous KOH and 2.00 mL of deionized water. Next, 5.00 mL of the PVP-stabilized Pd nanoparticle solution was added to the reactant mixture. The reaction was carried out for

15 h with stirring in room temperature, and then it was quenched with the addition of 50 mL of 5% aqueous HCl. The aqueous mixture was then treated with diethyl ether to extract the organic products three times, and then the organic layer was dried with $MgSO_4$ and filtered. 4-tertbuthylphenol (TBP) was then added as an internal standard and the solvent was removed in a rotary evaporator. Finally, the product was analyzed (without additional purification) by ^1H NMR in $CDCl_3$ solvent. All the reactions were performed once except for 4-chlorobenzoic acid, which was repeated once again for confirmation of results.

2.2.3.2 The Suzuki Reaction

The procedure used was based on that used by the Guo group [23]. 408 mg (2.00 mmol) amount of iodobenzene and 293 mg (2.40 mmol) of phenylboronic acid were completely dissolved in 8.00 mM aqueous KOH in 40.00 mL of deionized water. Next, 5.00 mL of the PVP-stabilized Pd nanoparticle solution was added to the reactant mixture. The reaction was carried out for 1.67 h with stirring in 80^oC, and then was quenched with 50 mL of 5% aqueous HCl. The aqueous mixture was treated with diethyl ether to extract the organic products three times, and then the organic layer was dried with $MgSO_4$ and filtered. 300mg (2.00mmol) of 4-tertbuthylphenol (TBP) was then added as an internal standard and the solvent was removed in a rotary evaporator. The product was analyzed (without additional purification) by ^1H NMR in $CDCl_3$. Most reactions were performed once; however, several reactions were done multiple times with reproducible results.

2.2.4 Characterization

Yields were calculated by ^{1}H-NMR using TBP as an internal standard. The ^{1}H NMR spectra were obtained using a Bruker 500MHz Advance NMR spectrometer. ^{1}H NMR chemical shifts of the crude reaction products obtained were referenced with respect to the residual protons of deuterated chloroform in a standard 5 mm NMR tube. UV-Vis absorbance spectra were obtained at 23 $\pm$ 2 ^{o}C using quartz cells with an optical path length of 1.0 cm and a Varian Cary 50 Bio UV-Vis spectrophotometer with a scan range of 300-900 nm. UV-Vis spectra of aqueous metal nanoparticle solutions were collected using deionized water as the reference.

2.3 Results and Discussion

2.3.1 Synthesis of PVP-stabilized Pd and Au Nanoparticles

Poly(N-vinyl-2-pyrrolidone) (PVP)-stabilized Pd and Au nanoparticles were synthesized following synthesis procedures developed in our group, which involves reducing aqueous solutions of the metal salts with an excess of $NaBH_4$ in the presence of the polymer [28]. The metal nanoparticles are known to be weakly stabilized through multiple coordination of the -N-C=O sites on PVP, and the final particles are not passivated, such that the reactants can access the surface of particles [31]. Figure 2.1 shows representative UV-Vis spectra of the Pd and Au nanoparticles after reduction with sodium borohydride. The PVP-stabilized Au nanoparticles show a broad, weak plasmon

band around 515 nm after reduction, which indicates the average diameter of particles is greater than 2 nm [28]. The exponentially decaying absorption with increasing wavelength seen for the Pd nanoparticles is characteristic of Pd nanoparticle systems and is similar to the findings of other groups [29]. The absence of d-d bands in the low-wavelength region suggests all of the Pd^{2+} salt has been reduced to form Pd nanoparticles.

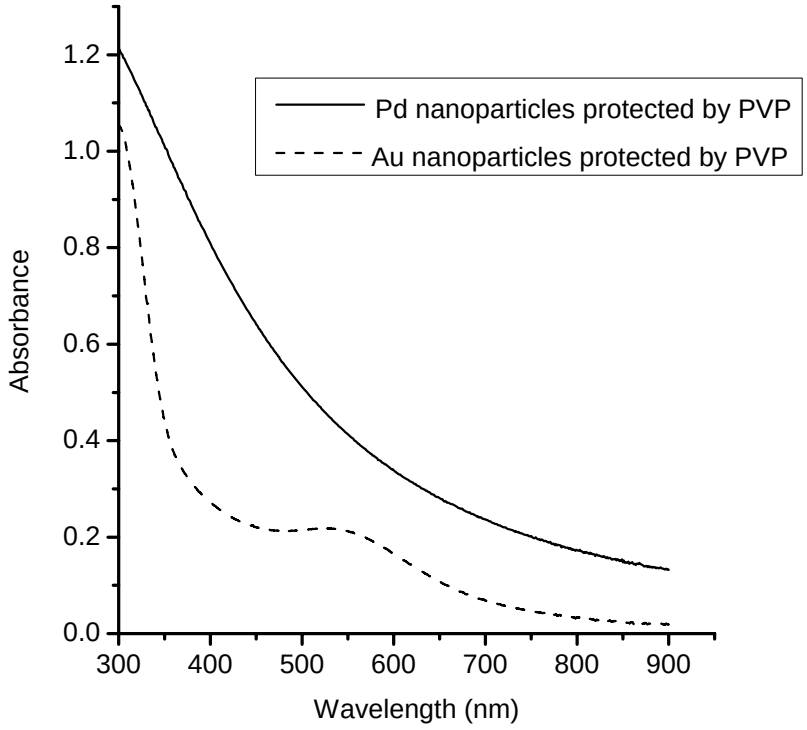

Figure 2. 1 UV-Visible spectra of Pd and Au nanoparticles protected by PVP stabilizer.

2.3.2 Catalytic Activity for Stille Reaction

In this study the activity of PVP stabilized-Pd nanoparticles as catalysts for the

Stille coupling reaction between aryl halides and trichloro-organostannanes using aqueous KOH as the solvent was investigated. This process can be considered greener than typical Stille coupling procedures as it takes place in aqueous solution and toxic tri- and tetra-organostannane precursors are avoided [30]. The reaction scheme is found below in Scheme 2.1:

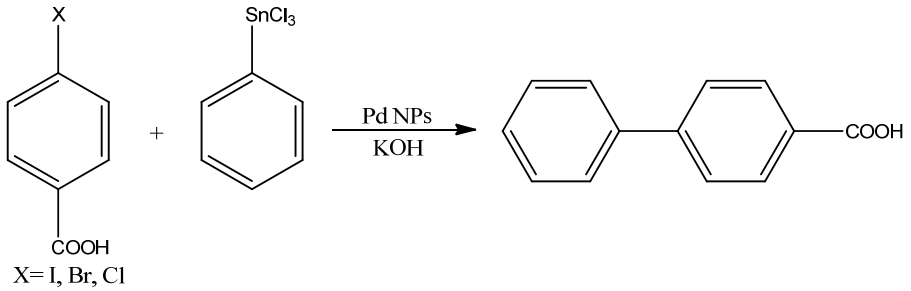

Scheme 2.1 The Stille coupling reaction of aryl halides with trichlorophenyltin in aqueous KOH.

The initial test for the Stille reaction involved using 4-iodobenzoic acid and phenyltin trichloride because 4-iodobenzoic acid is the most active among aryl halides. Figure 2.2a shows the ^{1}H NMR spectrum of 4-iodobenzoic acid dissolved in $CDCl_3$. The doublets at 7.87 and 7.83 ppm can be assigned to the phenyl protons of 4-iodobenzoic acid. Figure 2.2b is the ^{1}H NMR spectrum of the crude reaction product. The signal appearing at 8.22 ppm corresponds to the 4-disubstituted benzene rings of the anticipated Stille coupling product 4-biphenylcarboxylic acid. Note that the characteristic peaks of the starting material of phenyltin trichloride between 7.65 and 7.71 ppm are still present

in Figure 2.2b with low signals. The signals at 7.63, 7.51 and 7.39 ppm (labeled as a, b, c) corresponding to the homo-coupling product 1,1'-biphenyl and other multiplets at 7.73, 7.57 and 7.45 ppm are associated with the phenyl moiety of 4-biphenylcarboxylic acid. The presence of both the hetero and homo-coupling products is interesting given that others did not report similar observations with dendrimer-stabilized Pd nanoparticles [30], however, Terroros and coworkers recently reported similar findings with respect to the homo-coupling product [32]. Large phenyltin trichloride excesses (4 times) were used such that the homocoupling reaction would not deplete available substrate for the heterocoupling reaction.

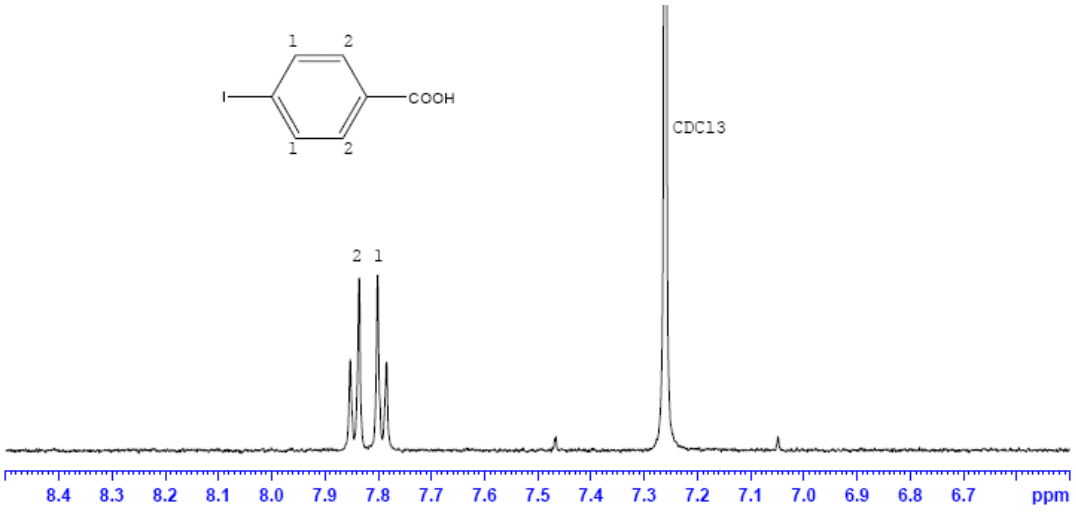

(a)

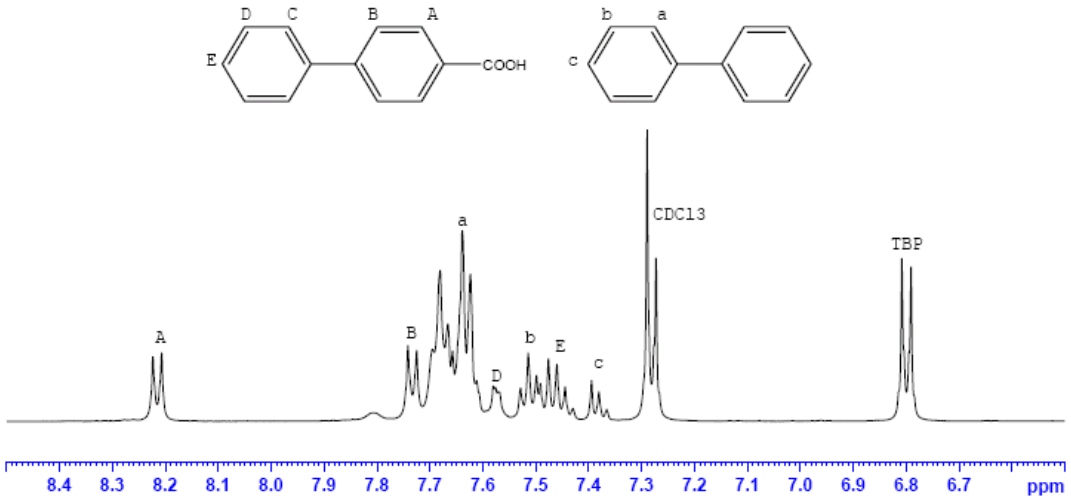

(b)

Figure 2.2 ^{1}H NMR spectra in $CDCl_3$ of (a) 4-iodobenzoic acid and (b) the crude product of the Stille reaction.

In addition to 4-iodobenzoic acid, a number of other aryl halide substrates and different reaction conditions were tested to evaluate the generality of the Pd nanoparticle-catalyzed Stille reaction. Table 2.1 lists these reactions and the corresponding yields determined from ^{1}H NMR. The results indicate that the coupling of the substrates 4-iodobenzoic acid and 4-bromobenzoic acid with phenyltin trichloride (entry 1 and 5) show decreasing yields when the iodide was replaced by bromide. However, for 4-chlorobenzoic acid, the yield (entry 6) was higher than 4-bromobenzoic acid. Indeed, in the absence of the Pd catalyst, a significant yield of 21% of the hetero-coupling product was produced using 4-chlorobenzoic acid, while no yields were seen in either the 4-iodobenzoic acid and 4-bromobenzoic acid reactions in the absence of catalyst. The relatively high yield of the homocoupling byproduct is also possible

evidence of a different mechanism for the Stille reaction for 4-chlorobenzoic acid.

Table 2.1 Reaction yields for the Stille reaction determined by ^{1}H NMR. All the reactions were performed with a 1000:1 substrate:catalyst ratio.

#	Ar-X	Condition	Yield (%) 4-Biphenylcarboxylic acid	Yield (%) Biphenyl
1	4-Iodobenzoic acid	15 h, 22 °C	52	33
2		2 h, 40 °C, N_2,	6	0
3		6 h, 22 °C, 1 mmol KI	27	30
4		6 h, 22 °C, without KI	9	0
5	4-Bromobenzoic acid	15 h, 22 °C	6	30
6	4-Chlorobenzoic acid	15 h, 22 °C	11	84
7	4-Chlorobenzoic acid	15 h, 22 °C, no catalyst	21	32

To better understand the mechanism of the Stille reaction several key control experiments for the 4-iodobenzoic acid substrate were performed due to its high activity

and yield, thus making the reaction easy to monitor. In addition, a higher temperature of 40 ^{o}C was used to reduce the reaction duration to 2 h. The results of these experiments can be seen in Table 2.2. First, the reaction was carried out using the same procedure and conditions with K_2PdCl_4 as the Pd source instead of Pd nanoparticles. The yield of biphenyl-4-carboxylic acid was 41% with a similar yield for the homo-coupling byproduct. This indicates that either Pd^{2+} is catalytically active for this reaction, or that *in-situ* reduction to Pd^0 is occurring leading to nanoparticle formation. If Pd^{2+} is the active catalyst, this would suggest that nanoparticle oxidation is occurring during the reaction in air which would then lead to leaching of Pd^{2+} from the particles [29].

Table 2.2 Reaction yields of 4-iodobenzoic acid for the Stille reaction determined by ^{1}H NMR. All the reactions were performed at 40^{o}C for 2 hours with a 1000:1 substrate:catalyst ratio.

#	Ar-X	Condition	Yield (%) 4-Biphenylcarboxylic acid	Yield (%) Biphenyl
1	4-Iodobenzoic acid	Pd Nanoparticles	66	33
2		K_2PdCl_4	41	36

Further control reactions were done under inert atmosphere to further determine which mechanism might be at play, and results are also shown in Table 2.1. The same reaction taking place under N_2 yields only a small amount of the heterocoupling products

(entry 2 of Table 2.1). The most likely possibility for the low yield of reaction under N_2 is that oxygen is part of reaction cycle to oxidize Pd^0 to the active catalyst Pd^{2+}. To test this hypothesis the reaction under air at room temperature was carried out in the presence of KI (1 mmol), which was added as a promoter of Pd oxidation and should facilitate the oxidation of Pd^0 to Pd^{2+} in air. From Table 2.1, entry 3, the rate of reaction over short time periods increased with KI addition and the yield of the homocoupling product, biphenyl is as high as seen for the heterocoupling product. In comparison, entry 4 shows that the room temperature coupling reaction proceeds very slowly over short time periods in the absence of KI. Additionally, it can also be seen the rate of reaction is non linear and increases with time when comparing the yield between reaction taken place for 15 h and 6 h (entry 1 and 4) from Table 2.1.

The reactions with K_2PdCl_4 and Pd nanoparticles under nitrogen above indicate that the catalyst is likely a Pd^{2+} species and the increased yields at higher temperatures could also be due to faster rates of Pd oxidation and leaching from sample. However, Trzeciak speculated that the oxidative addition of aryl halides to Pd^0 is a key stage of carbon–carbon coupling reactions catalyzed by palladium with aryl halides as substrates [29]. As shown in Scheme 2.2, in reactions catalyzed by Pd^0 nanoparticles the product of oxidative addition containing the [X–Pd^{2+}–Ar] core which can be attached to the surface of the nanoparticle or can leach from the surface of particles to the solution as a soluble Pd^{2+} monomolecular complex. In the Stille reaction, the oxidative addition step would be followed by a transmetallation step in which the phenyl tin trichloride precursor would

ligand exchange the halide to form tin tetrachloride and a $Pd(R_1R_2)^{2+}$ complex, as shown in Scheme 2.2. This complex would then undergo reductive elimination to form the hetero-coupling product and regenerate the Pd^0 catalyst. However, while this mechanism may be occurring in the reaction, it does not explain the formation the inactivity of the Pd nanoparticle catalysts under air or the presence of significant amounts of homo-coupling products.

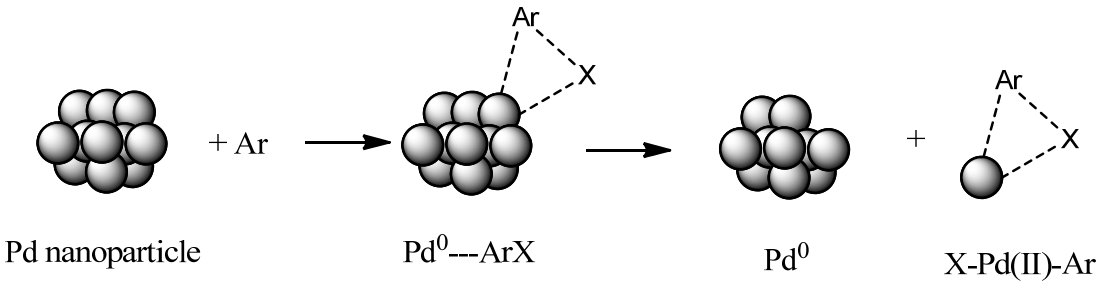

Scheme 2.2 Leaching of Pd^{2+} atom from nanoparticles as a consequence of oxidative addition of an aryl halide [29].

The actual mechanism of the Stille reaction of the Pd nanoparticle catalysts may involve several pathways. It has been postulated the coupling reaction over Pd salts that the Pd^{2+} could act as a precursor and be reduced *in-situ* to Pd^0, followed by oxidative addition and reductive elimination, which is consist with Espinet and Echavarren's work [33] with similar triorganotin compounds as shown in Scheme 2.3. The above results under nitrogen and air show that some Pd atoms are likely oxidized to form Pd^{2+} complexes which may or may not leach from the particles; these complexes can undergo transmetallation reactions with two equivalents of phenyltin trichloride to yield $Pd(R_2)_2^{2+}$

species which would then generate the homo-coupling product and form Pd^0 again upon reductive elimination. This could partially explain why abundant amounts of homo-coupling products are seen. However, it still is not apparent why low yields are seen for reactions under nitrogen.

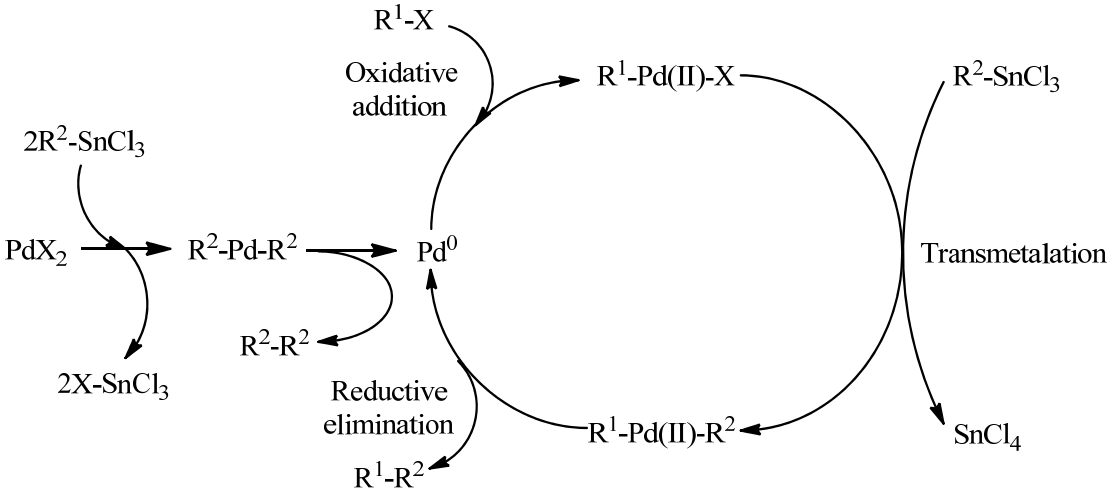

Scheme 2.3 An adapted representation of the Pd-catalyzed coupling of stannanes with organic electrophiles [33].

Crooks and co-workers have reported the Stille reaction with the same substrates and similar mild reaction conditions using dendrimer-encapsulated Pd nanoparticles [17]. Their results showed a 4-biphenylcarboxylic acid yield of 100% for both 4-iodobenzoic acid and 4-bromobenzoic acid as substrates over 15 h, which is greater than the experiment results in this study probably due to the smaller size of dendrimer-encapsulated Pd nanoparticles. However, they did not observe the formation of the homocoupling byproduct, which is quite different from the findings in this study in

which abundant amount of biphenyl were seen. Terreros's group compared the catalytic activity of Pd^{2+} acetate and dendrimer-encapsulated Pd nanoparticles [32] for the Stille reaction in water. The activity of $Pd(OAc)_2$ and dendrimer-encapsulated Pd nanoparticles was similar under these conditions, with both affording complete conversion of iodobenzoic acid; however, only in the case of Pd^{2+} acetate was the homocoupling byproduct observed. TEM images taken from the $Pd(OAc)_2$-catalyzed reaction medium at 80° C showed a few nanoparticles as big as 50 nm were formed after 2 h. They assumed the existence of a dynamic equilibrium between the Pd nanoparticles and molecular palladium species during the catalytic process and postulated that the molecular species are most likely responsible for the catalytic activity. These findings support findings in this work in which Pd(II) species are involved in the mechanism of the Stille reaction.

Finally, the last important factor for the Stille coupling reaction is that the substrates must be activated with strong base. It is obvious from Table 2.3 that reactions are indeed activated by KOH and higher yields are seen with increasing amount of base. Decreasing the amount of base resulted in lower yields, showing the need for a base to neutralize HI from the hydrolysis of the resulting Cl_3SnI from the transmetallation process and in particular to help dissolve the phenylstannane compounds in aqueous solution for the cross-coupling reaction [34, 35]. However, at such high pH's in air the Pd nanoparticle surfaces likely predominately exists as PdO [36], hence no oxidative addition reactions can readily occur and little leaching of Pd species from the particles will occur. The relative oxidation potentials and reactions of Pd under alkaline and acidic

conditions are described in equations (2.1 - 2.7):

In basic media: $Pd^0 + 2OH^- \rightarrow Pd(OH)_2 + 2e^-$ $E^o = -0.07$ V (2.1)

$O_2 + 2H_2O + 4e^- \rightarrow 4OH^-$ $E^o = 0.401$ V (2.2)

$2Pd^0 + 2H_2O + O_2 \rightarrow 2Pd(OH)_2$ $E^o = 0.394$ V (2.3)

$Pd(OH)_2 + 2OH^- \rightarrow Pd(OH)_4^{2-} \rightarrow PdO + H_2O + 2OH^-$ (2.4)

In acidic media: $Pd^0 \rightarrow Pd^{2+} + 2e^-$ $E^o = -0.951$ V (2.5)

$O_2 + 4H^+ + 4e^- \rightarrow 2H_2O$ $E^o = 1.229$ V (2.6)

$2Pd^0 + 4H^+ + O_2 \rightarrow 2Pd^{2+} + 2H_2O$ $E^o = 0.278$ V (2.7)

Table 2.3 Reaction yields for the Stille reaction in different base concentrations as determined by ^1H NMR. All the reactions were performed at 25 ^oC for 6.5 hours with a 1000:1 substrate:catalyst ratio.

#	Ar-X	Condition	Yield (%) 4-Biphenylcarboxylic acid	Yield (%) Biphenyl
1	4-Iodobenzoic Acid	KOH=0.2M	0	0
2		KOH=0.5M	1	0
3		KOH=1.0M	44	37

It can be seen clearly that under alkaline condition, Pd^0 is quite easily oxidized to $Pd(OH)_2$, which will form $Pd(OH)_4^{2-}$ in the presence of high concentration of OH^-.

Meanwhile, $Pd(OH)_4^{2-}$ has high tendency to decompose to PdO on the surface of the Pd nanoparticles and passivates the surface of the Pd nanoparticles, thus low yields are obtained. Acidic media may slightly decrease the potential of oxidation of Pd^0 to Pd^{2+} (equations 2.1 - 2.7), however, the solubility of phenylstannane compounds becomes problematic.

2.3.3 Catalytic Activity for the Suzuki Reaction

In order to find out if the findings from the Stille reaction are generic for the catalytic activity of Pd nanoparticles protected by PVP for other coupling reactions, the Suzuki-Miyaura reaction was used as a test reaction. The reaction examined is shown below in Scheme 2.4:

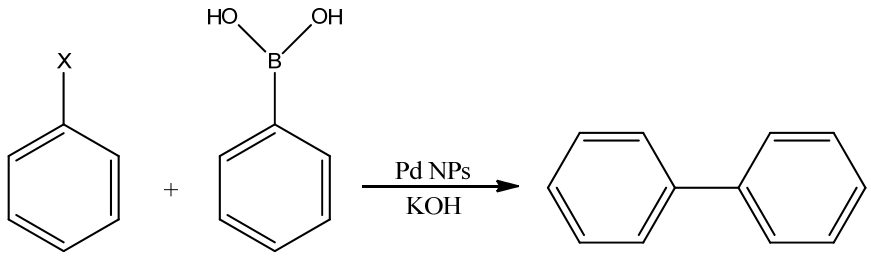

Scheme 2.4 Suzuki coupling of phenylboronic acid with aryl halides with Pd nanoparticle catalysts.

Results of the catalytic trials are shown in Table 2.4. The Pd nanoparticles have substantial catalytic activity for the Suzuki reaction, with a 63% yield seen at 80°C after 1.67 h. Pd^{2+} is also catalytically active for the reaction (entry 2 of Table 2.5) with 100%

yield under the same conditions. The presence of KI increases the yield of the Pd nanoparticle catalyzed reaction to 81%, which may be due to increased oxidation of Pd^0 to Pd^{2+}. However, in contrast to the Stille reaction results, when the Suzuki reaction was performed under N_2 atmosphere, a 100% yield of the final product 1, 1'-biphenyl was obtained. This suggests the surface of Pd nanoparticles is more active for the Suzuki reaction than the Stille reaction. The results are consistent with the literature, which suggest that the lack of O_2 is generally more favorable for higher yields [37]. By comparing the reaction conditions of Suzuki reaction with Stille reaction under N_2, an important difference between these reactions is the amount of base needed. The concentration of base for Stille reaction is much higher than Suzuki reaction which means that the Pd surfaces are likely not completely oxidized under experimental conditions for the Suzuki reaction, which explains the major differences in the results. However, it is hard to identify the percentage of product coming from homo- vs. hetero-coupling reactions using iodobenzene as substrate and more work would be needed with other substrates to determine the exact mechanisms at work.

Table 2.4 Reaction yields for the Suzuki reaction determined by ^{1}H NMR. All the reactions were performed at 80^{o}C for 1.67 hours with a 4000:1 substrate:catalyst ratio.

#	Ar-X	Condition	Yield (%) Biphenyl
1	Iodobenzene	Pd nanoparticles	63
2		K_2PdCl_4	100
3		Pd nanoparticles, 4mmol KI	81
4		Pd nanoparticles, N_2	100

2.3.4 Catalytic Activity of Au nanoparticles

Au nanoparticles were also investigated as catalysts for the Stille reaction (Table 2.5, entry 1 and 2) and Suzuki reaction (Table 2.5, entry 3) following the same procedure as Guo's group [23]. The results from Table 2.6 indicate that no product is formed starting from $HAuCl_4$ or Au nanoparticles under different reaction conditions, which is quite different from the results of Gou, though there are some significant differences between the Au nanoparticle preparations. First, in the Guo work, the Au nanoparticles are prepared from $HAuCl_4$ using poly(2-aminothiophenol) (PATP) stabilizers, whereas PVP was used as a stabilizer here. Secondly, the ratio of Au salt to PATP stabilizer used in Guo's work is 1:2 which gives nanoparticles of 1.0 nm in diameter, which is much smaller than Au nanoparticles protected by PVP used here (3.3 nm, 1:1 ratio). So it is

clear that the stabilizer and size of Au nanoparticles may play important roles in determining the catalytic activity of gold nanoparticles for carbon-carbon coupling reaction. Even a slight change of size will significantly affect the results, possibly due to stronger affinity of the substrate for smaller nanoparticles. All these results reveal that precise control over the size of gold nanoparticles and thickness of stabilizer is crucial to the efficiency of catalyst which may cause some difficulty for the application of Au nanoparticles in coupling reactions.

Table 2.5 Investigation of Au nanoparticle and salt catalysts for Stille and Suzuki reactions in air. #

	Ar-X	Condition	Yield (%) 4-Biphenylcarboxylicacid	Yield (%) Biphenyl
1	4-Iodobenzoic acid	1hour, 60^{o}C, Au NPs	0	0
2		2hours, 40^{o}C, $HAuCl_4$	0	0
3	Iodobenzene	4hours, 80^{o}C, Au NPs	None	0

2.4 Conclusions

To summarize, Pd nanoparticles stabilized by PVP were used to catalyze carbon-coupling reactions, specifically the Stille and Suzuki reactions. Results show that while the Stille reaction proceeds with the nanoparticles under air, they are nearly inert under nitrogen, and the K_2PdCl_4 precursor is itself quite active for the Stille reaction. This

suggests the likely mechanism involves formation of the Pd^{2+} species which is the catalyst precursor for the Stille coupling reaction. On the other hand, Pd nanoparticles have better catalytic activity for Suzuki reaction under N_2. The yields for seen for the Stille reaction of 4-chlorobenzoic acid and phenyltrichlorotin are higher than that of the 4-bromobenzoic acid and occur for un-catalyzed reactions, for reasons that are still unknown. Au nanoparticles protected by PVP stabilizers showed no activity for the reaction, which may be due to a limitation of their larger sizes than particles used in the literature. Looking to the future, more work is still needed to completely clarify the mechanisms of the Stille reaction and Suzuki reaction and find out the determining factor(s) for optimal yields using 4-chlorobenzoic acid substrates. In addition, the possible oxidation of Pd surfaces in strong basic conditions must be taken into account for Pd nanoparticle catalysts. Future work will be done on the coupling reactions carried out in ionic liquid solvents and comparing the results with reactions performed in aqueous solutions.

2.5 References

[1] G. Schmid, *Chem. Rev.*, **1992**, 92, 1709-1727

[2] N. Toshima and T. Yonezawa, *New J. Chem.*, **1998**, 22, 1179-1201

[3] M. T. Reetz and G. Lohmer, *Chem. Commun.*, **1996**, 1921-1922

[4] G. Schmid and B. Corain, *Eur. J. Inorg. Chem.*, **2003**, 3081-3098

[5] R. M. Crooks, M. Zhao., *Acc. Chem. Res.*, **2001**, 34, 181-190

[6] A. B. R. Mayer, *Polym. Adv. Technol.*, **2001**, 12, 96-106

[7] D. Astruc, *Inorg. Chem.*, **2007**, 46, 1884–1894

[8] C. Ornelas, D. Méry., *Angew. Chem. Int. Ed.*, **2005**, 44, 7399 –7404

[9] S. Sawooa, D. Srimania., *Tetrahedron*, **2009**, 65, 4367-4374

[10] S. Jana, S. Haldar, and S. Koner, *Tetrahedron Lett.*, **2009**, 50, 4820–4823

[11] J. P. Genet and M. Savignac, *J. Organome.t Chem*, **1999**, 576, 305–317

[12] A. F. Littke and G. C. Fu, *Angew. Chem. Int. Ed.*, **1998**, 37, 3387-3388

[13] N. Miyaura and A. Suzuki, *Chem. Rev.*, **1995**, 95, 2457-2483

[14] M. Moreno-Man˜as, M. Pe´rez, and R. Pleixats, *J. Org. Chem.*, **1996**, 61, 2346-2351

[15] IJ.Boyer, *Toxicology*, **1989**, 55, 253-98

[16] K. E. Appel, *Drug Metab. Rev.*, **2004**, 36, 763-786

[17] J. C, Garcia-Martinez., *J. Am. Chem. Soc.*, **2005**, 127, 5097-5103

[18] R. Narayanana and M. A. El-Sayed, *J. Catal.*, **2005**, 234, 348-355

[19] F. Lu, J. Ruiz, and D. Astruc, *Tetrahedron Lett.*, **2004**, 45, 9443–9445

[20] Y. Li, E. Boone, and M. A. El-Sayed, *Langmuir*, **2002**, 18, 4921-4925

[21] R. Narayanan and M. A. El-Sayed, *J. Am. Chem. Soc.*, **2003**, 125, 8340-8347

[22] V. Calo, A. Nacci., *J. Org. Chem.*, **2005**, 70, 6040-6044

[23] J. Han, Y. Liu, and R. Guo, *J. Am. Chem. Soc.*, **2009**, 131, 2060–2061

[24] A. F. Littke, C. Dai, and G. C. Fu, *J. Am. Chem. Soc.*, **2000**, 122, 4020–4028

[25] J. P. Wolfe, R. A. Singer., *J. Am. Chem. Soc.*, **1999**, 121, 9550–9561

[26] A. Ricci, F. Angelucci., *J. Am. Chem. Soc.*, **2002**, 124, 1060-1071

[27] T. MB, K. PJ., *Adv. Synth. Catal.*, **2005**, 347, 1965-1968

[28] W. Hou, N. A. Dehm, and R. W. J. Scott, *J. Catal.*, **2008**, 253, 22-27

[29] A. Gniewek, A. M. Trzeciak., *J. Catal.*, **2005**, 229, 332-343

[30] J. C. Garcia-Martinez, R. Lezutekong, and R. M. Crooks, *J. Am. Chem. Soc.*, **2005**, 127, 5097-5103

[31] H. Tsunoyama, H. Sakurai., *J. Am. Chem. Soc.*, **2005**, 127, 9374-9375

[32] M. a. Bernechea., *Inorg. Chem.*, **2009**, 48, 4491-4496

[33] P. Espinet and A. M. Echavarren, *Angew. Chem. Int. Ed.*, **2004**, 43, 4704-4734

[34] T. Z. Nichele and A. L. Monteiro, *Tetrahedron Lett.*, **2007**, 48, 7472-7475

[35] W. J. Zhou, K. H. Wang, and J. X. Wang, *Adv. Synth. Catal.*, **2009**, 351, 1378-1382

[36] C. C. Hu and T. C. Wen, *Electrochimica Acta.*, **1996**, 41, 1505-1514

[37] H. Wei, L. Chun, and J. Z. Lin, *Org. Lett.*, **2007**, 9, 4005-4007

CHAPTER 3: STABILITY AND CATALYTIC ACTIVITY OF GOLD AND PALLADIUM MONOLAYER-PROTECTED CLUSTERS WITH METAL - CARBON BONDS

3.1 Introduction

Metal and semiconductor nanoparticles have attracted intense research interest due to their unique chemical and physical properties which differ greatly from those of their constituent atoms and bulk forms [1-3]. Among metal nanoparticles, Au and Pd have been extensively studied because of their interesting optical [4, 5], electronic properties [6, 7] and high catalytic activity for diverse reactions [8-11]. However, metal particles are often stable only as suspensions and tend to irreversibly aggregate over time or when removed from solvent, which limits both their manipulation and the range of analytical tools that can be applied to them [12, 13]. Stabilization of metal clusters by ligand coatings can, however, enable further manipulation, control stability characterization, and facilitate characterization [14, 15]. Specifically, thiol chemistry has been successfully employed for the attachment of different capping ligands onto metal surfaces and for the synthesis of nanoparticles with narrow size distributions [16]. Brust-Schiffrin [17] and Murray [18] have synthesized 1-3 nm diameter ligand-stabilized Au and Pd clusters by protecting the metal with a self-assembled monolayer of thiolate ligands, and the resulting nanoparticles are known as monolayer protected clusters (MPCs). While MPCs tend to be quite stable, their surfaces are often thought to be passivated due to complete

monolayer coverage. However, thiolate exchange and oxidation reactions have been observed [19, 20] and several groups [21, 22] have reported that thiolate-protected Pt and Pd MPCs have catalytic activities for hydrogenation and Suzuki cross-coupling reactions, although their catalytic activities were low and the particles were reported to precipitate during catalytic reactions. Jin's group used Au MPCs for the selective oxidation of styrene by O_2 and hydrogenation of benzalacetone, which demonstrated the remarkable catalytic properties and remarkable chemoselectivity of small $Au_n(SR)_m$ clusters [23]. Herein the synthesis of Au and Pd MPCs stabilized by metal-carbon bonds via diazonium reduction is reported, along with demonstrations of their activity for carbon-carbon coupling and hydrogenation reactions.

The range of metals for which stable MPCs can be prepared is limited by the stability of the metal-sulfur bond, and often the final MPCs are catalytically inactive due to surface passivation. A general synthetic approach for the preparation of metal and alloy nanoparticles with stronger metal covalent bonds and accessible surface areas would be advantageous [24]. Recently, several groups have studied metal nanoparticles passivated by carbon-metal covalent bonds. In fact, the bonding energy for a Pd–C single bond has been reported to be 436 kJ /mol, which is even larger than that of the Pd–S linkage (380 kJ /mol)[25]. McDermott [26] and coworkers compared the stability of aryl diazonium derived self-assembled monolayer (SAM) films in terms of resistance to sonication, exposure to refluxing solvents, and displacement using thiolated molecules and reported that the films are, under certain conditions, more strongly bound to gold than their

corresponding alkanethiol SAMs. Schiffrin and coworkers [27] reported a new synthetic route based on the formation of carbon-metal bonds by the chemical reduction of alkylphenyl diazonium salts in the presence of Au salts, while Chen and coworkers applied the same strategy to make Pd nanoparticles passivated by metal-carbon covalent linkages [25]. Both groups characterized the final particles by TEM and various other spectroscopic techniques. Specifically, Chen's group performed solid-state conductivity studies which showed that the Pd-C stabilized particles exhibited drastically enhanced conductivity properties as compared to their alkanethiolate protected counterparts. Stable ruthenium nanoparticles with Ru=C carbene bonds were synthesized by Chen's group via the reaction of diazo species that reacted readily with the ruthenium surface [28]. They found the exchange rate constant of surface place exchange reactions on the ruthenium particles with other vinyl derivatives was substantially faster than that of Au thiolate MPCs with another thiol. However, to date, no groups have reported the catalytic activity of Au or Pd nanoparticles stabilized by metal-carbon bonds formed via diazonium reduction.

In this chapter, the synthesis of Au and Pd MPCs with metal carbon covalent linkages is examined, and the stability of the resulting MPCs is tested. UV-Vis spectra and TEM images show the formation of Au and Pd nanoparticles and ^{1}H NMR was used to characterize the ligands attached to the surface of the nanoparticles. The decylphenyl-stabilized Pd MPCs were synthesized successfully and quite stable in air, while decylphenyl-stabilized Au MPCs prepared with the same protocol showed less

stability and were easily decomposed. XPS spectra indicate the composition of decylphenyl-stabilized Pd MPCs is a combination of Pd^0 and Pd^{2+} with the Pd^{2+} complex in excess. In addition, alkylphenyl-stabilized Pd nanoparticles are shown to be effective catalysts for carbon-carbon coupling reaction such as Suzuki and Stille reactions as well as hydrogenation reactions. All results indicated that the decylphenyl-stabilized Pd MPCs are efficient catalysts for both carbon-carbon coupling reactions and hydrogenation reactions. Finally, it was noted that Pd-C bonds could be easily reduced by H_2 when performing hydrogenation reactions resulting in nanoparticle aggregation and precipitation under hydrogenation conditions.

3.2 Experimental

3.2.1 Materials

All solvents (ACS grade toluene, acetonitrile, chloroform, acetone, ethyl ether, tetrahydrofuran and methanol) were purchased from EMD Chemicals Inc. and used as received. Deuterated solvents were purchased from Cambridge Isotope Laboratories. 4-decylaniline, tetrafluouoboric acid, sodium nitrite, 4-tert-buthylphenyl (99%) and sodium borohydride were purchased from Aldrich. Iodobenzene, hydrogen tetrachloroaurate (III) trihydrate, potassium tetrachloropalladate, potassium hydroxide and benzeneboronic acid was purchased from Alfa Aesar. All the chemicals were used without further purification. 18 MΩ.Cm Milli-Q deionized water (Millipore, Bedford,

MA) was used throughout.

3.2.2 Synthesis of Diazonium Ligands

The decylphenyl diazonium tetrafluoroborate salt was synthesized by following a standard literature synthetic protocol [27]. 467 mg (2.00 mmol) of the amine precursor, 4-decylaniline, was dissolved in ice-cold 48 wt% fluoroboric acid (732 mg, 8.00 mmol), followed by the addition of a 2:1 stoichiometric amount of sodium nitrite (276 mg, 4.00 mmol) which was added dropwise. The solution turned to light yellow suggesting the formation of the decylphenyl diazonium salt. The solution was allowed to stir for one hour, and then the products were washed thoroughly with cold water and cold ethyl ether to remove any impurities, affording the corresponding white compound decylphenyl diazonium tetrafluoroborate, which was then used to prepare metal nanoparticles as detailed below. The yield of decylphenyl diazonium salt was 85%. The procedure for the synthesis of the hydroxyethylphenyl diazonium tetrafluoroborate salt is quite similar to that of the decylphenyl diazonium salt. The differences were that 1.0 ml of acetonitrile was added to reaction solution when synthesizing the hydroxyethylphenyl diazonium salt and the final product was stored in deionized water in the fridge. The yield of the hydroxyethylphenyl diazonium salt is 80%.

3.2.3 Synthesis of Au and Pd MPCs

3.2.3.1 Decylphenyl-stabilized metal nanoparticles

Decylphenyl-stabilized metal nanoparticles were synthesized by following a literature synthetic protocol [25]. The following procedure was used for the synthesis of decylphenyl-protected Au nanoparticles; the procedure for the synthesis of the Pd nanoparticles is quite similar except with substitution of K_2PdCl_4 as the Pd precursor. Briefly, 35.8 mg (0.091 mmol) of hydrogen tetrachloroaurate trihydrate was dissolved in 50 mL of deionized water. 100 mg (0.364 mmol) of the decylphenyl diazonium tetrafluoroborate salt was dissolved in 75 mL of toluene. These two solutions were then mixed under rigorous stirring for about 30 min. The aqueous phase was found to become colorless whereas the organic phase turned yellow, signifying that the Au ions had been transferred into the organic phase by complexion with the diazonium ions [27]. The aqueous phase was then separated and discarded. 688 mg (18.20 mmol) of sodium borohydride was dissolved in 40 ml methanol and then added dropwise to the stirred organic phase. The solution colour changed rapidly from yellow to dark red/black signifying the formation of gold nanoparticles. The solution was allowed to stir for another 30 min. All the reactions were performed under N_2. Subsequently, solvents were removed under reduced pressure with a rotary evaporator. The resulting sample was washed several times with ethanol, acetonitrile and acetone to remove any excess ligands and other impurities.

3.2.3.2 Hydroxyethylphenyl-stabilized Pd MPCs

Hydroxyethylphenyl-stabilized Pd MPCs were synthesized using a similar procedure as shown for the decylphenyl-stabilized metal nanoparticles above. For a 4:1 ligand:metal mole ratio reaction, 0.0413g (0.127mmol) of K_2PdCl_4 was dissolved in 5 ml of H_2O and then added with stirring to hydroxyethylphenyl diazonium tetrafluoroborate dissolved in 80 ml of methanol in a 250 ml round bottom flask. The solution was stirred 15-20 min, followed by slow addition of 0.6 mmol of $NaBH_4$ dissolved in 20 ml methanol, whereupon the solution quickly turned red/orange. The solution was allowed to stir for 2 hours followed by solvent evaporation. The product was purified using a silica chromatographic column and the impurities were eluted by acetonitrile, and then, the last band at the top of column was eluted using methanol. The solvent was evaporated in a vacuum rotary evaporator leaving a dark red residue.

3.2.4 Characterization of metal MPCs with different ligands

MPCs were characterized by UV-Vis absorption spectra on a Varian Cary 50 Bio UV-Vis spectrometer with an optical path length of 1.0 cm with a wavelength range of 300 to 900 nm. TEM samples were prepared by placing a drop of solution on a holey-carbon-coated Cu TEM grid (Electron Microscopy Scientific) and allowing the solvent to evaporate in air. For each sample, an average of 50 particles was counted for size distribution analysis. The presence of organic ligands on the nanoparticles was

confirmed by ^{1}H NMR measurements which were carried out with concentrated solutions of the nanoparticles dissolved in deuterated chloroform solvent, recorded on a Bruker 500 MHz Advance spectrometer. TGA measurements were performed on a TGA Q5000IR (TA Instruments). The MPCs were placed in a high temperature Pt TGA pan and heated from 25 to 800 °C at a rate of 5 °C min^{-1} under a nitrogen atmosphere, and the weight loss was recorded as a function of temperature. X-ray photoelectron spectra (XPS) were performed on an Axis Ultra Kratos photoelectron spectrometer. The binding energies (BEs) were corrected by referencing the C 1s BE to 284.8 eV. The spectra were processed using peak-fitting routines in Casa XPS v.2.3.15 software.

3.2.5 Stability of Hydroxyethylphenyl-stabilized Pd MPCs

For HCl etching studies, 0.50 mL of a freshly prepared aqueous solution of HCl (40 mM) was added to a 3.0 mL solution of the Pd MPCs in THF (1.0 mM in Pd). The reaction was monitored every hour by UV-Vis spectroscopy.

3.2.6 Catalytic Reactions Using Decylphenyl-stabilized Pd MPCs

3.2.6.1 Stille Reaction

The same procedure was used for most of the catalytic reactions, but small deviations were necessary in some cases. These are identified in the appropriate locations in the results and discussion section. The reaction catalyzed by decylphenyl-stabilized Pd

MPCs for the coupling of 4-bromobenzoic acid with phenyltin trichloride are presented as an example of the default procedure [29]. 124 mg (0.50 mmol) of 4-bromobenzoic acid and 604 mg (2.00 mmol) of phenyltin trichloride were completely dissolved in 6.00 mL of 3.0 M aqueous KOH and 2.00 mL of deionized water. Next, 5.00 mL of the decylphenyl-stabilized Pd nanoparticles (5.0×10^{-4} mmol) in THF was added to the reactant mixture. The reaction was carried out for 2 hours with stirring at 60°C, and then was quenched with 50 mL of 5% aqueous HCl. The aqueous mixture was treated with diethyl ether to extract the organic products three times, and then the organic layer was dried with $MgSO_4$ and filtered. An internal standard, 4-tertbuthylphenol (TBP), was then added, followed by removing the solvent in a rotary evaporator. The product was then analyzed without additional purification by ^1H NMR. Most reactions were performed once; however, several reactions were done multiple times with reproducible results.

3.2.6.2 Suzuki Reaction

The Suzuki reaction between phenylboronic acid and iodobenzene was catalyzed using the decylphenyl-stabilized Pd nanoparticles following the procedure as described below: For this reaction, 204 mg (1.00 mmol) of iodobenzene, 146 mg (1.20 mmol) of phenylboronic acid, and 224 mg (4.00 mmol) of potassium hydroxide was added to 20 mL of 3:1 THF:water solvent. The solution was heated to 66°C and 1.00 mL ($5x10^{-4}$ mmol) of the decylphenyl-stabilized Pd MPCs dissolved in THF was added. The reaction mixture was refluxed at 80°C for a total of 1.7 h. After the reaction, THF was evaporated

and diethyl ether was used to extract the organic products from the remaining water phase three times. 1.00 mmol of TBP was added as an internal standard to the diethyl ether solution and then the solvent was evaporated by rotary evaporator. ^{1}H NMR was used to characterize the final product. Most reactions were performed once; however, several reactions were done multiple times with reproducible results.

3.2.6.3 Hydrogenation Reactions

The hydrogenation of allyl alcohol was performed in a three-necked round-bottomed flask at 40°C. The procedure for the hydrogenation reaction was followed using previous procedures developed in the group [30]. A H_2 gas source was connected to one end of the flask, while a differential pressure gauge (Model 407910, Extech Instruments Corp. with a resolution of 0.001 atm and accuracy of 2% at 25°C) was attached at the other end and the central portion was closed with a rubber septum. Initially, 10 mL ($6.5x10^{-3}$ mmol) of the nanoparticle catalyst dissolved in THF was placed in the flask, followed by purging the system with H_2 for 10 min. Next, 0.50 mL of the allyl alcohol substrate (600:1 mole ratio of allyl alcohol:Pd) was added under vigorous stirring conditions, followed by measurement of the H_2 uptake via differential pressure measurements every 10 s. The amount of hydrogen consumed was determined from the pressure decrease assuming hydrogen behaves as an ideal gas. Correlation of hydrogen consumption and the hydrogenation product formation (1-propanol) was found to be 100% via ^{1}H NMR experiments. This allowed the turnover frequency (TOF, (mol of

product/mol of metal) h^{-1}) to be determined from the slope of linear plots of TON (mol of product/mol of metal) versus time. ^1H NMR was used to determine the amounts of isomerization products obtained. Most reactions were performed once; however, several reactions were done multiple times with reproducible results.

3.3 Results and Discussion

3.3.1 Synthesis of Diazonium Salts

The decylphenyl diazonium tetrafluoroborate salt used in this work was synthesized according to Scheme 3.1 below. ^1H NMR ($CDCl_3$, 500 MHz) analysis indicates the decylphenyl ligands were formed with a yield of 85% by using 4-tertbuthylphenol as an internal standard. Figure 3.1 shows a representative labeled ^1H NMR spectra; the four phenyl protons can be clearly identified at 7.6 ppm (2H) and 8.6 ppm (2H), which are labeled as 11 and 12 in Figure 3.1. Additional characteristic peaks can be observed at 0.9, 1.6-1.8 and 1.3 ppm for the methyl and methylene protons, respectively, while the methylene peak for the methylene off the phenyl ring is found at 2.8 ppm.

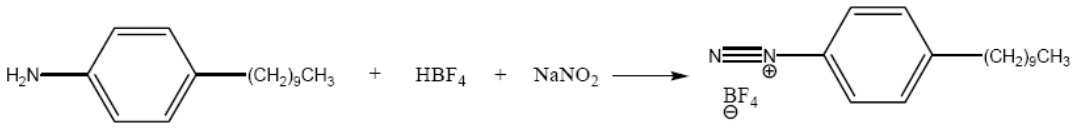

Scheme 3.1 Synthetic protocol for the formation of decylphenyl diazonium tetrafluoroborate.

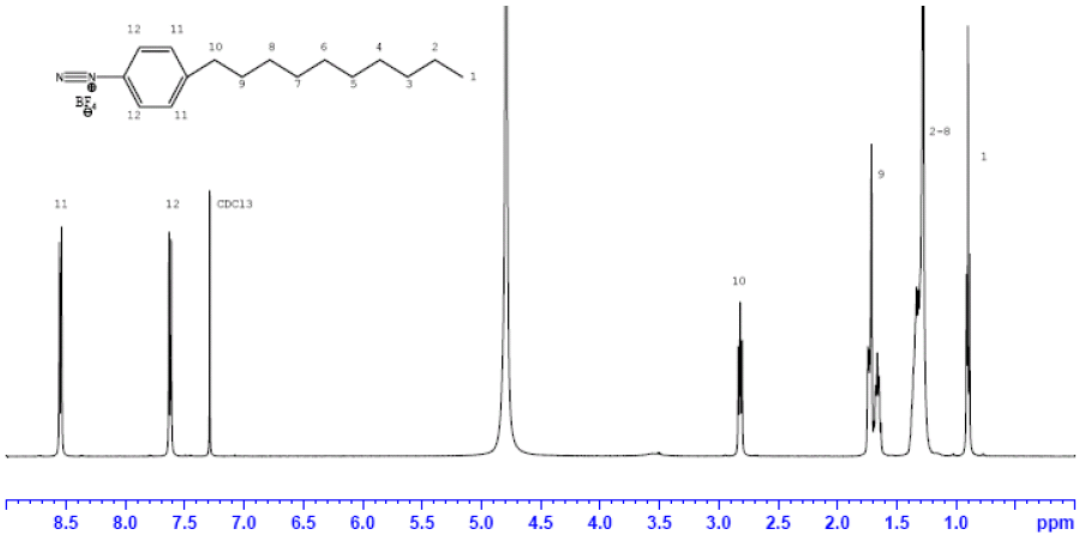

Figure 3.1 ^{1}H NMR of decylphenyl ligands in $CDCl_3$.

The hydroxyethyl phenyl diazonium tetrafluoroborate salt which was used in this work was synthesized according to Scheme 3.2 below. ^{1}H NMR (CD_3CN, 500 MHz) analysis indicates the desired diazonium ligands were formed. Figure 3.2 shows representative NMR spectra of these ligands. The aromatic region shows two sharp peaks at 7.8 ppm and 8.4 ppm, corresponding to four protons. The peaks at 3.1 and 3.8 ppm correspond to the four methylene protons, respectively. The large peak at 2.9 ppm is likely H_2O remaining in final product. The hydroxylic peak for the hydroxyl group is absent, which is likely due to hydrogen bonding interactions with water.

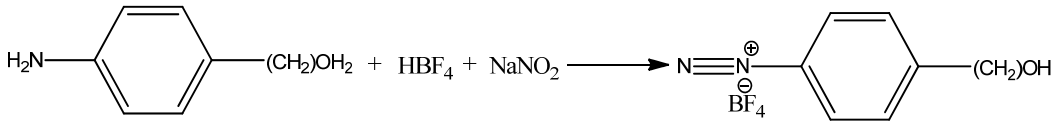

Scheme 3.2 Synthetic protocol for the formation of hydroxyethylphenyl diazonium tetrafluoroborate

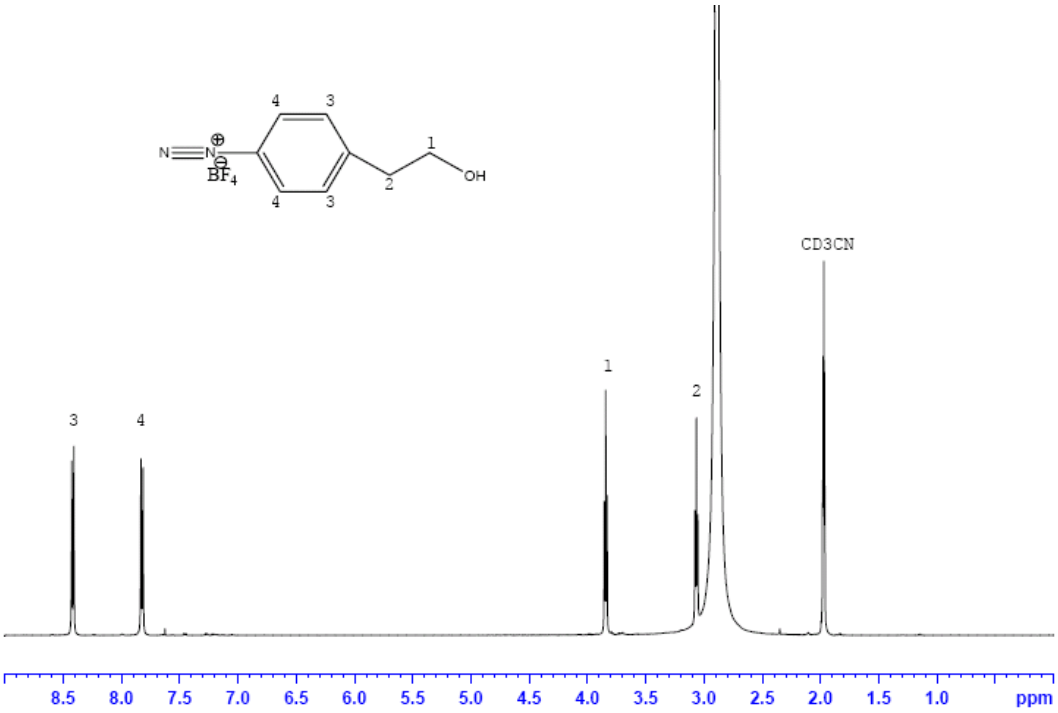

Figure 3.2 ^{1}H NMR of hydroxyethyl phenyl diazonium ligands in CD_3CN.

3.3.2 Synthesis of decylphenyl-protected Au MPCs

Au nanoparticles stabilized by decylphenyl linkages were synthesized following the procedure from Schiffrin's group [27]. When the Au salt and decylphenyl diazonium salt were reduced in the presence of sodium borohydride a clear red solution along with a large amount of precipitate was obtained. Figure 3.3 shows the UV-Vis spectra of the

decylphenyl-protected Au MPCs solution immediately after preparation. The weak plasmon shoulder of the decylphenyl-stabilized Au MPCs can be seen at approximately 523 nm and is indicative of gold nanoparticles over 3 nm in size [31, 32]. After keeping the decylphenyl-stabilized Au nanoparticles in air for two hours, almost all the Au nanoparticles precipitated out of solution and the remaining solution was light yellow. Figure 3.3 also shows the UV-Vis spectra of the decylphenyl-stabilized Au MPCs two hours later, there is no visible Au plasmon band remaining which indicates the most of nanoparticles have decomposed; thus Au nanoparticles protected by this ligand are quite unstable in air, likely due to ligand decomposition. The band at 360 nm likely comes from decomposition products forming during the decomposition. We are unsure at this point what the final organic species are, but several possibilities include 4,4'-didecyl-(1,1'-biphenyl), decylbenzene, 1,2-(4-decylphenyl)- diazene and 4-decylphenol compounds [33]. However, the decylphenyl-stabilized Au MPCs are relatively stable when all the solvent is removed and the MPCs are kept under N_2, which enabled purification and characterization. This synthetic method was also not feasible for the synthesis of phenyl-protected Au MPCs, as the Au nanoparticles precipitate in the form of black solid when adding the reducing agent $NaBH_4$ to the stirring solution. Thus the role of the decylphenyl group seems to be that of a moderate steric stabilizer which prevents Au MPC aggregation from occurring over short time periods.

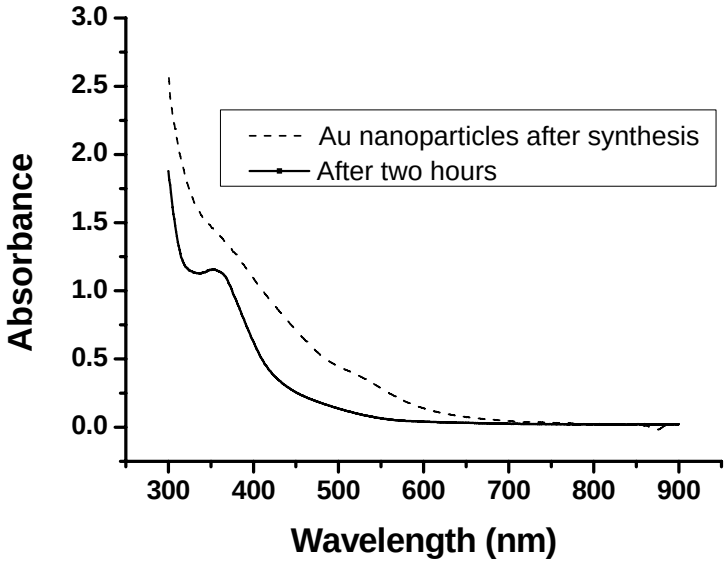

Figure 3.3 UV-Vis spectra of decylphenyl-protected Au MPCs as-synthesis and after exposure to air for 2 hours.

Figure 3.4 shows a TEM of decylphenyl-stabilized Au MPCs and its size distribution after synthesis. The average diameter of Au nanoparticles is 6.2±1.6 nm, which is relatively smaller than decylphenyl-stabilized Au MPCs (8.1±0.8 nm) made by the Schiffrin group. It seems reasonable to postulate that smaller nanoparticles were obtained because a 4:1 ratio of diazonium salt to Au^{3+} salt was used while the Schiffrin work only used a 2:1 ratio [27]. It can be seen that by increasing the initial ratio of diazonium to metal salt, the average diameter of the resulting particles decreases. This is in good agreement with work by other groups in which a larger excess of protecting ligands generally results in a smaller diameter of the particle core, as a consequence of arresting nanoparticle growth [34].

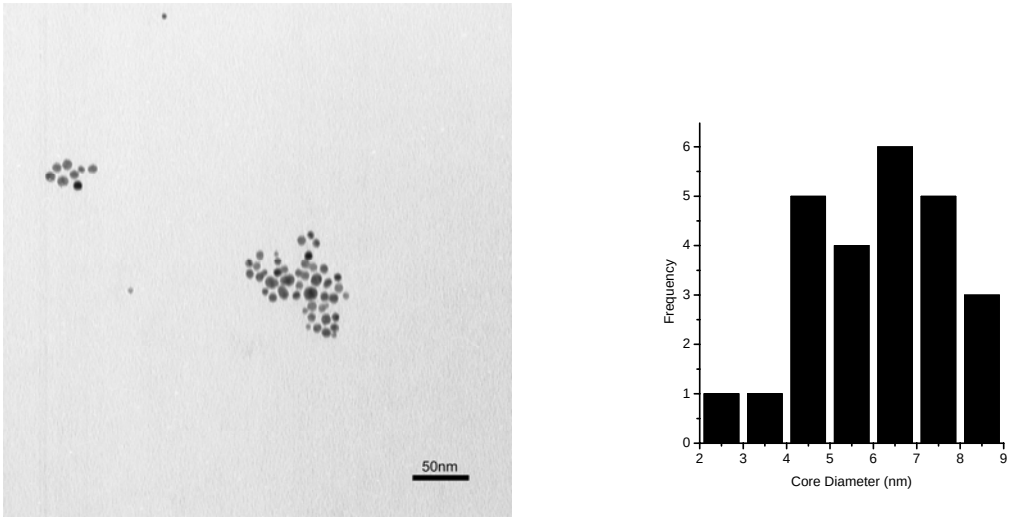

Figure 3.4 TEM of decylphenyl-stabilized Au MPCs as-synthesized and histogram of size distribution.

After purification of the decylphenyl-stabilized Au nanoparticles, the particles were characterized by ^{1}H NMR, which is shown in Figure 3.5.

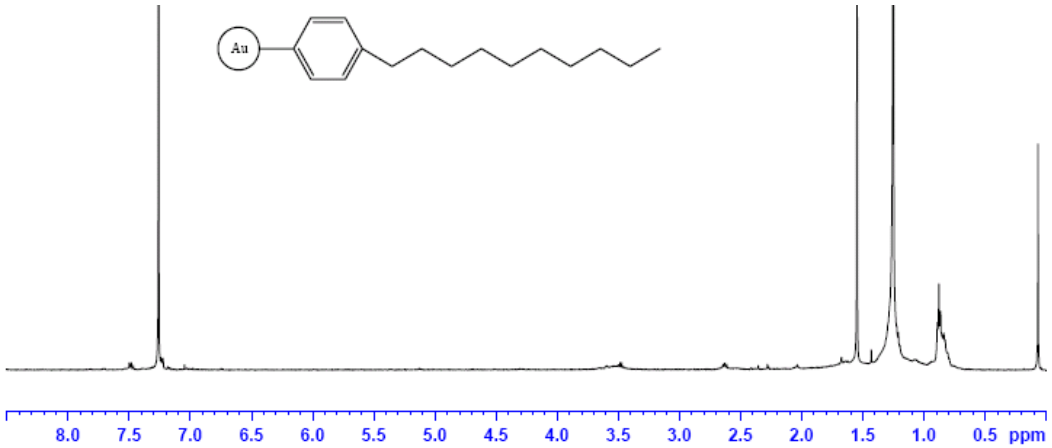

Figure 3.5 ^{1}H NMR spectra of decylphenyl-stabilized Au MPCs.

For the decylphenyl-protected Au nanoparticles, only the peaks for the methyl and

the methylene protons can now be seen and they are substantially broadened, as compared to their counterparts in the free ligands, whereas the peaks for the phenyl protons and methylene next to the phenyl group vanish completely. This is likely occurring because the peaks are become broadened. When the functional moieties are closer to the particle core, the broadening becomes more pronounced. Several structural variables have been used to explain such broadening effects by other groups [19, 25, 27], and three significant contributing factors are: (1) the chain packing near the core is more "solid-like" because of the small Au core radius and the high ligand packing density near the Au core; especially for the phenyl groups, which experience a much higher average surrounding chain packing density as compared to the end group. The resultant lowered mobility of the phenyl group should cause its NMR resonance to be much broader than the end groups; (2) the rate of tumbling of the MPCs in solution causes spin-spin relaxation (T2) broadening; and (3) the crystalline facets and curvature of the cores causes a distribution of chemical shifts for the packing ligands on the solid-like nanoparticle surfaces. The absence of any peaks in the high field region of the ^{1}H NMR spectra strongly indicates that the obtained nanoparticles are free of any solution-phase diazonium ligands or their reduced products.

3.3.3 Synthesis of decylphenyl-stabilized Pd MPCs

We alternatively tried to synthesize decylphenyl-stabilized Pd MPCs using the same procedure as the Au system; Pd MPCs were synthesized by reducing the

decylphenyl diazonium salt and Pd^{2+} salt together with $NaBH_4$ in toluene with vigorously stirring, which gives a dark red/black solution. After synthesis, the unpurified decylphenyl-stabilized Pd MPCs made using a 2:1 ratio of ligand:Pd^{2+} salt was characterized by UV-Vis spectroscopy. Figure 3.6 displays the UV-Vis absorption spectra of the decylphenyl-stabilized Pd MPCs in toluene. The spectrum exhibits a broad and monotonic increase in absorption from the visible to UV region, which is consistent with the spectrum of Pd nanoparticles in the literature [35].

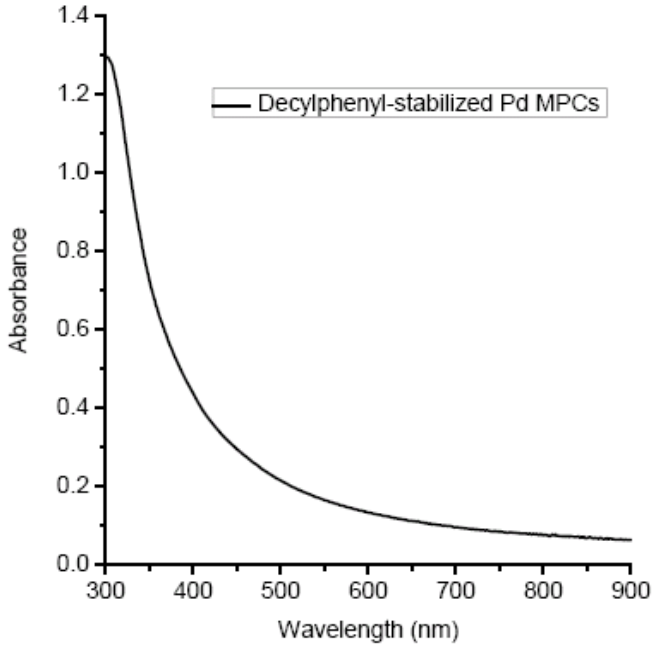

Figure 3.6 UV-Vis spectroscopy of decylphenyl-stabilized Pd MPCs.

TEM images and size-distribution plots of the decylphenyl-stabilized Pd MPCs are shown in Figure 3.7. The average sizes of Pd nanoparticles prepared with a 2:1 ratio of ligand:Pd^{2+} salt was 2.2 ± 0.4 nm before purification and 2.4 ± 0.4 nm after

purification by chromatography. The difference in average nanoparticle size is within statistical error; no significant change was seen for the diameter of the decylphenyl-stabilized Pd MPCs. It is also possible that Ostwald ripening led to a small increase in particle size [36].

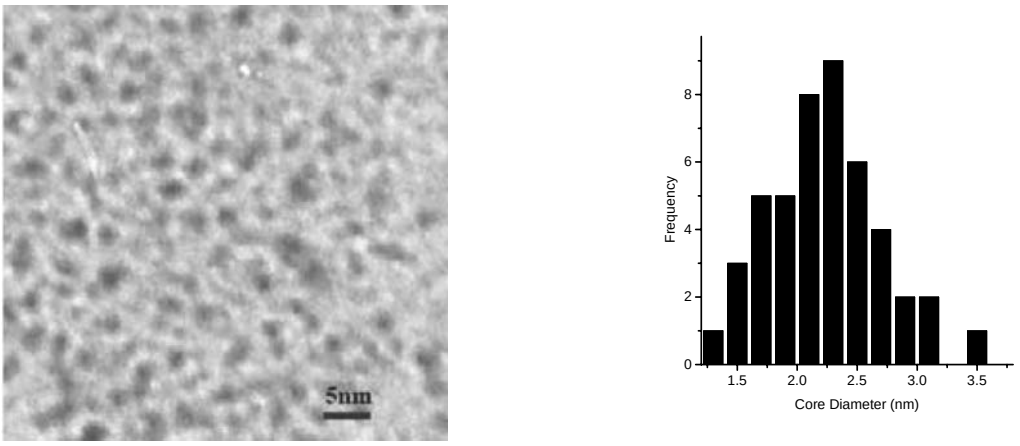

(a)

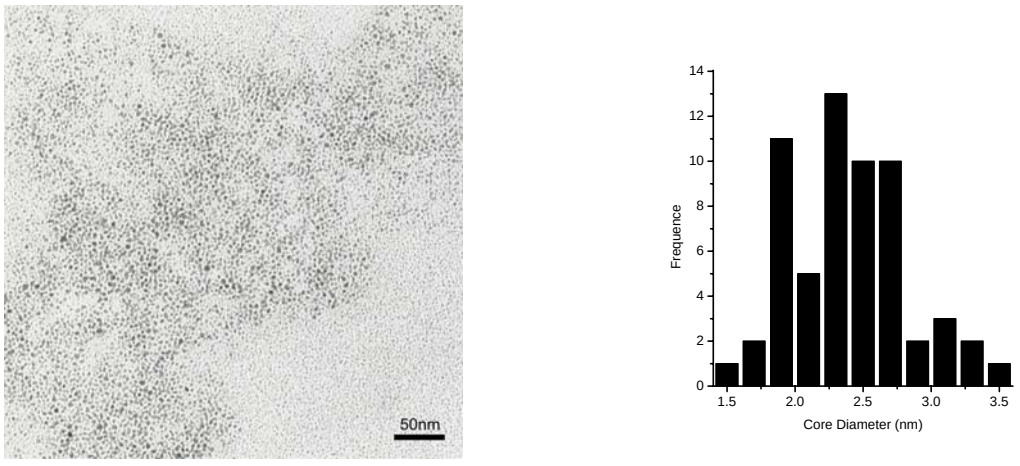

(b)

Figure 3.7 TEM and size distribution of (a) 2:1 ligand:metal decylphenyl-stabilized Pd nanoparticles before purification, and (b) after purification.

In Figure 3.8, the ^{1}H NMR spectra of the decylphenyl diazonium salt and the corresponding Pd nanoparticles before and after purification by chromatography are compared. For the Pd nanoparticles washed only by regular method, with methanol, acetonitrile and ethanol, peaks from protons on the phenyl ring are clearly identified from ^{1}H NMR, though shifted significantly when compared to the decylphenyl diazonium salt. This result indicates the routine washing procedure does not completely clean the nanoparticle solution. The solution was then purified using a silica chromatographic column and the impurities were eliminated thoroughly by eluting with toluene and chloroform followed by the elution of the nanoparticle band using acetone. As seen in Figure 3.8c, the purified particles have almost the same ^{1}H NMR spectra as the previous decylphenyl-stabilized Au MPCs, as the four phenyl protons vanish completely and only the peaks for the methyl and methylene protons can still be clearly identified at 0.9 ppm and 1.2 ppm when the ligands are attached onto the Pd particle surface. The peak at 1.5 ppm probably belongs to protons on the methylene groups, which was not verified by 2D-NMR. Additional peaks at lower fields arise from traces of solvents from the particle purification process, such as methanol and acetone at 3.0-3.5 and 2.1 ppm. Although chromatography is an efficient way to purify decylphenyl-stabilized Pd MPCs, only a small amount of pure Pd nanoparticles could be obtained.

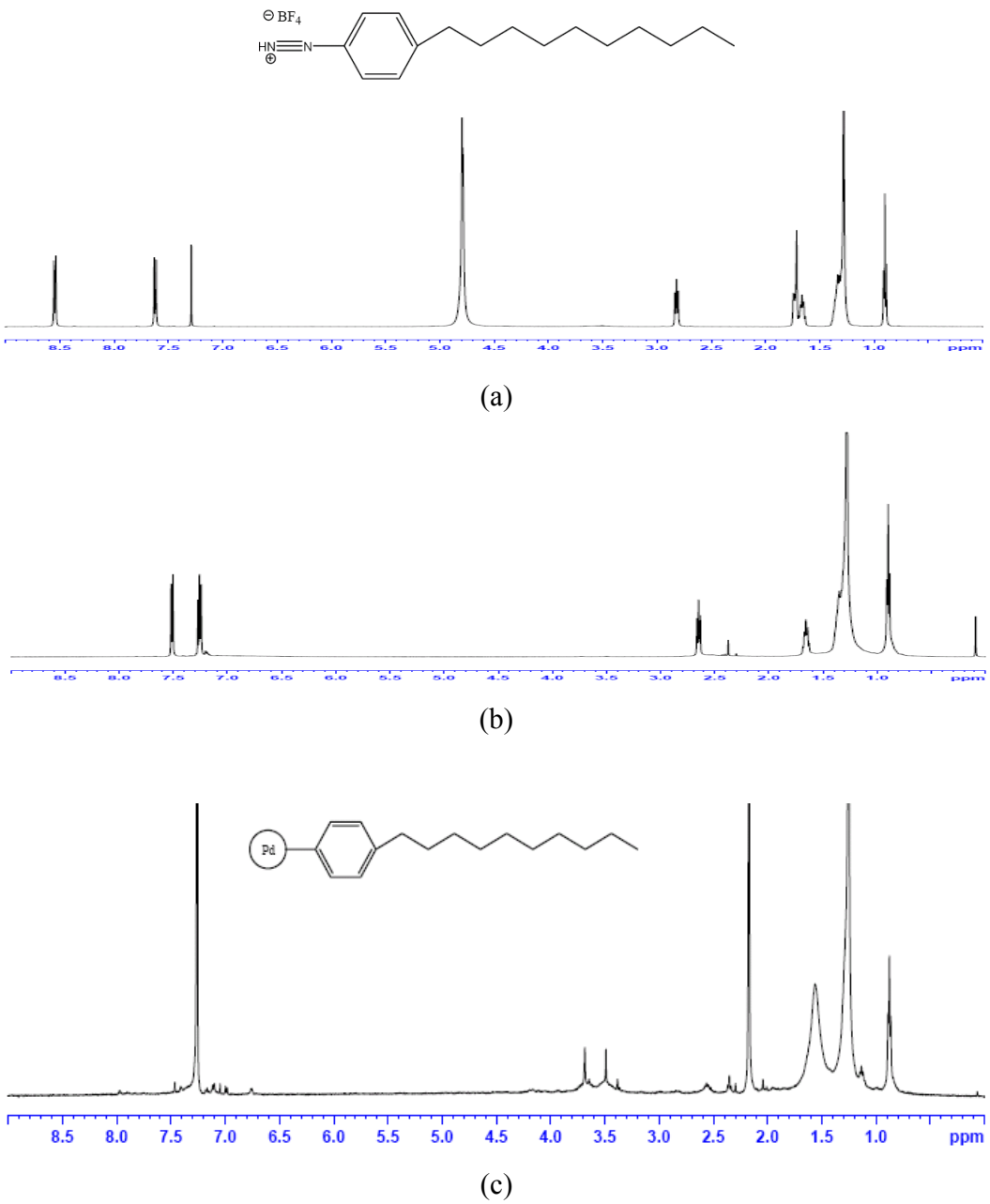

Figure 3.8 ^{1}H NMR of (a) the decylphenyl diazonium salt, and (b) the final product made from the reduction of the decylphenyl diazonium salt and Pd salt and after washing by methanol, acetonitrile and ethanol, and (c) decylphenyl-stabilized Pd MPCs after washing by column chromatography.

To obtain further information of the oxidation state of Pd in the decylphenyl-stabilized Pd nanoparticles, XPS analysis of the Pd nanoparticle samples synthesized with a 2:1 ratio of decylphenyl diazonium ligand:K_2PdCl_4 salt was performed before purification by chromatography. Figure 3.9 displays the Pd 3d core level XPS spectra of these Pd nanoparticle samples. When inspected carefully, it was observed that each Pd 3d peak is quite broad, implying that they possibly are composed of two overlapping peaks. As such, the experimental data (red lines) were deconvoluted by a curve-fitting program (Casa XPS v.2.3.15 software) to two separate components, with the minor component having a lower binding energy than the major one. The binding energies of the major components are 342.8 and 337.6 eV, which match well with the binding energies for the Pd^{2+} $3d_{3/2}$ and $3d_{5/2}$ peaks in PdO [37]. The minor peaks were fit to values of 335.0 and 340.5 eV, which correspond fairly well to Pd^0 [38] peaks. The binding energy values extrapolated from the data are displayed in Table 3.1 below.

Table 3.1 The binding energies of Pd^0 and Pd^{2+} for the decylphenyl-stabilized Pd nanoparticles extrapolated from XPS spectra.

Binding Energy (eV)			
$Pd^0 3d_{3/2}$	$Pd^0 3d_{5/2}$	$Pd^{2+} 3d_{3/2}$	$Pd^{2+} 3d_{5/2}$
340.6	335.8	342.8	337.6

By comparing the areas under the $Pd^0_{5/2}$ and $Pd^{2+}_{5/2}$ peaks, the relative ratio of Pd^0:Pd^{2+} is roughly 1:2. There are several possible reasons for this result. First, since the surface of Pd nanoparticles is prone to oxidation, there might be a layer of PdO on the surface of the Pd particles [39]. In addition, it is possible that a portion of the surface Pd atoms are present as Pd^{2+} species complexed to decylphenyl ligands, which coat the nanoparticles and prevent them from precipitation. This would be similar to the alkylamine-stabilized Pd MPCs, in which surface atoms of Pd nanoparticles exist as Pd^0 and Pd^{2+} species [40]. However, the most likely possibility is that not all the Pd is being reduced in the presence of the diazonium salt, possibly due to the formation of reductively-stable Pd salts upon reaction with diazonium radicals. Murray's group has found that stable Pd^{2+} alkanethiolate complexes form when synthesizing thiolate-stabilized Pd MPCs [34].

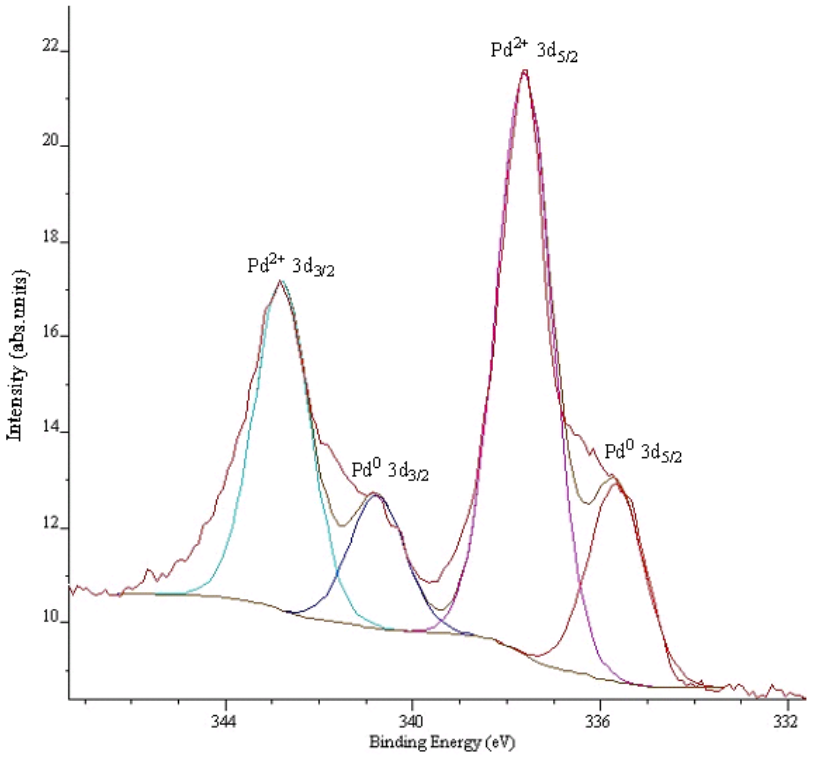

Figure 3.9 XPS spectra of Pd 3d of the final product made from the reduction of a Pd salt and decylphenyl ligands.

The C 1s spectra of decylphenyl-stabilized Pd MPCs are displayed in Figure 3.10. The wide carbon peak was observed and deconvoluted to two components by the curve-fitting program, which contains contributions from carbon atoms in various chemically different environments: the main peak centered at 284.8 eV BE derives from the alkyl chain of decylphenyl ligands. The minor component on the low BE side can be assigned to C atoms directly bound to Pd [41, 42]. Again, these results indicate that decylphenyl ligands linked on the surface of Pd nanoparticles chemically.

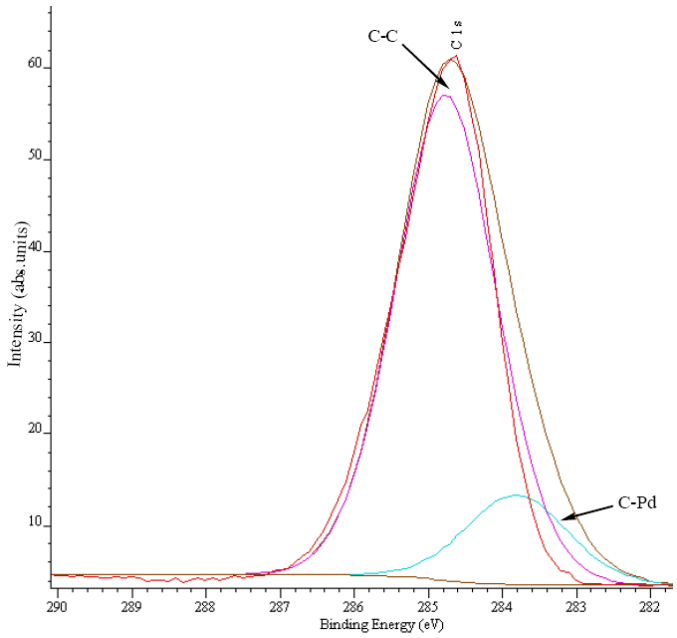

Figure 3.10 XPS spectra of C 1s spectra of decylphenyl-stabilized Pd MPCs

Thermal gravimetric analysis (TGA) is a very useful technique to estimate the organic content of organic-inorganic hybrid materials. For the 2:1 ratio of ligand:Pd salt decylphenyl-stabilized Pd MPCs (before purification by chromatography) the TGA curve (Figure 3.11 a) displays four steps of mass loss during the heating from 25 to 500^{o}C. The mass change is plotted against temperature; such mass losses reflect the decomposition and removal of decylphenyl ligands from the Pd surface. Meanwhile, the derivative curve was plotted and the positions of the derivative peaks reflect the thermal stability of the organic ligands. In the first step (167-253^{o}C), the small mass loss is likely caused by the loss of residual decylphenyl diazonium salts and/or the BF_4 anion; the pure diazonium salt completely decomposes by 200^{o}C as observed from Figure 3.11 (b). Continued heating from 253 to 365^{o}C results in a slow mass loss due to the decomposition of

organic impurities. These impurities are likely species such as 4,4'-didecyl-(1, 1'-biphenyl), decylbenzene, 1, 2-(4-decylphenyl)-diazene and 4-decylphenol compounds [33] which were introduced during the process of synthesizing Pd nanoparticles from decylphenyl diazonium salt and K_2PdCl_4, and were difficult to completely remove from the sample. There are two more processes between 365 and 500°C corresponding to the decomposition of the decylphenyl ligands. The first process (365-396°C) involves almost 40% of total organic content, which is 2.5 times more than the second mass loss process (396-455°C). Referring to the results of XPS, it is likely that these mass losses are due to different decylphenyl-palladium systems, the first being Pd^{2+} species while the second likely belongs to Pd nanoparticles (15.7%) protected by decylphenyl ligands. However, more thorough analysis of purified particles and/or salts would need to be done in order to confirm these assignments.

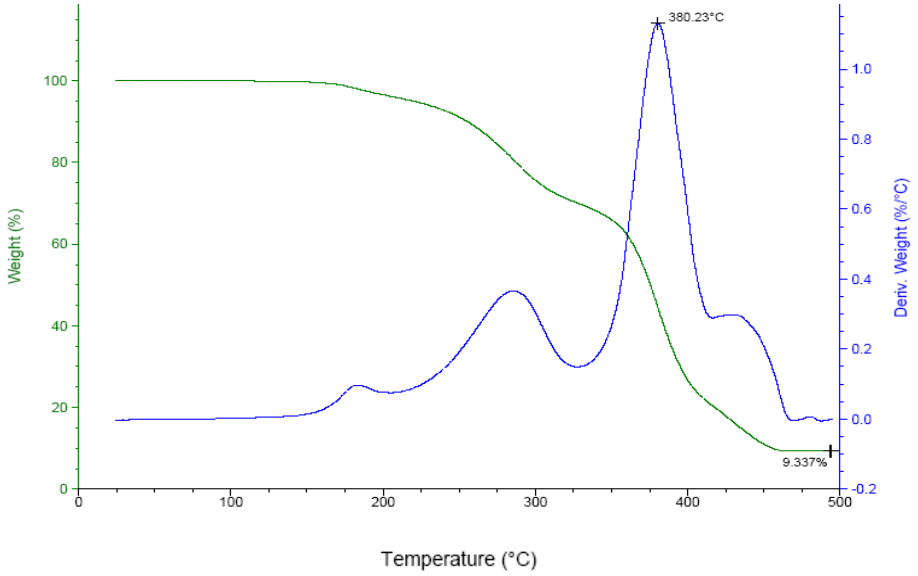

(a)

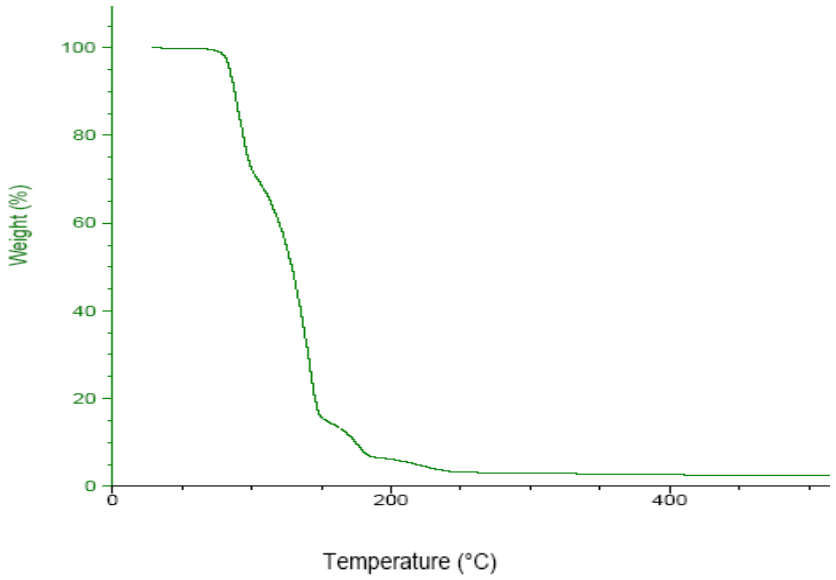

(b)

Figure 3.11 Thermal gravimetric analysis curve and derivative thermogravimetric curve of (a) decylphenyl ligands protected Pd nanoparticles, and (b) decylphenyl diazonium salt.

The surface accessibility of decylphenyl-protected Pd MPCs was probed by examining HCl-induced etching of the Pd cores. Figure 3.12 shows an etching experiment of decylphenyl-stabilized Pd MPCs. The concentration of HCl was treated as a constant during the reaction given its concentration was much higher than the initial concentration of Pd MPCs. The Pd MPCs were almost completely etched in the presence of HCl, giving light yellow solutions comprising of Pd^{2+} complexes from the initial light brown solutions. No shoulder at 375nm could be observed at the beginning and the band at 375nm increased over time as the Pd cores were etched and all the etching process was finished in 20 hours. The likely assignment of this band at 375 nm is likely a Pd^{2+} -

decylphenyl decomposition species. Figure 3.13 shows a fit for experimental data based on the 1st order decomposition of the decylphenyl-stabilized Pd MPCs, which gives a R^2 value of 0.9976 and a pseudo-first-order rate constant for the HCl etching of 2.08 x 10^{-2} ± 2.47 x 10^{-4} h^{-1}. This is relative slow etching rate when comparing to 1-dodecanethiolate-protected Au MPCs etching by KCN [43], which reveals the surfaces of decylphenyl-stabilized Pd MPCs are only mildly accessible to HCl.

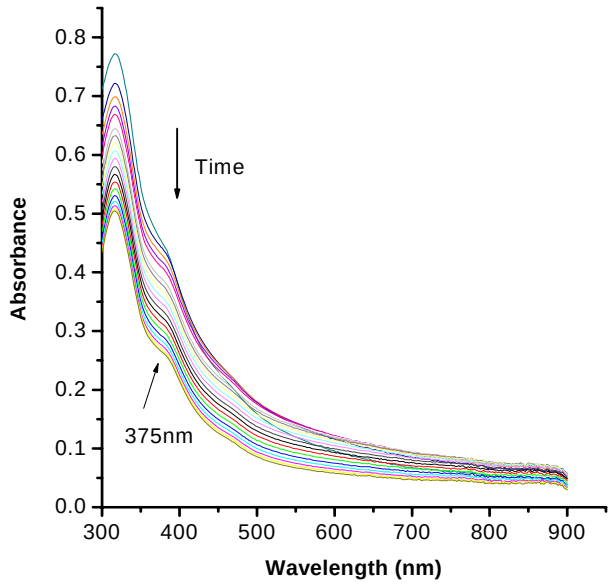

Figure 3.12 UV-Vis spectra of decylphenyl-stabilized Pd MPCs upon exposure to HCl. Each plot represents a 1 hour interval.

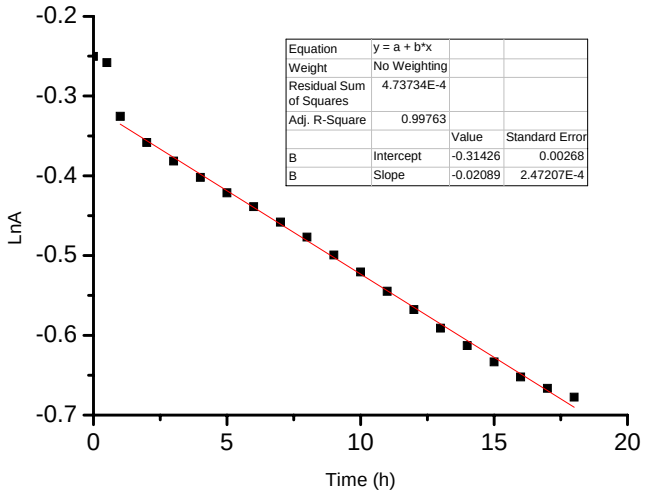

Figure 3.13 The 1st order fit of UV-Vis absorption changes of Pd MPCs at 316 nm in the presence of HCl at room temperature.

3.3.4 Attempted synthesis of Hydroxyethylphenyl-stabilized Pd MPCs

As previous results showed that decylphenyl-stabilized Pd MPCs were synthesized successfully in air, we alternatively tried to synthesize Pd nanoparticles with similar procedures with different diazonium ligands. The first ligand used was the hydroxyethylphenyl diazonium tetrafluoroborate salt which is a more favorable ligand for solubilization of the particles in aqueous solutions. For a typical 4:1 of ligand:metal mole ratio reaction, the K_2PdCl_4 and hydroxyethylphenyl diazonium salt were dissolved in a mixture of methanol and water and both reduced by $NaBH_4$ with vigorous stirring. Unlike above attempts with decylphenyl-stabilized Au MPCs, no metal precipitate formed when adding $NaBH_4$ to the solution containing hydroxyethylphenyl diazonium salt and K_2PdCl_4. A dark red product was obtained in a decent yield, which could be purified with

chromatographic column and was redissolvable in water and methanol.

TEM measurements show that Pd nanoparticles were formed with an average particle size of 2.5 ± 1.0 nm (Figure 3.14). The UV-Vis spectra of the final product is shown in Figure 3.15, the spectra shows a band at 330 nm followed by broad exponentially decreasing absorbance to high wavelength. By comparing with dithiolate [1, 5-bis (2-mercaptoethyl)-1, 5-diazacyclooctane] Pd^{2+} complexes, the peak near 330 nm likely corresponds to a metal-to-ligand charge transfer band [44]. The UV-Vis spectrum (Figure 3.14) after 400 nm is similar to that of Pd nanoparticles protected by PVP, showing an exponentially decaying absorption spectra with increasing wavelength [35]. These comparisons infer that the final dark red solid corresponds to a mixture of some form of Pd^{2+} complex and Pd nanoparticles rather than pure Pd nanoparticles protected by hydroxyethylphenyl ligands.

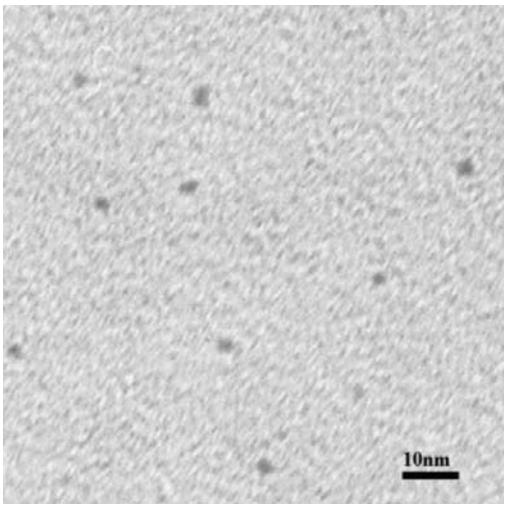

Figure 3.14 TEM of final dark red solid made from reduction of hydroxyethyl phenyl diazonium salt and K_2PdCl_4.

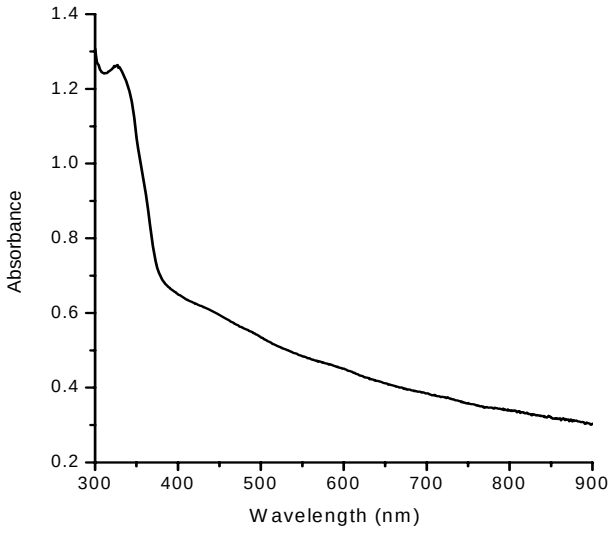

Figure 3.15 UV-vis spectra of Pd MPCs synthesized using hydroxyethyl phenyl ligands.

The final product was characterized by ^{1}H NMR after purification by chromatography; the ^{1}H NMR spectra shown in Figure 3.16. The absence of two features in the high field region (above 8 ppm) in the final purified product indicates that the product is free of any leftover diazonium salts. However, two pairs of sharp peaks coming from four phenyl protons can clearly be identified at 7.3 and 7.6 ppm and also, at a lower intensity at 6.7 and 7.1 ppm, which were not seen for decylphenyl-stabilized Au or Pd MPCs with similar diameter. It seems reasonable to propose that the product obtained is composed of multiple species. One of pairs of peaks likely belongs to a Pd^{2+} hydroxyethylphenyl complexes and the other weak pairs of peaks at 6.7 and 7.1 ppm may come from protons from phenyl groups which are linked to protecting ligands of hydroxyethylphenyl – stabilized Pd MPCs.

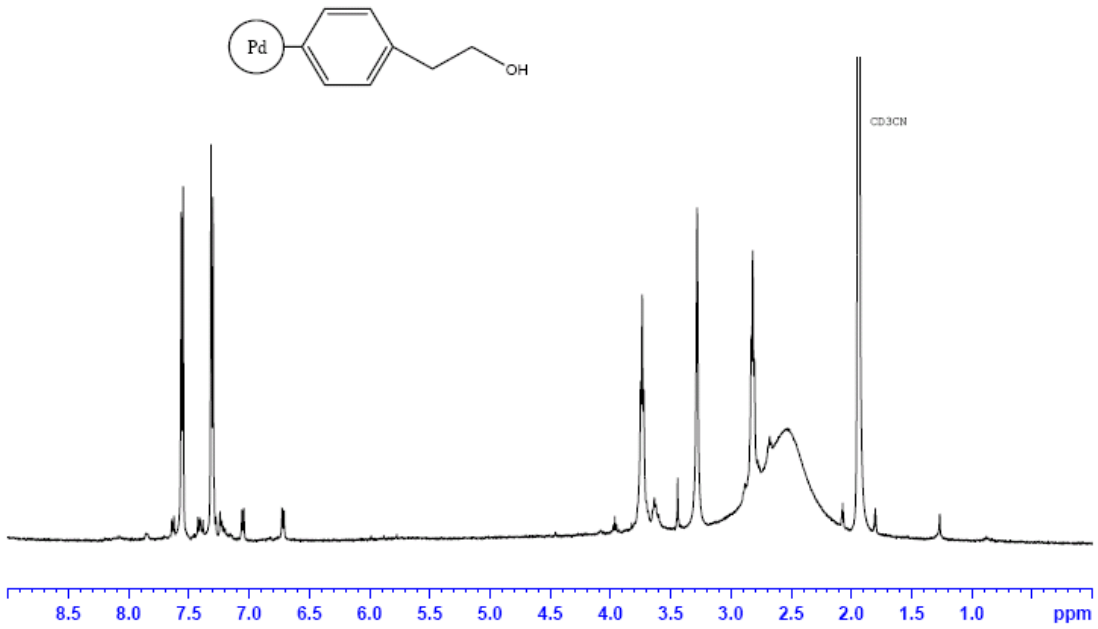

Figure 3.16 ^{1}H NMR of dark red product of synthesis of Pd nanoparticles protected by hydroxyethylpheny ligands.

To obtain further information on the oxidation state of Pd the final product, x-ray photoelectron spectroscopy (XPS) analysis of the sample synthesized from Pd^{2+} and the hydroxyethylphenyl diazonium salt was performed. Figure 3.17 displays the Pd 3d core level XPS spectra for this sample. The core level binding energies and full width at half maximum (FWHM) of the XPS peaks were analyzed with particular attention to the binding energies of the Pd 3d spin-orbit components, which are of major interest for assessing the oxidation state of Pd atom. The Pd $3d_{5/2}$ and Pd $3d_{3/2}$ peaks in the final product are at 337.8 and 343.1 eV. It has been reported that the Pd^{0} 3d spectra of Pd nanoparticles comprise of two spin-orbit components of Pd $3d_{5/2}$ and Pd $3d_{3/2}$ at 335.0 and 340.5 eV, whereas and the PdO $3d_{5/2}$ and Pd^{2+} $3d_{3/2}$ components correspond to peaks

at 337.5 and 342.5 eV, respectively [37, 38]. The observed results are similar to the binding energy of Pd^{2+} species found in the literature, inferring that the major product of the reaction is a Pd^{2+} complex. When inspected carefully, it is observed that Pd^{2+} $3d_{5/2}$ peak is broad and a small peak is present at 335.0 eV. In addition, a small shoulder on the Pd^{2+} $3d_{3/2}$ peak is seen at 341.5 eV. The minor component has lower BE than the major one, which match well with the BE for Pd^0. These results indicate that the final dark red product comprises two compounds: Pd nanoparticles capped by hydroxyethanolphenyl ligands and a Pd^{2+} complex, with the Pd^{2+} species being present in large excess.

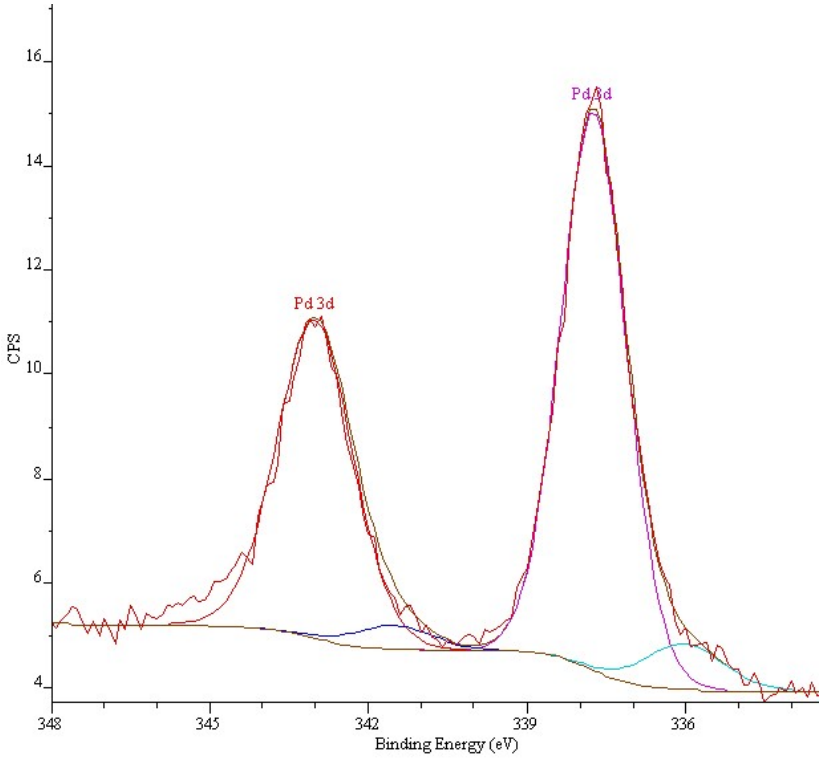

Figure 3.17 The Pd 3d core level XPS spectra for the attempted synthesis of hydroxyethylphenyl-stabilized Pd MPCs.

3.3.5 Comparison of Catalytic Acitvity of decylphenyl-stabilized Pd Nanoparticles and PVP-stabilized Pd Nanoparticles

Our investigations of catalytic activity of decylphenyl-stabilized Pd MPCs started with the study of the Suzuki reaction, one extremely important methodology for the generation of new carbon−carbon bonds specifically applied to the synthesis of biaryls, which is shown in Scheme 3.3:

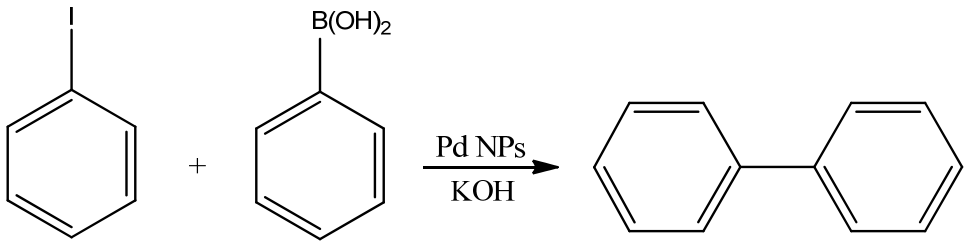

Scheme 3.3 Suzuki reaction with iodobenzene as substrate.

Table 3.2 shows the results of catalytic activity of Pd nanoparticles protected by different stabilizers. It is found that the decylphenyl-stabilized Pd nanoparticles could catalyze the Suzuki reaction completely when compared to PVP stabilized-particles which only gave a 60% yield (see Chapter 2). Since the synthesized decylphenyl-stabilized Pd nanoparticles also contain Pd^{2+} complexes, it is possible that Pd^{2+} species play a role in catalyzing the Suzuki reaction.

Table 3.2 Comparison of catalytic activity of Pd nanoparticles protected by PVP and decylphenyl ligands.

Stablizer	Substrate	Condition	Yield (%)
Poly (vinylpyrrolidone)	Iodobenzene	22 hours, 23°C, in air	0%
		1.7 hours,80°C, in air	63%
Decylphenyl ligand		1.7 hours, 80°C, in air	98%

To investigate the change of size and state of Pd nanoparticles, UV-Vis spectra was carried out to test the Pd nanoparticles solution before and after the Suzuki reaction as shown in Figure 3.18. After the reaction there is no observable exponential band at high wavelengths characteristic of Pd nanoparticles and an enhanced peak at 375 nm, suggesting that all the Pd^0 has been oxidized to Pd^{2+}. This result can be explained by examining the hypothesized mechanism of the Suzuki reaction, as shown in Scheme 3.4. The first step of the reaction is the oxidative addition of the aryl halide to Pd to the halide to form a Pd^{2+} species, which can then lead to leaching of Pd from the surface. However, the process of reductive elimination of the desired product should restore the original Pd^0 catalyst. This phenomenon has never been observed in the same reaction catalyzed by Pd nanoparticles protected by PVP, suggesting the resulting Pd^{2+} species formed in the decylphenyl system are significantly more stable to reductive elimination.

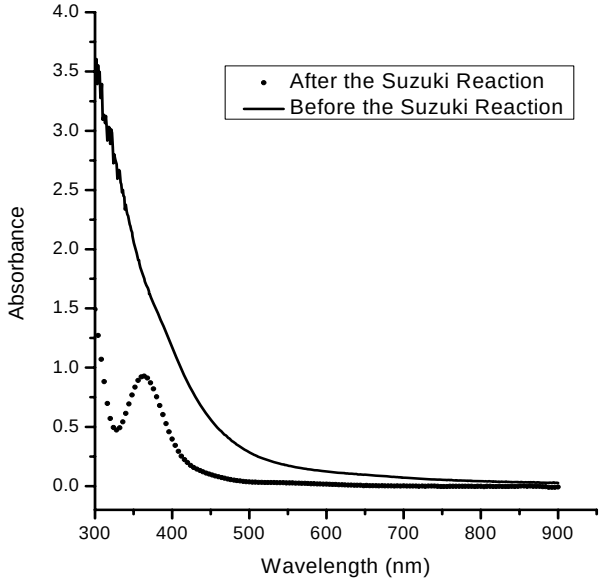

Figure 3.18 UV-Visible spectra of decylphenyl-stabilized Pd MPCs before and after the Suzuki reaction.

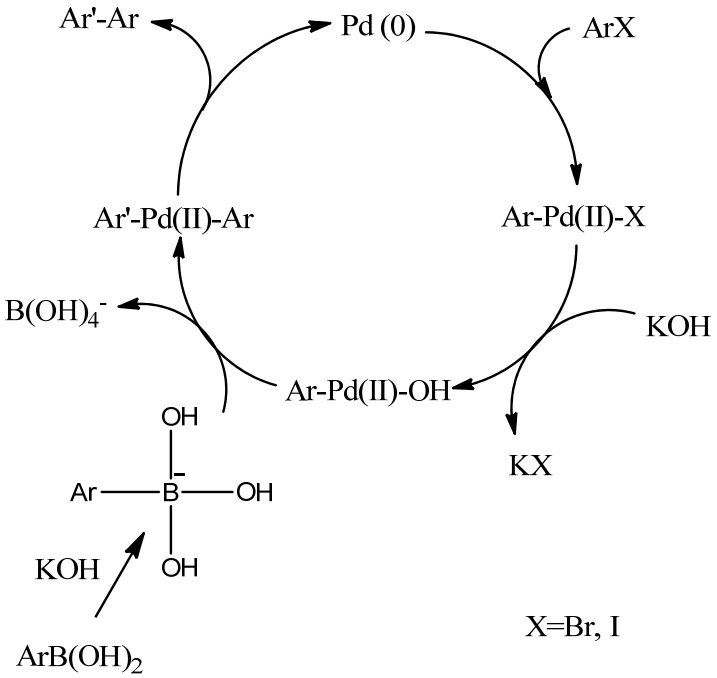

Scheme 3.4 Speculated mechanism of the Suzuki reaction.

In order to test the diversity of the catalytic activity of Pd nanoparticles protected by decylphenyl ligands, another catalytic reaction, the Stille reaction was performed. The catalyst was tested for the Stille reactions using 4-bromobenzoic acid and phenyltin trichloride. The reaction follows Scheme 3.5 shown below:

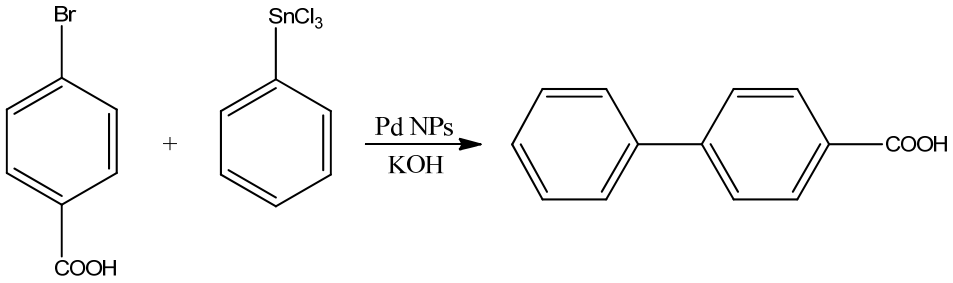

Scheme 3.5 Stille reaction with 4-borombenzoic acid as the substrate.

The whole reaction was carried out in mild reaction conditions (60^{o}C, air) and after extracting the final product from aqueous phase by ether, the organic layer changed to light red without any precipitate formed, which indicates the decylphenyl-stabilized Pd MPCs are oxidised to Pd^{2+} during the reaction as the Stille reaction proceeds. In order to evaluate the generality of the decylphenyl-stabilized Pd MPCs-catalyzed Stille reaction, the results were compared with a Pd catalyst protected by PVP (see Chapter 2). Table 3.3 shows the corresponding yields calculated from ^{1}H NMR. It is quite clear from the table that the decylphenyl-stabilized Pd nanoparticle sample has a higher catalytic activity than PVP-stabilized particles. These results indicate that even though the Pd nanoparticles are covered with protected carbon bond linked ligands, the substrate can still access the Pd nanoparticle surface. As Pd^{2+} complexes are present in the the decylphenyl-stabilized Pd

MPCs sample, it is possible that Pd^{2+} species are involved in the catalytic reaction as well.

Table 3.3 Different protection of nanoparticles and the corresponding yields for the Stille Reaction.

Stablizer	Substrate	Condition	Yield
Poly (vinylpyrrolidone)	4-Bromobenzoic Acid	2 hours, 60°C, in air	5%
Decylphenyl Ligand			20%

Another important reaction which can occur over Pd surfaces is hydrogenation reactions of olefins; to test their activity the hydrogenation of allyl alcohol was examined, as shown in Scheme 3.6 below:

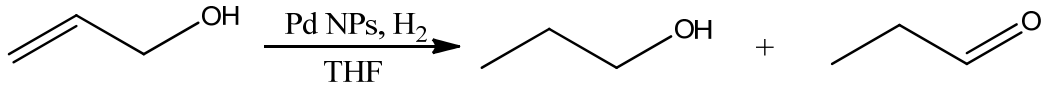

Scheme 3.6 Hydrogenation reaction with allyl alcohol as the substrate catalyzed by Pd nanoparticles.

Table 3.4 shows the results of the catalytic hydrogenation reactions; compared to PVP-stabilized Pd nanoparticles, the decylphenyl-stabilized particles show excellent selectivity (for 3:1 ligand:Pd ratio) and efficiency for the hydrogenation of allyl alcohol (for 2:1 and 3:1 ligand:Pd ratios), which indicates that the decylphenyl-stabilized Pd

MPCs are an efficient catalysts for hydrogenation reactions.

Table 3.4 The results of hydrogenation reactions of Pd nanoparticles with different stabilizers.

Stabilizer	Substrate	Conversion	Selectivity	TOF (h^{-1})
Poly (vinylpyrrolidone)	Allyl Alcohol	100%	63%	1110
Decylphenyl Ligand (2:1)		100%	40%	2280
Decylphenyl Ligand (3:1)		100%	94%	5237

It is noticeable that during the catalysis reaction with decylphenyl-stabilized Pd MPCs that the colour of reaction solution becomes darker and after several minutes, and a precipitate was formed at the bottom of reaction flask. Correspondingly, the pressure of H_2 dropped rapidly at the beginning of reaction and slowed down significantly when the black precipitate was visible. These results indicate the decylphenyl-stabilized Pd MPCs are not stable under H_2 atmosphere and the dramatic activity at the initial reaction conditions suggests at least some of the ligands are being removed such that the Pd nanoparticles are becoming quite active. In order to find out the reason of high activity of nanoparticles and how the H_2 gas affects the ligands, decylphenyl-stabilized Pd nanoparticle solutions exposed to H_2 was monitored by UV-Visible spectroscopy and TEM.

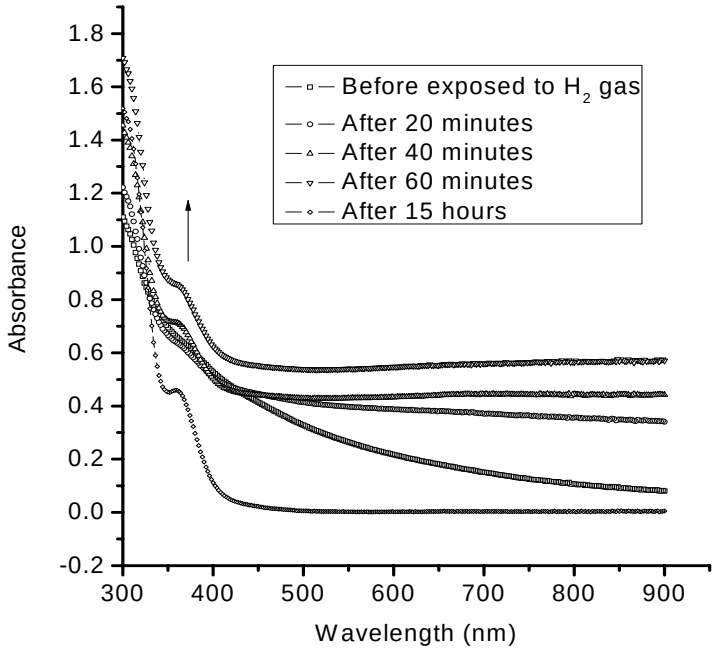

Figure 3.19 UV-Visible spectroscopy of decylphenyl-stabilized Pd MPCs exposed to H_2 gas for different times.

Figure 3.19 shows the changes of UV-Vis spectra of particles exposed to H_2 gas for different times. Before H_2 gas exposure, there is a gradually decreasing curve from 300 nm to 900 nm, which is characteristic of Pd nanoparticles. After exposure to H_2 gas for 20 minutes, the solutions turned black and the baseline of the UV-Vis spectra increased, which is due to scattering by larger colloids in the solution. After 40 and 60 minutes, the baseline increases signficantly and a peak around 375 nm appears. The diamond-shaped line is the UV-Vis spectra of the Pd nanoparticles under H_2 for 15 hours. The spectra show that the decylphenyl ligands are removed from the surface of Pd

nanoparticles and the particles start to aggregate and precipitate, suggesting that H_2 could reduce the ligands from the particle surface. Figure 3.20 illustrates the obvious change of colour of decylphenyl-stabilized Pd MPCs before and after H_2 exposure.

(a) (b)

Figure 3.20 Picture of Pd nanoparticles protected by carbon bond before (a) and after (b) exposed to H_2 for 15 hours.

Figure 3.21 shows a TEM image of decylphenyl-stabilized Pd MPCs after exposure to H_2 gas for 15 hours. A great deal of particles have aggregated and precipitated, while for unaggregated particles, it can be seen the diameter increases from 2.4 ± 0.4 nm to 8.0 ± 2.1 nm. The large change of size of decylphenyl-stabilized Pd MPCs suggests the protecting ligands partly decompose from the surface of particles, which causes the size of nanoparticles to increase. This TEM result further supports the hypothesis that H_2 gas can reduce protecting ligands and remove them from nanoparticle

surfaces. However, we were unable to exactly determine the final decomposition product after the reaction from ^{1}H NMR. Some of these products might be decylbenzene and p-decylphenol. Due to the ligands have been removed from the particles, the exposed surface of the Pd nanoparticles is much higher for allyl alcohol and H_2 to access and the hydrogenation reaction was quite fast. However, without the protection of organic ligands, the particles tend to aggregate and the catalytic activity drops as the precipitate is formed.

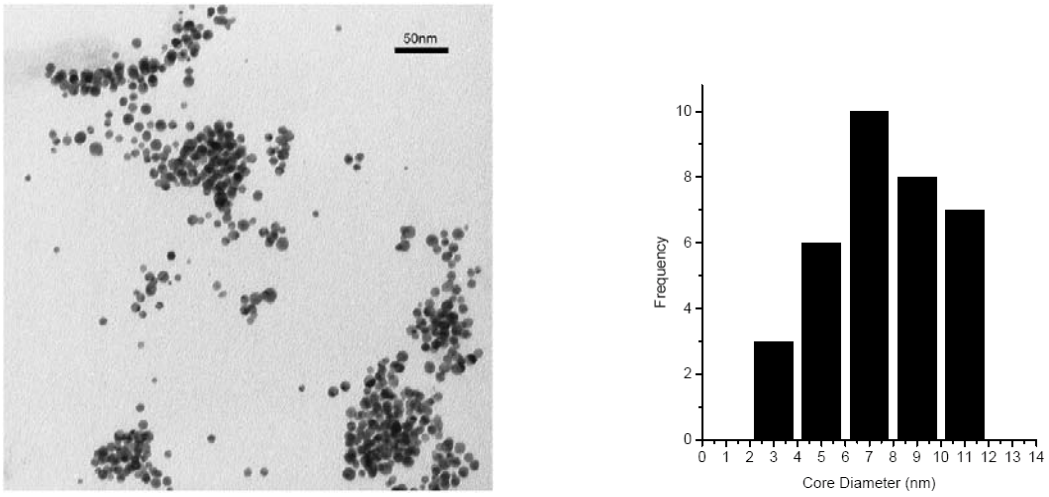

Figure 3.21 TEM and size distribution of decylphenyl-stabilized Pd MPCs after exposed to H_2 gas for 15 hours.

It is notable that the decylphenyl-stabilized Pd MPCs with a 2:1 ratio of ligand to metal salt has relatively low product selectivity of product than the PVP-stabilized particles compared to the 3:1 decylphenyl-stabilized Pd MPCs, which might arise from the competition of hydrogenation and isomerisation reactions. Alkene hydrogenation

occurs via the Horiuti-Polanyi mechanism, which involves dissociative adsorption of H_2 onto the catalyst surface, followed by stepwise hydrogenation of the C=C double bond [45]. For allyl alcohol, there are usually two products obtained in the reaction, one from hydrogenation and the other an isomerisation product. The possible mechanism is depicted in Scheme 3.7 [46]. It is reasonable to believe that other than the effect of size, the bonding ligands are an important factor to influence the selectivity of Pd nanoparticles. As mentioned in the first chapter, the structure of Pd nanoparticles is cuboctahedron showing different types of surface atoms [47] and the active site of particle correlates to the relative number of atoms on face, vertex and edge sites, which modulate the catalytic selectivity of Pd nanoparticles. Kang's work found the thermodynamic competition of the adsorption of acrolein between faces, vertex and edges determined the hydrogenation selectivity [48]. Similarly, the competition of the adsorption of ally alcohol on the surface of Pd nanoparticles is the main factor to selectivity. For a 2:1 ratio of ligand to metal, the active sites of Pd nanoparticles may have a strong tendency to produce the isomerization product rather than hydrogenation product. On the contrary, the hydrogenation reaction may occur preferentially on the active sites of the 3:1 decylphenyl-stabilized Pd MPCs and propanol is the main product. The exploration on the details of favourable sites to form propanol will be performed in the future.

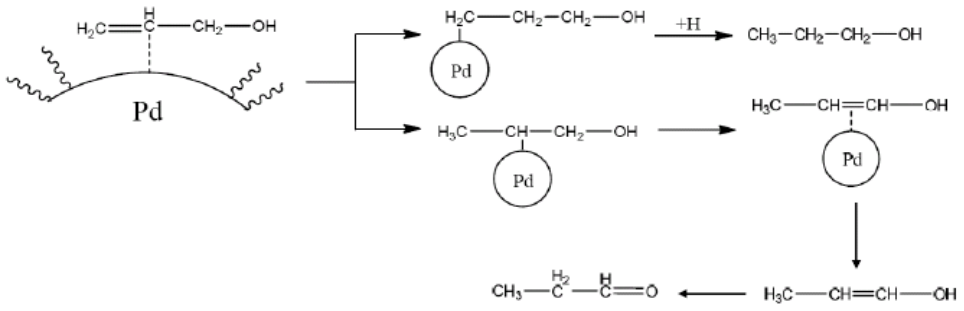

Scheme 3.7 Reaction pathways of allyl alcohol to form different products [46].

3.4 Conclusions

Several alkylphenyl-stabilized nanoparticles have been synthesized following previous literature syntheses. UV-Vis spectra and TEM images of the final Au and Pd nanoparticles were obtained to identify the diameter of metal core, and ^{1}H NMR was used to characterize the ligand attached to the surface of nanoparticles. The results show that the stability of the final decylphenyl-stabilized Au MPCs is quite weak; however, decylphenyl-stabilized Pd MPCs were quite stable in toluene for months. XPS spectra indicate the composition of Pd nanoparticles is a combination of Pd^{0} and Pd^{2+} with the Pd^{2+} complex in excess. An attempt was made to synthesize hydroxyethylphenyl-stabilized Pd MPCs but the major product was a Pd^{2+} complex. Finally, Pd nanoparticles with decylphenyl stabilizers were employed as catalysts for the Stille and Suzuki coupling reactions and hydrogenation reactions. Comparisons of the catalytic activity of PVP–stabilized and decylphenyl-stabilized Pd nanoparticles found that for these three reactions, the decylphenyl-stabilized Pd MPCs are more efficient than Pd nanoparticles protected by PVP stabilizers.

3.5 **References**

[1] C. B. Murray, C. R. Kagan, and M. G. Bawendi, *Sci.*, **1995,** 270, 1335 - 1338

[2] G. Schmid and G. L. Hornyak, *Curr. Opin. Solid St. M.*, **1997,** 2, 204-212

[3] R. E. Benfield and D. Grandjean, *J. Phys. Chem. B*, **2001,** 105, 1961-1970

[4] M. M. Alvarez, J. T. Khoury., *J. Phys. Chem. B*, **1997,** 101, 3706–3712

[5] T. G. Schaaff, M. N. Shafigullin., *J. Phys. Chem. B*, **1997,** 101, 7885–7891

[6] S. Link and M. A. El-Sayed, *J. Phys. Chem. B*, **1999,** 103, 8410–8426

[7] J. P. Wolfe, H. Tomori., *J. Org. Chem.*, **2000,** 65, 1158–1174

[8] R. Meiersa, U. Dingerdissenb, and W. F. Hölderich, *J. Catal.*, **1998,** 176, 376-386

[9] T. Hayashi, K. Tanaka, and M. Haruta, *J. Catal.*, **1998,** 178, 566-575

[10] L. Prati and M. Rossi, *J. Catal.*, **1998,** 176, 552-560

[11] S. Carrettin, P. McMorn., *Phys. Chem. Chem. Phys.*, **2003,** 5, 1329-1336

[12] M. Antonietti, E. Wenz., *Adv. Mater.*, **1995,** 7, 1000 - 1005

[13] I. Pastoriza-Santos and L. M. Liz-Marzán, *Langmuir*, **2002,** 18, 2888–2894

[14] A. C. Templeton, W. P. Wuelfing, and R. W. Murray, *Acc. Chem. Res.*, **2000,** 33, 27–36

[15] R. L. Whetten, M. N. Shafigullin., *Acc. Chem. Res.*, **1999,** 32, 397–406

[16] S. Chen and R. W. Murray, *Langmuir*, **1999,** 15, 682–689

[17] M. Brust, M. Walker., *J. Chem. Soc., Chem. Commun.*, **1994,** 801-802,

[18] F. P. Zamborini, S. M. Gross, and R. W. Murray, *Langmuir*, **2000,** 17, 481–488

[19] R. S. Ingram, M. J. Hostetler, and R. W. Murray, *J. Am. Chem. Soc.*, **1997,** 119, 9175-9178

[20] G. H. Woehrle and J. E. Hutchison, *Inorg. Chem.*, **2005,** 44, 6149–6158

[21] Y. Murakami and K. Konishi, *J. Am. Chem. Soc.*, **2007,** 129, 14401–14407

[22] J. Alvarez, J. Liu., *Chem. Commun.*, **2000,** 1151-1152

[23] Y. Zhu, H. Qian., *Adv. Mater.*, **2010,** 22, 1915-1920

[24] C.-J. Zhong and M. M. Maye, *Adv. Mater.*, **2001**, 13, 1507-1511

[25] D. Ghosh and S. Chen, *J. Mater. Chem.*, **2008**, 18, 755–762

[26] D. M. Shewchuk and M. T. McDermott, *Langmuir*, **2009,** 25, 4556–4563

[27] F. Mirkhalaf, J. Paprotny, and D. J. Schiffrin, *J. Am. Chem. Soc.*, **2006,** 128, 7400-7401

[28] W. Chen, J. R. Davies., *Chem. Mater.*, **2006,** 18, 5253-5259

[29] J. C. Garcia-Martinez, R. Lezutekong, and R. M. Crooks, *J. Am. Chem. Soc.*, **2005,** 127, 5097-5103

[30] P. Dash, N. A. Dehm, and R. W. J. Scott, *J. Mol. Catal. A-Chem.*, **2008,** 286, 114–119

[31] Y.-S. Shon, C. Mazzitelli, and R. W. Murray, *Langmuir*, **2001,** 17, 7735-7741

[32] D. V. Leff, P. C. Ohara., *J. Phys. Chem.*, **1995,** 99, 7036-7041

[33] S. Patai, *The chemistry of diazonium and diazo groups*. The chemistry of diazonium and diazo groups, ed. W. Ando, D.A. Ben-Efraim, and A.J. Fry. **1978,** Bristol: Wiley.

[34] M. J. Hostetler, J. E. Wingate., *Langmuir*, **1998,** 14, 17-30

[35] A. Gniewek, A. M. Trzeciak., *J Catal.*, **2005,** 229, 332-343

[36] R. Narayanan and M. A. El-Sayed, *J. Am. Chem. Soc.*, **2003,** 125, 8340-8347

[37] M. C. Militello and S. J. Simko, ***Surf. Sci. Spectra*, 1997**, 3, 395-401

[38] M. C. Militello and S. J. Simko, ***Surf. Sci. Spectra,* 1997,** 3, 387-394

[39] S. Penner, P. Bera., *J. Phys. Chem. B*, **2006,** 110, 24577-24584

[40] Z. Li, J. Gao., *J. Phys. Chem. C*, **2010,** 114, 723–733

[41] N. Karousis, G.-E. Tsotsou., *J. Phys. Chem. C*, **2008,** 112, 13463–13469

[42] Y.-F. Han, D. Kumar., *Catal. Lett.*, **2004,** 96, 131-135

[43] W. Hou, M. Dasog, and R. W. J. Scott, *Langmuir*, **2009,** 25, 12954–12961

[44] C. A. Grapperhaus, M. J. Maguire., *Inorg. Chem.*, **1997,** 36, 1860-1866

[45] I. Horiuti and M. Polanyi, *Trans. Faraday Soc.* , **1934,** 30, 1164 - 1172

[46] L. K. Freidlin, Y. A. Kopyttsev, and N. M. Nazarova, *Izvestiya Akademii Nauk SSSR, Seriya Khimicheskaya*, **1973,** 3, 700-701

[47] Y. Li, E. Boone, and M. A. El-Sayed, *Langmuir*, **2002,** 18, 4921-4925

[48] X. He, Z.-X. Chen, and G.-J. Kang, *J. Phys. Chem. C*, **2009,** 113, 12325–12330

CHAPTER 4: SUMMARY AND FUTURE WORK

4.1 Summary of Previous Work

In Chapter 2, Pd nanoparticles stabilized by PVP were used to catalyze carbon-carbon coupling reactions, specifically Stille and Suzuki reactions. The results showed that leached Pd^{2+} salts are the precursor for the actual catalytic species for the Stille coupling reaction, which is re-reduced to Pd^0 to produce homocoupling products. O_2 is crucial to the Stille reaction, and nearly no product is obtained under N_2 atmosphere even with heating, and much higher yields are seen in the presence of KI acting as an oxidization promoter. However, O_2 is unfavorable for the Suzuki reaction which might be due to the high activity of Pd nanoparticles to Suzuki reaction. Meanwhile, Au nanoparticles have been tested by the same experimental procedure and have no catalytic activity for these two reactions. The yield for 4-chlorobenzoic acid is higher than 4-bromobenzoic acid even in the absence of catalysts, but the reasons for this result are still unknown.

In Chapter 3, several alkylphenyl-stabilized nanoparticles have been synthesized, including decylphenyl-protected Au and Pd nanoparticles and ethanolphenyl-protected Pd particles. UV-Vis spectra and TEM images of the final Au and Pd nanoparticles were obtained to identify the diameter of metal core, and ^1H NMR was used to characterize the ligand attached to the surface of nanoparticles. Results show that the stability of the decylphenyl–protected Au nanoparticles is quite poor; however, decylphenyl-protected Pd

nanoparticles were quite stable to air in toluene for months. However, x-ray photoelectron spectra (XPS) indicated the composition of the decylphenyl-protected Pd nanoparticles includes both Pd^0 and Pd^{2+} species in a 1:2 ratio. An attempt to synthesize ethanolphenyl-protected Pd nanoparticles was made, but the major product was a Pd^{2+} complex which was confirmed by UV-Visible spectroscopy and XPS spectra, and particles were only formed with minor yields. Finally, Pd nanoparticles with carbon-metal bonds were employed as catalysts for the Stille and Suzuki coupling reactions and hydrogenation reactions. Comparisons of the catalytic activity of PVP-stabilized and decylphenyl–stabilized particles have shown decylphenyl-stabilized Pd nanoparticles have excellent catalytic activity, though the particles tend to fall apart under hydrogenation conditions, likely due to ligand reduction.

4.2 Future Work for Carbon-Carbon Coupling Reactions

Looking to the future, it may eventually be possible to clarify the mechanism of the Stille reaction and Suzuki reaction over nanoparticle catalysts, especially to find out the determining factor(s) for optimal yields using 4-chlorobenzoic acid or chlorobenzene as substrates. Recently, El-Sayed and coworkers have extensively studied the Suzuki reaction with phenylboronic acid and iodobenzene as substrates [1]. They found the addition of biphenyl, which is the main product, to a reaction mixture consisting of Pd nanoparticle catalysts for the Suzuki reaction results in poisoning the active sites and gives rise to a low product yield [1]. Meanwhile, the addition of phenylboronic acid was

found to increase the stability of the Pd nanoparticles as it binds to the particle surface through the O^- of the OH group and acts as a stabilizer and the addition of iodobenzene was found to have no effect on the stability of particles and thus probably does not bind strongly to the surface during the catalytic process. These results might shed light on the catalytic mechanism of the Suzuki reaction. Based on our previous study, Pd nanoparticles usually demonstrate high activity for the Suzuki reaction when heated above certain temperatures and little or no yields were obtained at room temperature. In future work involving Pd nanoparticles catalyzing the Suzuki coupling reaction, several control experiments will be conducted to examine whether biphenyl has an effect on Pd nanoparticle stability and catalytic activity and which factors indeed influence the yield of final product. Meanwhile, more work needed to be done to investigate the homo-coupling reaction for Suzuki reaction. Several groups have demonstrated that Au and Pd nanoparticles could catalyze homocoupling of phenylboronic acid in water to form biphenyl [2-4]. Tsunoyama and Tsukuda [3] proposed a possible mechanism, shown in Scheme 4.1, for the homocoupling of phenylboronic acid catalyzed by Au:PVP nanoparticles in which the catalytic process is mediated by the interaction of O_2 on small Au nanoparticles. In the future, more work should be done to investigate the selectivity of Au and Pd nanoparticles catalysts by applying different substrates to the Suzuki reaction and to determine optimal reaction conditions to obtain high yields of hetero-coupling reaction products, and to investigate the conditions/sizes for which Au nanoparticles are catalytically active.

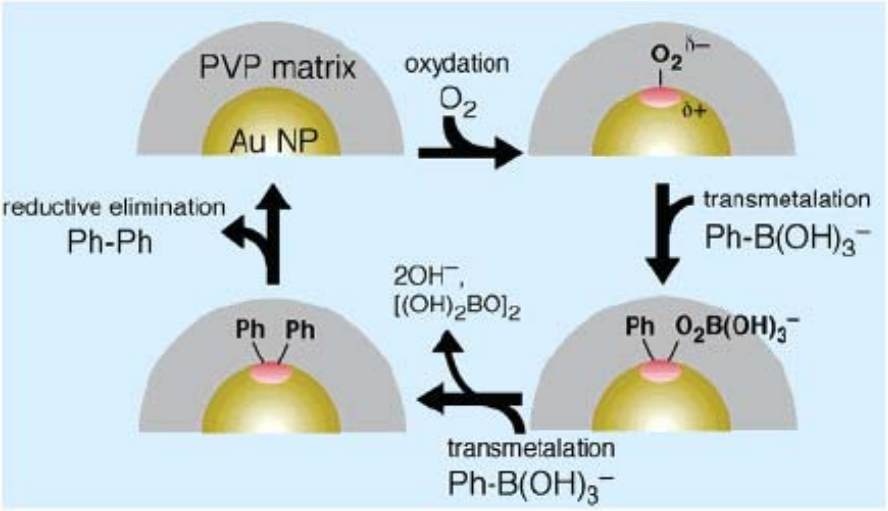

Scheme 4.1. Scheme of homocoupling of phenylboronic acid catalyzed by Au:PVP nanoparticles. Reprinted with permission from [3]. Copyright 2004 American Chemical Society.

4.3 Future Work for Metal Monolayer-Protected Cluster Catalysts

Inspired by the ligand exchange reaction to functionalize monolayer protected clusters (MPCs) with different surface functionalities [5-7], a new method of synthesizing metal nanoparticles protected by metal-carbon bonds via a ligand exchange strategy is proposed. This ligand exchange method would involve the direct synthesis of thiolate protected metal nanoparticles, followed by a ligand exchange step where the original ligand shell is displaced by reducing the thiolate species off the nanoparticle surface in the presence of the diazonium salt to introduce metal-carbon bonds to the surface of nanoparticles. An attempt to synthesize Au nanoparticles by this ligand exchange method was made and the final product was characterized by ^{1}H NMR, UV-Visible spectroscopy,

and TEM. 1-dodecanethiolate-protected Au MPCs were synthesized via a modified Brust-Schiffrin method using standard literature procedures [8]. All solvents were degassed with N_2 and reactions were kept under an N_2 atmosphere unless otherwise noted. A typical synthesis is as follows: 15 ml of an aqueous solution of $HAuCl_4.3H_2O$ (0.25g, 1 mmol) was stirred with a solution of tetraoctylammonium bromide (TOAB, 0.34 g, 2 mmol) in 80 ml of toluene for 2 hours until all the $HAuCl_4$ was transferred to the organic layer, giving it an orange color and the water layer is colorless. The organic phase was separated from the water layer and 0.81 g (4 mmol) of 1-dodecanethiol was then added to the organic phase. After stirring for 15 minutes, 15.0 ml of a freshly prepared 0.67 M $NaBH_4$ solution was added over 20 minutes and the solution was stirred overnight. Excess thiol ligands, disulfides, and TOAB impurities were removed by sequential washing with ethanol, acetonitrile, and acetone. After obtaining purified thiolate protected Au MPCs, the ligand exchange reaction was performed as follows: first 0.0262g of 1-dodecanethiolate-protected Au particles was dissolved in 80 mL of toluene along with freshly made decylphenyl diazonium salt (0.89 g, 3.24 mmol). 1.23M of $NaBH_4$ was dissolved in 15.0 ml MeOH solution and was then added dropwise to the stirring toluene solution over 30 minutes, followed by stirring for one hour. Finally, the solvent was removed and the final product was washed by ethanol, acetonitrile, and acetone thoroughly.

Figure 4.1 shows the UV-Vis spectrum of Au nanoparticles before and after the attempted ligand exchange method, which indicates there are Au particles existing with

small sizes about 2 nm after reaction [9]. The band around 370 nm belongs to remnant side product, which may be azobenzene [10, 11] coming from reduction of the decylphenyl diazonium salt. TEM measurements shows the average particle size of Au nanoparticles after ligands exchange reaction is 1.7 ± 0.3 nm (Figure 4.2), which is slightly larger than the average diameter of the 1-dodecanethiolate-protected Au MPCs before the reaction (1.6 ± 0.2 nm). These results indicate the ligand exchange reaction, if it occurred, did not vary the size of metal core to a large extent.

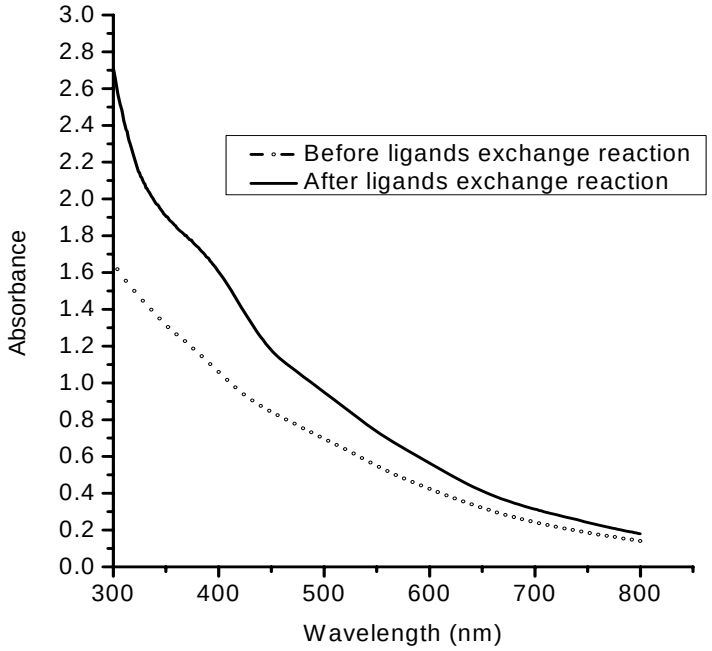

Figure 4.1 UV-Visible spectroscopy of Au nanoparticles before and after the attempted ligand exchange.

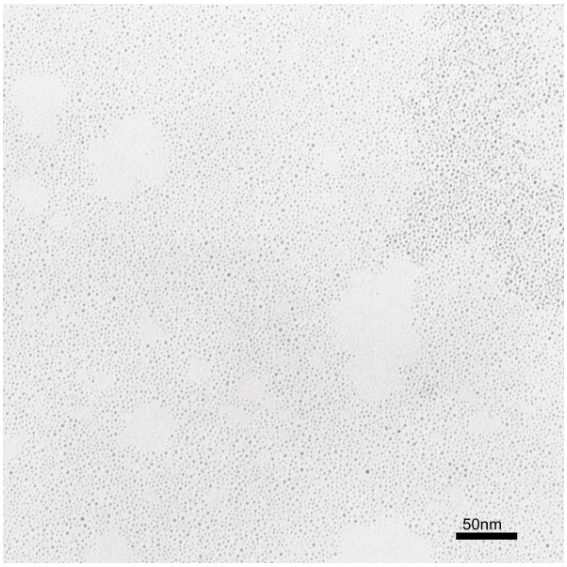

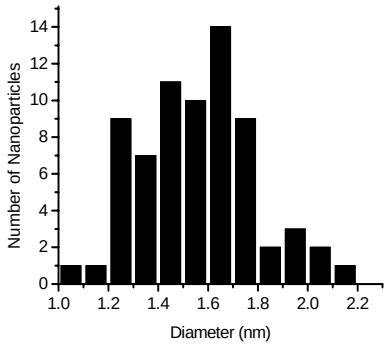

(a)

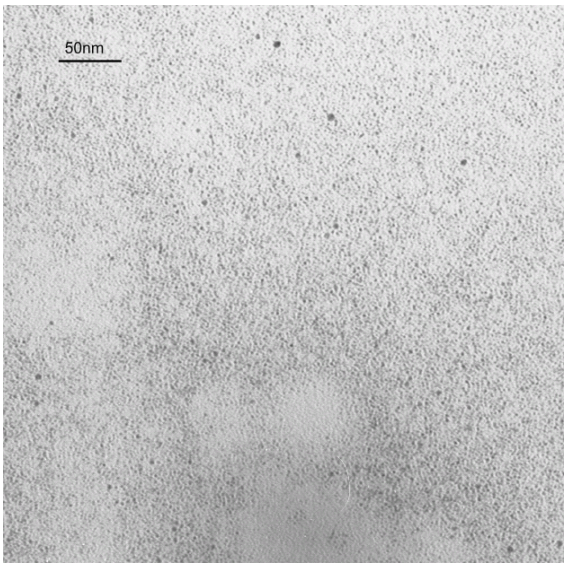

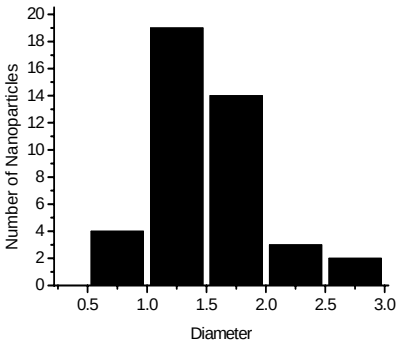

(b)

Figure 4.2 TEMs of Au nanoparticles and size distribution plots before (a) and after (b) the attempted ligand exchange.

After purification of the nanoparticles, the particles were characterized by ^{1}H NMR. The ^{1}H NMR spectrum of the final particles is shown in Figure 4.3. Only the peaks

for the methyl and methylene protons can now be seen and no significant peaks for the protons of phenylene group can be seen. When comparing with original thiolate protected Au particles, we find no obvious change illustrated other than one broadened peak at 2.58 ppm which belongs to proton of methylene off the phenyl group. There are three ways to explain the ^{1}H NMR spectrum of Au MPCs after ligand exchange reaction. First, decylphenyl ligands completely replace original 1-dodecanethiolate ligands and the peaks belong to protons of phenyl broadened to the baseline due to slow tumbling of the particles in solution. Alternatively, some of the original ligands were exchanged by metal-carbon bond linkages but it is difficult to assess the extent of replacement. Finally, due to the strong affinity of sulfur to metal atoms, the decylphenyl ligands are not able to replace the original thiolate ligands, so this product is still primarily the 1-dodecanethiolate protected Au nanoparticles and the peak around 2.58 ppm are likely impurity products remaining in the system. By examining the integration of methyl vs. methylene peaks at 1.25 ppm for both ^{1}H NMR spectra, we believe the reaction has happened in some extent because the methylene:methyl intensity ratio is higher after the reaction, which means longer chains of organic ligands (16 carbons) have linked to Au nanoparticles.

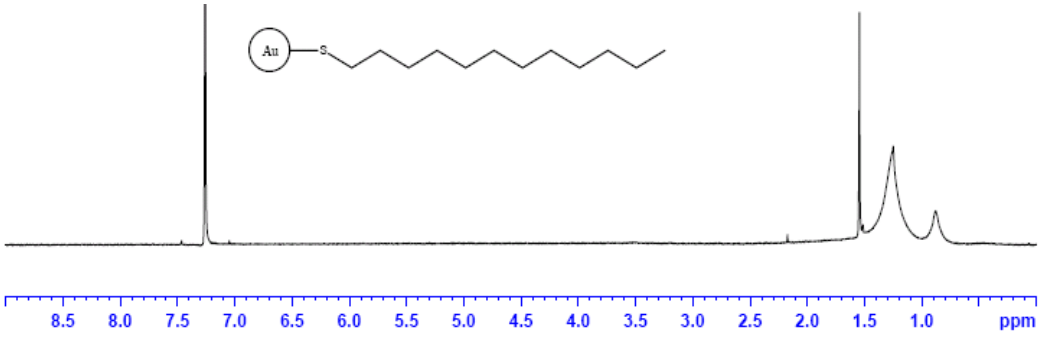

(a)

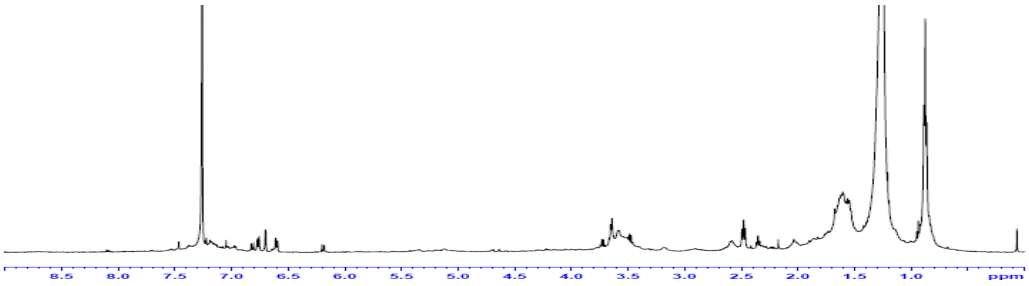

(b)

Figure 4.3 ^{1}H NMR spectra of Au MPCs before (a) and after (b) the attempted ligand exchange reaction.

The above experimental results cannot determine precisely whether the ligand exchange method to synthesize metal-carbon bonds on the Au nanoparticles was successful. However, it still provides one possibility of new technique to prepare metal nanoparticles. In the future, several diverse replacement ligands with more identifiable functional groups (by NMR) can be attempted and more labile ligand- protected nanoparticles can be chosen. The product will be characterized further via XPS, FTIR, and other techniques to obtain information on the extent of ligand exchange [12, 13].

Furthermore, different diazonium ligands such as more sterically bulky ligands will be synthesized as protecting groups for metal nanoparticles, especially Pd and Au nanoparticles, and attempts will to be made to improve their stabilities. Finally, the catalytic activities of different ligand-stabilized nanoparticles will be tested to find out which ligands can give high stability to the final particles and at the same time excellent catalytic activity for catalysis reactions. Comparison of the catalytic mechanisms of coupling reaction and hydrogenation reaction with Pd nanoparticles protected by carbon bond linkages and PVP will be carried out in hope of discovering more effective catalysts.

4.4 References

[1] Narayanan, R. and M.A. El-Sayed, *J. Am. Chem. Soc.*, **2003**, 125, 8340-8347

[2] Cravotto, G., M. Beggiato., *Tetrahedron Lett.*, **2005**, 46, 2267-2271

[3] Tsunoyama, H., H. Sakurai., *Langmuir*, **2004**, 20, 11293-11296

[4] Seganish, W.M., M.E. Mowery., *Tetrahedron*, **2005**, 61, 2117-2121

[5] Ingram, R.S., M.J. Hostetler, and R.W. Murray, *J. Am. Chem. Soc.*, **1997**, 119, 9175-9178

[6] Dahl, J.A., B.L.S. Maddux, and J.E. Hutchison, *Chem. Rev.*, **2007**, 107, 2228-2269

[7] Templeton, A.C., W.P. Wuelfing, and R.W. Murray, *Acc. Chem. Res.*, **2000**, 33, 27–36

[8] Brust, M., M. Walker., *J. Chem. Soc., Chem. Commun.*, **1994**, 801-802,

[9] Hou, W., M. Dasog, and R.W.J. Scott, *Langmuir*, **2009**, 25, 12954–12961

[10] Wang, Y., B. Tang., *Chinese J. Org. Chem*, **2010**, 30, 330-337

[11] Kawai, T., J. Umemura, and T. Takenaka, *Langmuir*, **1989**, 5, 1378-1383

[12] Gniewek, A., A.M. Trzeciak., *J Catal.*, **2005**, 229, 332-343

[13] Ghosh, D. and S. Chen, *J. Mater. Chem.*, **2008**, 18, 755–762